Multi-Band Subsynchronous Damping Controller for Type III DFIG Wind Turbines with Single Mass and Multi-Mass Rotor Models

A Thesis Submitted
to the College of Graduate and Postdoctoral Studies
in Partial Fulfillment of the Requirements
for the Degree of Master of Science
in the Department of Electrical and Computer Engineering
University of Saskatchewan

by

Jason B. Pannell

Saskatoon, Saskatchewan, Canada

Permission to Use

In presenting this thesis in partial fulfillment of the requirements for a Postgraduate degree from the University of Saskatchewan, it is agreed that the Libraries of this University may make it freely available for inspection. Permission for copying of this thesis in any manner, in whole or in part, for scholarly purposes may be granted by the professors who supervised this thesis work or, in their absence, by the Head of the Department of Electrical and Computer Engineering or the Dean of the College of Graduate Studies and Research at the University of Saskatchewan. Any copying, publication, or use of this thesis, or parts thereof, for financial gain without the written permission of the author is strictly prohibited. Proper recognition shall be given to the author and to the University of Saskatchewan in any scholarly use which may be made of any material in this thesis.

Request for permission to copy or to make any other use of material in this thesis in whole or in part should be addressed to:

Head of the Department of Electrical and Computer Engineering
57 Campus Drive
University of Saskatchewan
Saskatoon, Saskatchewan, Canada
S7N 5A9

Abstract

Wind energy provides a needed source of renewable energy to the electrical market however, connecting this renewable energy to the grid can cause some challenges. With the quick increase of the proportion of renewables in the composition of electrical generation, these complexities, such as sub-synchronous oscillations, are becoming more and more important.

The largest addition of renewable energy to the electrical grid has come from wind generation. The most popular type of wind generators are the Type III or Doubly Fed Induction Generators, which have a power-electronics based control system running the excitation control of the generator.

Sub-Synchronous Interactions (SSI), are a family of issues involving the exchange of energy between the generation system and the transmission system, most often found in situations involving series compensated transmission lines. These sub-synchronous oscillations present a hazard to generation systems, transmission systems, and connected equipment that can result and have resulted in catastrophic failure.

A subset of SSI are known as Sub-Synchronous Control Interactions (SSCI). SSCI involves the interaction between the power electronic based excitation control of a Type III wind generator and the transmission system. A key feature of SSCI is the fact that they are a completely electrical interaction and as a result, large oscillations can develop much more quickly than with an electro-mechanical oscillation such as the well-studied Sub-Synchronous Resonance (SSR).

Because of the speed with which SSCI's develop, quick corrective action must be taken to eliminate these incidents. Doubly Fed Induction Generators (DFIG) have been observed to have experienced SSCI's when connected radially through a series compensated transmission line.

This thesis develops a Multi-Band Sub-Synchronous Damping Controller (MBSSDC), which will leave the existing generator protection and control system in place while adding protection against SSCI. The MBSSDC is run in parallel with the main control loop of the

generator. The solution envisioned uses a two band controller.

This represents a simple and elegant solution to the problem of sub-synchronous control interactions between Type III wind generators and series compensated transmission lines. A solution to a problem of particular interest to North American utilities, due to the influx of wind power to their systems and the prevalence of long transmission lines in their systems, compared to the shorter lines typical in Europe.

The MBSSDC has demonstrated an improvement in the stability of the model wind generation system, providing stable operation at compensation levels in excess of 95% for the single mass rotor model. The MBSSDC has also improved the response of the system to faults on the system generation bus, allowing a quicker return to steady state operation after a fault has been removed from the system. The normal operation of the system has not been altered, but the response to SSCI events and to various line faults has been greatly improved, virtually eliminating the stability loss seen with the base wind farm.

For validation and verification of the research results, a wind farm consisting of 150 - 3 MW Type III Doubly Fed Induction Generators (DFIG) connected to a stiff voltage source through a 240 km transmission line was modeled using electromagnetic transient simulations (EMT) in PSCAD/EMTDC. A capacitor was placed in series with the transmission line, allowing adjustable levels of compensation. A selectable fault was added to the generator bus to verify the operation of the system during faults.

The thesis shows the results of placing the MBSSDC on generator models using a single mass rotor model and on the more realistic multi-mass rotor model, and it discusses results from both these models.

After completion of the initial design of the MBSSDC, both the single mass rotor model and the multi-mass rotor model results were further refined using a non-linear time domain simplex optimization (multi-run) process within the electromagnetic transient simulation. The optimization process improved the response of both system models settling time and increased the maximum level of compensation the single mass rotor model was stable to significantly.

Acknowledgments

I have a number of people I must thank for the help they have given me through this process.

Foremost, I must express my appreciation and gratitude to my supervisor Dr. Ramakrishna Gokaraju. This thesis could not have happened without your support, advice and guidance. I extend gratitude to my fellow grad students, especially Sriram Chandreshekar and Binay Thakur, in the Real-Time Simulation Laboratory at the University of Saskatchewan. Thank you to the Electrical and Computer Engineering Department at the University of Saskatchewan for providing support, as well as a comfortable environment for my studies.

Thank you to my parents, Vicki and Bernie, and my sister Christy, for encouraging me to enter into graduate studies and for all the encouragement and support along the way. Thank you to my wife Sarah, our son Winston, and our dog Daisy, for the encouragement, the laughs and for reminding me about what is really important in life.

Thank you to Olivier Larocque, with whom I completed my undergraduate degree, for the initial research we did together on our capstone design project.

Thank you to SaskPower for their generous support through an NSERC Industrial Postgraduate Scholarship. Thanks to Don Robinson of SaskPower for all the real world knowledge and advice he passed to me while I was working with Plant Services at SaskPower. Thank you to Dr. Amit Jindal and Electranix Corporation for their help with the PSCAD Windfarm model.

A special thanks must go to Guy Fuller, my father in law, who helped me with the editing and proofing of this thesis. Guy provided valuable insights on how to clearly express my thoughts in a way that is easy for the reader to follow.

Lately it occurs to me,

what a long strange

trip it's been...

- The Grateful Dead

Table of Contents

List of Tables

List of Figures

List of Symbols & Abbreviations

A	Ampere
AC	Alternating Current
BIBO	Bounded Input - Bounded Output
C	Capacitance
CT	Current Transformer
DC	Direct Current
DFIG	Doubly Fed Induction Generator
DG	Distributed Generation
DLG	Double Line to Ground
DSP	Digital Signal Processing
EMT	Electromagnetic Transient
EMTP	Electromagnetic Transient Program
ERCOT	Energy Reliability Council of Texas
FACTS	Flexible AC Transmission Systems
GSC	Grid Side Converter
IG	Induction Generator
IGBT	Insulated Gate Bipolar Transistor
IPP	Independent Power Producer
H	Inertia Constant
L	Inductance
L-L	Line to Line
LFPO	Low Frequency Power Oscillation
MBSSDC	Multi-Band Sub-Synchronous Damping Controller
MW	Mega Watt
P	Real Power
PSS	Power System Stabilizer
PT	Potential Transformer
PWM	Pulse Width Modulation

Q	Reactive Power
R	Resistance
RMS	Root Mean Square
RSC	Rotor Side Converter
RTDS	Real Time Digital Simulator
S	Apparent Power
SCIG	Squirrel Cage Induction Generator
SLG	Single Line to Ground
SMIB	Single Machine Infinite Bus
SSCI	Sub-Synchronous Control Interaction
SSI	Sub-Synchronous Interaction
SSO	Sub-Synchronous Oscillation
SSR	Sub-Synchronous Resonance
STATCOM	Static Compensator
SVC	Static VAR Compensator
TCSC	Thyristor Controlled Series Capacitor
TL	Transmission Line
TSAT	Transient Security Assessment Tool
V	Volt
VA	Volt-Ampere
VAR	Volt-Ampere Reactive
VSC	Voltage Source Converter
WRIG	Wound Rotor Induction Generator
Z	Impedance

Chapter 1

Renewable Energy and the Power System

1.1 Introduction

This chapter will discuss the current state of renewable energy in regards to power generation, and how the growth of renewable energy as a proportion of the total power generation has caused some issues with power system reliability. The various types of Sub-Synchronous Oscillations (SSO) affecting the power system will be discussed briefly with a focus on the phenomena more relevant to wind systems. The practice of series compensation of transmission lines will be discussed with a brief overview of the system model following. The Chapter concludes with a literature review discussing the current research and techniques in the area of Sub-Synchronous Control Interactions (SSCI) and Type III doubly fed induction generators (DFIG) wind turbines.

1.2 Growth of Renewable Energy

Renewable energy is appealing to the public as a source of 'green power' that causes a low environmental impact. Integration of renewable energy to the electrical system has seen a rapid increase over the past decade. Concern over carbon footprints and greenhouse gas emissions has led to the larger-scale incorporation of wind and photo-voltaic sources to augment the main grid.

Other forms of renewable energy such as bio-mass and geothermal have seen significant growth [2], but the bulk of the new non-conventional generation comes from wind and photo-

voltaic sources [3]. Renewable energy sources often appeal to utilities and independent power producers (IPP) since governments often subsidize the installation of these systems through tax breaks and other incentives, moreover public perception of the desirability of renewable energy is surely an impetus behind the growing adoption of renewable energy by utilities. In Canada, the province of Ontario has established an act, Green Energy and Green Economy, that pays above market prices for renewable energy generated power [4].

The composition of traditional and renewable generation capacity available worldwide as of 2014 is shown in Figure 1.1 [5]. The pie chart clearly shows that wind energy composes a large portion of the renewable energy production.

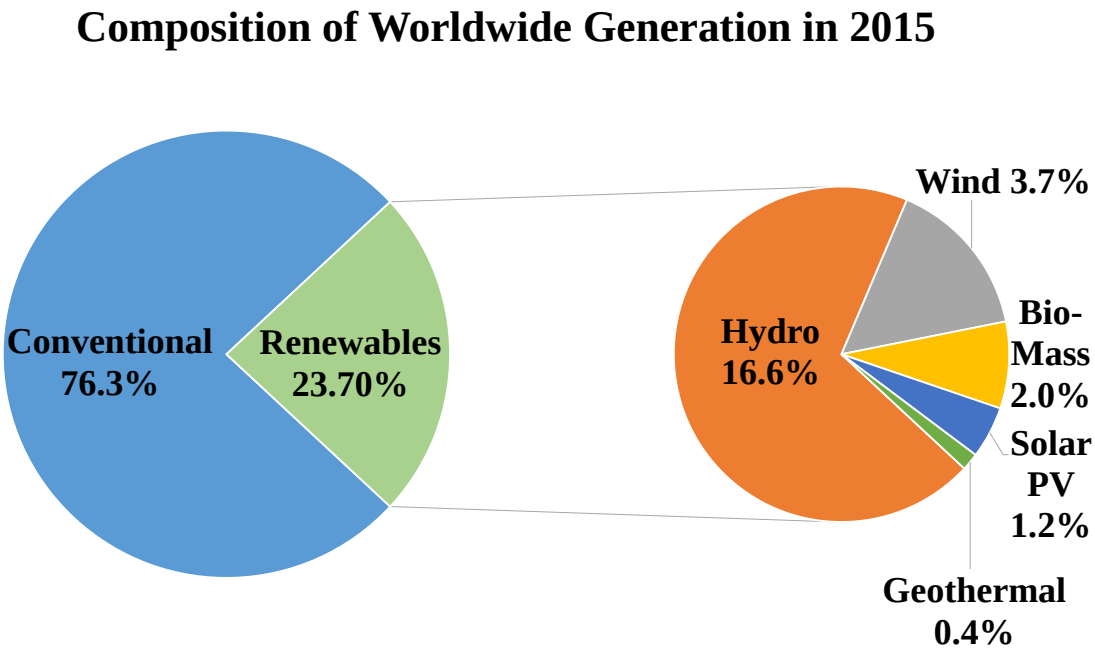

Figure 1.1: Composition of Available Generation Capacity Worldwide in 2015

Globally, renewable energy provided approximately 24% of the energy generated worldwide [5]. 2014 marked the first time in forty years that carbon emissions from power production remained stable despite an overall increase in energy use, no doubt due to the 107 GW increase from 2013 in the amount of renewable generation available [5]. Clearly, since the effects of adding this amount of non-conventional generation to the power system will have some unintended consequences, utilities must develop new techniques for control and

protection.

1.2.1 Growth of Wind Energy

The total worldwide installed wind generation capacity was 370 GW as of 2014; 51 GW of this was installed in 2014 alone. Such rapid increase of wind integration is perhaps due to its representing the lowest cost option for new installations [5]. A chart showing the worldwide growth of wind generation over an eleven year period from 2005 - 2015 is shown in Figure 1.2.

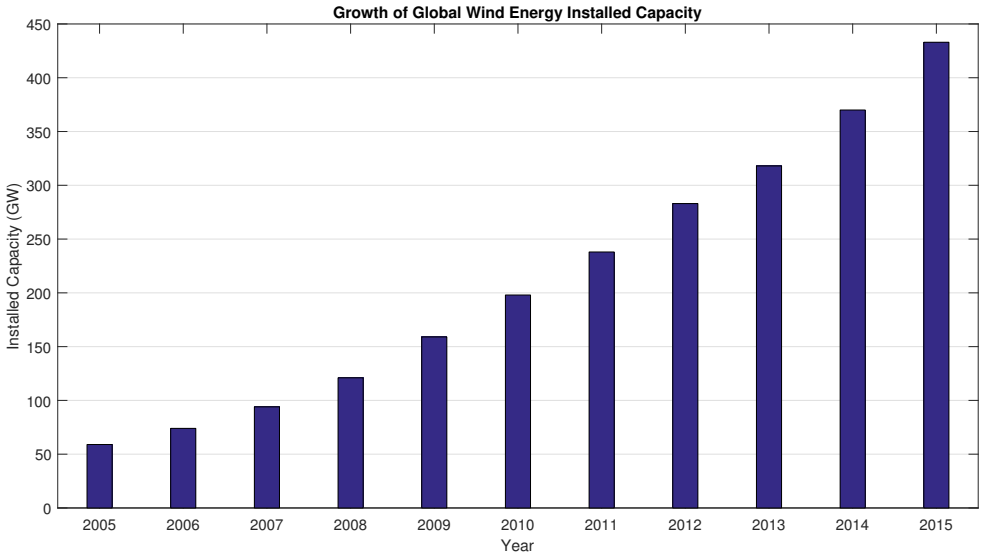

Figure 1.2: Growth of Wind Generation Globally

In Canada, the installed wind generation capacity has grown by 11 GW since the year 2000. Over the five year period of 2010 - 2015, the installed capacity has grown by over 7 GW [6].

Currently wind power represents about 6% of the installed electrical generation capacity in Canada. It is clear that wind energy is a rapidly growing component of Canada's installed capacity. Figure 1.3 illustrates this rapid year by year increase of installed wind generation capacity in Canada since the year 2000.

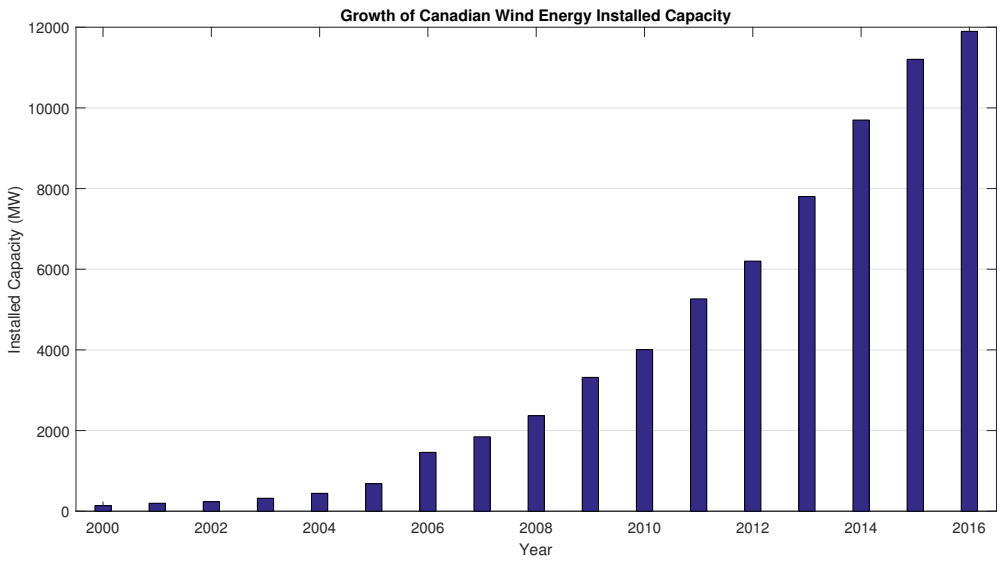

Figure 1.3: Growth of Wind Generation in Canada

1.3 Issues with Wind Generation

The growing supply of wind power being connected to the grid, frequently in areas far from population centers means that issues involved with the transmission of this energy to the main grid are likely to become very important in the near future [7].

Capacity factor is defined as the average output of a power generation plant divided by the rated output over a long period of time. Wind is an intermittent source, and is not always available or easily scheduled pr predicted. Wind is generally stated to have a capacity factor of between 20% and 40% [8] [9]. This is lower than the capacity factors of nuclear and fossil fuel units which are between 60% and 90% [9]. However wind does have a higher capacity factor than solar PV which has a daytime capacity factor of around 15% [10] [11].

Since wind-farms are frequently connected to the main grid through a radial transmission line, that is, a line where the wind-farm is connected to the main grid via a long single circuit, efficient use of the transmission line often dictates the installation of a series capacitor in the system. This radial connection may also occur during a contingency situation where a forced outage has removed other lines as was the case with the Zorillo wind farm incident [12].

The Energy Reliability Council of Texas (ERCOT) notes that the most widely used type of induction generator in their system is the Type III [13]. The Type III (Doubly Fed Induction Generator) is in widespread use across the wind generation industry. The DFIG is a type of induction generator where both the stator and rotor windings are attached to an electrical supply with the rotor windings having a back-to-back converter isolating it from the supply.

Under certain conditions it has been shown that the interaction between a Type III DFIG and a series compensated long transmission line output power oscillations can develop. These oscillations can lead to system instability and equipment damage [14] [15] [12].

1.4 Specifications of the System Model

Figure 1.4 shows the system model. This construct consists of a wind farm with 150 - 3 MW Type III DFIG generators connected to a series compensated 240 km transmission line which is radially connected to a stiff voltage source representing the infinite bus. This is known as a single machine infinite bus (SMIB) system although there is multiple small machines connected at the windfarm. The system generates 450 MW at its steady state operating condition with all turbines assumed to be receiving the same wind speed [16]. The windfarm has the 150 generators aggregated into a single equivalent generator [17]. The generators are equivalent to each other and will see the same wind speed.

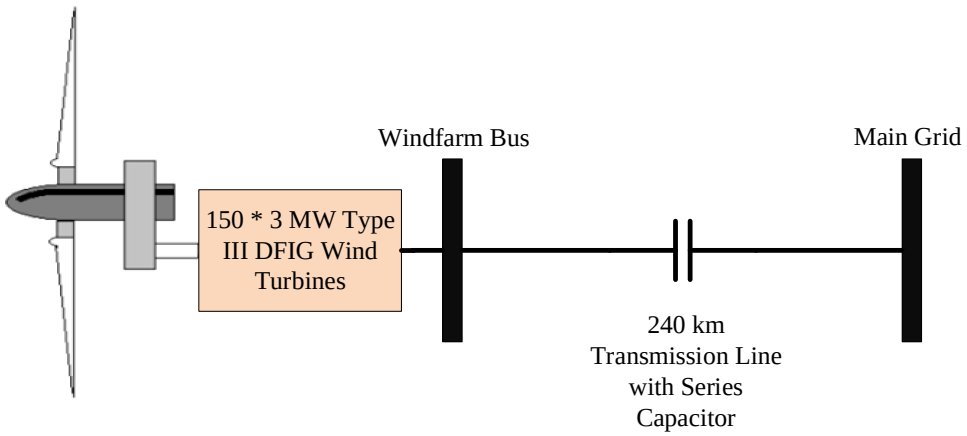

Figure 1.4: Model Windfarm

1.5 Literature Review

Several methods have been proposed for the problem of sub-synchronous oscillations on radially connected series compensated wind farms with type III DFIG's. This section will summarize these efforts and draw comparisons to my research construct, the Multi-Band Sub-Synchronous Damping Controller (MBSSDC) presented in this thesis.

The MBSSDC is a supplementary control system with frequency specific band(s) designed to damp out specific oscillations that have lead to system instability, in a Type III DFIG based windfarm. These bands are placed in parallel with the existing excitation control of a Type III DFIG wind generator in order to stabilize the system.

1.5.1 Doubly Fed Induction Generators

The Type III doubly-fed induction generator (DFIG) is the most commonly used wind generator due to its ability to capture wind power at variable wind speeds [11] [18]. The output power of a DFIG increase as the wind speed increases, and as the wind varies, the excitation of the generator must be altered to maintain operation of the machine at the desired frequency output set-point.

The DFIG consists of a wound rotor induction machine that has the stator windings connected directly from the three phase voltage supply, while the rotor windings are fed through a back-to-back converter that is powered by the grid side connection that is also connecting the stator. The back-to-back converter rectifies the grid voltage and uses an inverter to feed the rotor windings with a variable frequency AC voltage [19].

Wind farms typically consist of multiple wind turbines arranged on the site in a manner to maximize the wind capture, the farm is then connected to the main grid via a main bus. As the wind generators are often identical to each other leading to the modeling of the farm as a single equivalent generator [20] [17]. An aggregate model that views the multi-generator windfarm as a single entity has been used extensively in recent times, it is assumed that the generators all see the same wind [21] [16]. Reference [22] demonstrates that the aggregated model is virtually identical for modeling the transient behaviour of wind farms. The aggregated model is used in the model system developed in this thesis.

1.5.1.1 Multi-Mass Rotor Model

As the practical wind turbine will be constructed with several rotating masses on a single rotor shaft, it is necessary to model the rotor as a multi-mass shaft for more realistic results. This thesis has adopted both a single mass rotor model, as well as a two mass model (turbine and gearbox) for the rotor shaft which has been deemed sufficient for transient stability studies of wind turbines as show in [23].

This multi-mass model will have a number of natural frequencies that may be excited when a disturbance occurs. These modes will make the system more fragile than the same system modeled with the simpler single mass rotor model. If the oscillations triggered by the disturbance coincide with the natural mechanical modes of oscillation, instability can be triggered as the electrical and mechanical oscillations begin to grow due to torsional interactions [24].

1.5.2 Sub-Synchronous Interactions

In power generation and distribution, oscillation is a situation where the electro-mechanical system affected begins to oscillate at its natural frequency. This frequency is determined by the reactive elements (jX_L or jX_C) within the system and the particular generator configuration. Resistance within the system helps to damp out these oscillations, but if the level of damping is insufficient, system instability will result and the wind-farm will see oscillations in its output power.

These oscillations are outside of normal system operation and are often induced by a disturbance of some type. The disturbance can range from routine operations such as a simple change in the operating load or the addition of series compensation the to the transmission line, to emergency events such as the failure of a component in a connected system or a faulted line. These oscillations can quickly grow in magnitude and become destructive, possibly damaging the generation system, the transmission system, and connected equipment.

Oscillation in the output of a wind-farm involves the transfer to and from the generator and the transmission line. Such a situation is commonly referred to as Sub-Synchronous Interactions (SSI) in the power industry, as the frequency of oscillation is below the synchronous frequency (typically 50 Hz in Europe and 60 Hz in North America). The resonant frequency of a circuit can be determined by the following formula:

$$\omega_0 = \frac{1}{\sqrt{LC}} \tag{1.1}$$

In the most simplified model, the transmission line is represented by the inductive reactance and the series compensation applied to the transmission line is represented by the capacitive reactance.

1.5.3 Low Frequency Power Oscillations

The most common type of SSI's are known as Low Frequency Power Oscillations. There are two main types of Low Frequency Power Oscillations (LFPO): local modes of oscillation which resonate at approximately 1 - 2 Hz, and inter-area modes which occur around 0.1 - 0.7 Hz. These oscillations occur due to the interaction between the electro-mechanical systems of different generators on the same electrical system, and the interaction between separate electrical grids with 'weak ties' providing insufficient connection between them [25].

These oscillations can have a number of negative impacts on a power system. Both these modes of oscillation can cause reliability issues in the power system, over-voltage situations, where the low frequency oscillation effectively modulates the power output on the line damaging equipment, and causing premature generator failure [26].

Mechanical damage to the generator is also possible due to the torque applied on the generator shaft during these events. These oscillations are typically avoided through the use of a power system stabilizer. The installation of a power system stabilizer (PSS) in a generator system is becoming a standard practice to ensure stable operation [27].

1.5.4 Sub-Synchronous Resonance

A second group of SSI's known as Sub-Synchronous Resonance (SSR) involves an electro-mechanical interaction between a series compensated transmission line and the torsional modes contained within the generator's shaft. This is normally only seen with large synchronous generators. This problem has been noticed as early as 1937 [28], with Butler and Concordia noting that the hunting of synchronous generators increased as series capacitors were added to the transmission line.

An electrical resonance begins to excite a mechanical resonance that is present at approximately the same frequency as the electrical resonance, and a slow growing vibration will begin [1]. SSR damage is typically found in larger synchronous generators and is not normally a concern in a typical wind farm configuration with smaller induction generators.

SSR is characterized by a slow build-up of the oscillation over a period of one to two seconds.

Sub-Synchronous Resonance was responsible for two failures at the 1580 MW coal fired Mohave power plant in Nevada [26]. The first incident occurred in 1970 resulting in a fracture of the generator shaft. This incident was not initially identified to be the result of SSR and the same problem recurred in 1971, again destroying the generator shaft [29]. A photo of the damaged generator shaft appears in Figure 1.5 [1]. Further study after the second incident identified the cause of both shaft failures to be SSR.

Figure 1.5: Broken Mohave Power Plant Generator Shaft (Used With Permission) [1]

1.5.5 Series Compensation

Series compensation of transmission lines involves placing a series capacitor with the transmission line, providing an economical method of effectively shortening the transmission line [30], allowing the transmission of larger amounts of power, compared to the uncompensated line. This allows an existing transmission line to safely transmit a higher amount of power than would be possible without the series capacitor, thus better economizing the system capacity [31].

Series capacitors are often used when a generation station is far from a population center, and therefore connected with a 'long' transmission line. Such is often the case with windfarms located in remote areas [32].

Generally a transmission line is said to be 'long' if its length is more than 160 kilometers or 100 miles [31]. It is possible to experience SSCI events with a shorter transmission line, although transmission line length is an aggravating factor. As the length of the transmission line increases, the inductance of the entire line increases as well, and for a given level of compensation (x%) the resonant frequency will therefore decrease as well, bringing the electrical resonant frequency closer to the mechanical resonance (generally in the region of 20-40 Hz [26] [25].

Series compensation reduces the value of reactance between the source and the load of a transmission system by countering the $+jX_L$ reactance of the generator and transmission lines with $-jX_C$ reactance from the series capacitor installed on the transmission line. Series compensation allows the adjustment of the circuit parameters to allow larger power transfer [33]. The level of compensation, or how much of the inductive reactance is countered by the capacitive reactance, is defined as follows:

$$\%Compensation = \frac{X_{C_{Series}}}{X_{L_{Line}}} * 100\% \tag{1.2}$$

The new value of reactance for the transmission line will be found thus:

$$jX_{TL_{new}} = jX_{L_{Line_{original}}} - jX_{C_{Series}} \tag{1.3}$$

Typically transmission lines would be compensated no more than 50%, although values as high as 70% can be seen in practice. As the level of compensation increases, the fragility of the system also increases, and instability is more likely to occur.

As the level of compensation increases, the value of the capacitive reactance, $-jX_C$, approaches the value of the inductive reactance, $+jX_L$. At 100% compensation the value of these reactances are equal and the frequency of the resonant oscillation between the inductive and capacitive reactances is equal to the power system frequency (ω_{grid} in $\frac{rad}{s}$) as shown in equation 1.8. The following derivation shows this:

$$X_L = \omega_{Grid} L \tag{1.4}$$

and

$$X_C = \frac{1}{\omega_{Grid} C} \tag{1.5}$$

thus with X_L equal to X_C;

$$\omega_{Grid} L = \frac{1}{\omega_{Grid} C} \tag{1.6}$$

yielding

$$L = \frac{1}{\omega_{Grid}^2 C} \tag{1.7}$$

Substituting Equation 1.7 into Equation 1.8 gives;

$$\omega_{Resonant} = \frac{1}{\sqrt{\frac{1}{\omega_{Grid}^2 C} C}} = \frac{1}{\sqrt{\frac{1}{\omega_{Grid}^2}}} = \omega_{Grid} \tag{1.8}$$

Equivalent reactances will result in this resonant frequency being excited by the system and an oscillating circuit and system instability will result. Line resistance will provide some damping of the oscillation in general.

Series compensated lines are often found in a typical wind-farm application, where wind power is captured using an induction generator in a rural or remote area, and transmitted along the electrical grid to a population center. Even if the farm is not normally connected radially, it is possible for a wind-farm suddenly to find itself connected radially due to other faults on the system, causing lines to be removed as mentioned with the Zorillo wind farm case [12] [34].

1.5.6 Sub-Synchronous Control Interactions

A third type of SSI oscillation, which is the focus of this project – is an oscillation due to the interaction between an induction generator's power-electronic based excitation control and series compensated 'long' transmission lines [34]. Such an oscillation is referred to as a Sub-Synchronous Control Interaction (SSCI) [14] [35]. The purely electrical nature of this interaction means that stability can be lost nearly instantly, as opposed to the slower buildup of oscillations as seen in an SSR event [36]. This unanticipated consequence is of particular concern to North American utilities due to the abundance of long transmission lines, and the emergence of wind power that has been seen lately [37].

The frequency ranges of oscillation during an SSCI event have no fixed value. The frequency range of oscillations is dependent upon the specific generator control system configurations, the transmission line length and type, and the value of the series compensation connected to the transmission line. This SSCI can damage the generation system, equipment connected within the transmission system, such as series compensation capacitors, in a way similar to an SSR event, although the damage can occur much more rapidly due to the dramatic buildup of oscillations due to the purely electrical nature of the oscillations.

The Zorillo wind farm in Texas experienced such an event in October of 2009. A fault on an adjacent line left the wind farm radially connected to the grid and an SSI event was triggered. The line originally was series compensated to a value of 50% but the forced outage effectively increased the series compensation level to approximately 75% [34]. In 200 ms oscillations grew to such an extent that the voltage exceeded 1.5 P.U. (reaching nearly 2.0 P.U. [1]) and the generators suffered damage [15]. After 400 ms the voltage and current had reached levels of nearly 3 p.u. at the wind farm terminals [34]. The event may never have happened if the forced outage had not caused the radial connection of the wind farm to the grid through a series compensated line [1].

Several methods have been proposed to solve the issue of SSCI's developing between series compensated lines and DFIG based wind farms. This thesis develops a Multi-Band Sub-Synchronous Damping Controller (MBSSDC), which will leave the existing generator

protection and control system in place while adding protection against SSCI. The MBSSDC is run in parallel with the main control loop of the generator and tuned to damp out the offending frequencies during an SSCI event to maintain system stability.

ERCOT now recommends EMT studies to be performed with PSCAD for all types of generation connected to series compensated lines, including analysis of contingency situations due to forced outages. The recommendation is a for a reasonable number *(N-x)* to be studied. This 'reasonable' number of contingencies would be determined by the specific circumstances of the system [34] [38].

References [39] and [40] describe a method to mitigate the SSCI issue between series compensated lines and DFIG based wind farms through the installation of Static VAR Compensators (SVC) at the terminals of the induction generator. Reference [40] also proposes the use of a Thyristor Controlled Series Capacitor (TCSC) to replace the traditional series compensation capacitor in the transmission line. The cost and difficulty implementing these solutions is much higher than the proposed MBSSDC.

The use of band-stop filters in the control loop of the DFIG is discussed in references [41] and [42]. A band-stop filter set to the offending frequency would be placed in series with the control system for the DFIG. This has the disadvantage of being a series element, possibly interrupting normal system operation as opposed to a shunt element that does not pass the entire control signal through it at all times.

Placement of a Voltage Source Converter (VSC) in parallel with the collector bus of the windfarm is discussed in reference [43]. Reference [43] also calls for the modification of the DFIG control system to be done in concert with the addition of the VSC. This presents a similar issue to the solutions proposed in [39] and [40] in that relatively high powered equipment will have to be purchased and installed to implement the proposed methods.

Chowdhury et al. [44] propose the use of a non-linear controller based upon partial feedback linearization for the mitigation of SSCI in series compensated DFIG's. This method again places an element in series with the existing control, potentially suffering from the same issues as discussed with [41] and [42].

Reference [45] investigates the use of a traditional power system stabilizer (PSS) to control the SSCI both at an individual generator level and at the wind farm as a whole.

The addition of a lag controller in the PD control loop of a DFIG is discussed in [46]. Again as noted in references [41], [42], and [44], this leads to the addition of a series element in the control system potentially leading to undesired operation or system failure if the new element fails somehow. The addition of a series element in a control loop means the entire control signal will pass through the new element, whereas a shunt element will only pass the portion of the control signal filtered into the shunt loop.

1.5.7 Simplex Optimization

Once system stability has been achieved, final tuning of the parameters will be done using a nonlinear time domain method known as simplex optimization. The tuning of the parameters of the MBSSDC is non-trivial due to the wide frequency range that the SSCI oscillations contain. Conventional control system tuning techniques will not be effective [47].

Simplex optimization allows the minimization of an objective function in a multi-dimensional space. The variables in the function to be optimized are iterated in a nonlinear fashion until a minimum is found. This section explains the simplex optimization concept briefly (a more detailed description is found in [48]).

Optimization in an EMT program requires multiple simulation runs, iterating through all possible inputs to the system to find the optimum values. The choice of the 'next set' of variables will determine how long the system will take to converge. A brute force linear progression through all possible variables will take very large amounts of computer time to solve. Random use of possible input values such as in a Monte-Carlo type optimization require a large number of iterations to ensure that a sufficient range of inputs have been evaluated leading to large amounts of computer time similar to the linear search.

A strategic choice of the 'next set' of variables can greatly cut down on the time required for optimization. A simple example with some mock values of the objective function is

shown in Figure 1.6, the three points of the initial triangle represent three points where the objective function will be evaluated. The worst performing point (value of 18) is found (indicated by the red dot), and the remaining points (indicated by the points with values of 15 and 17) form the vertices for the triangle to be flipped upon to find the new evaluation point (value of 16).

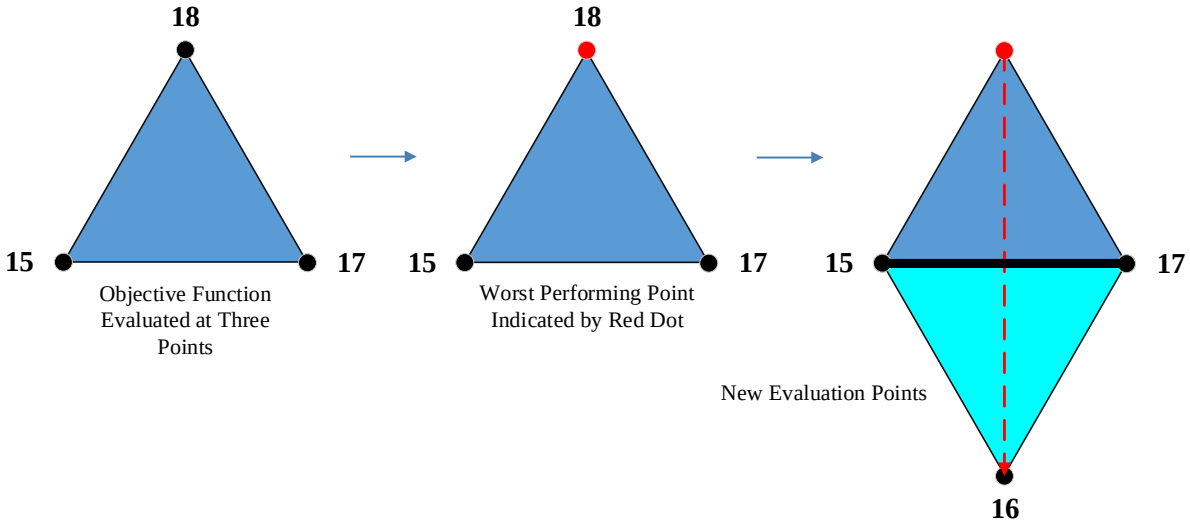

Figure 1.6: Simplex Optimization Initial Steps

A basic example of the nonlinear optimization path an optimization might take is shown in Figure 1.7 [48]. Each of the three points of a triangle represents an evaluation of the objective function. The mock values for the objective function are shown beside the points of each triangle. The point with the worst performance is then reflected with respect to the other two points. The axis of rotation is shown in black in Figure 1.7. The points are again compared and an appropriate reflection is executed. This continues until convergence is reached. The nonlinear path the optimization takes is demonstrated by the red arrows in Figure 1.7. Additional techniques to attempt to speed up the convergence such as skewing the reflection to take a larger step can be added to the algorithm.

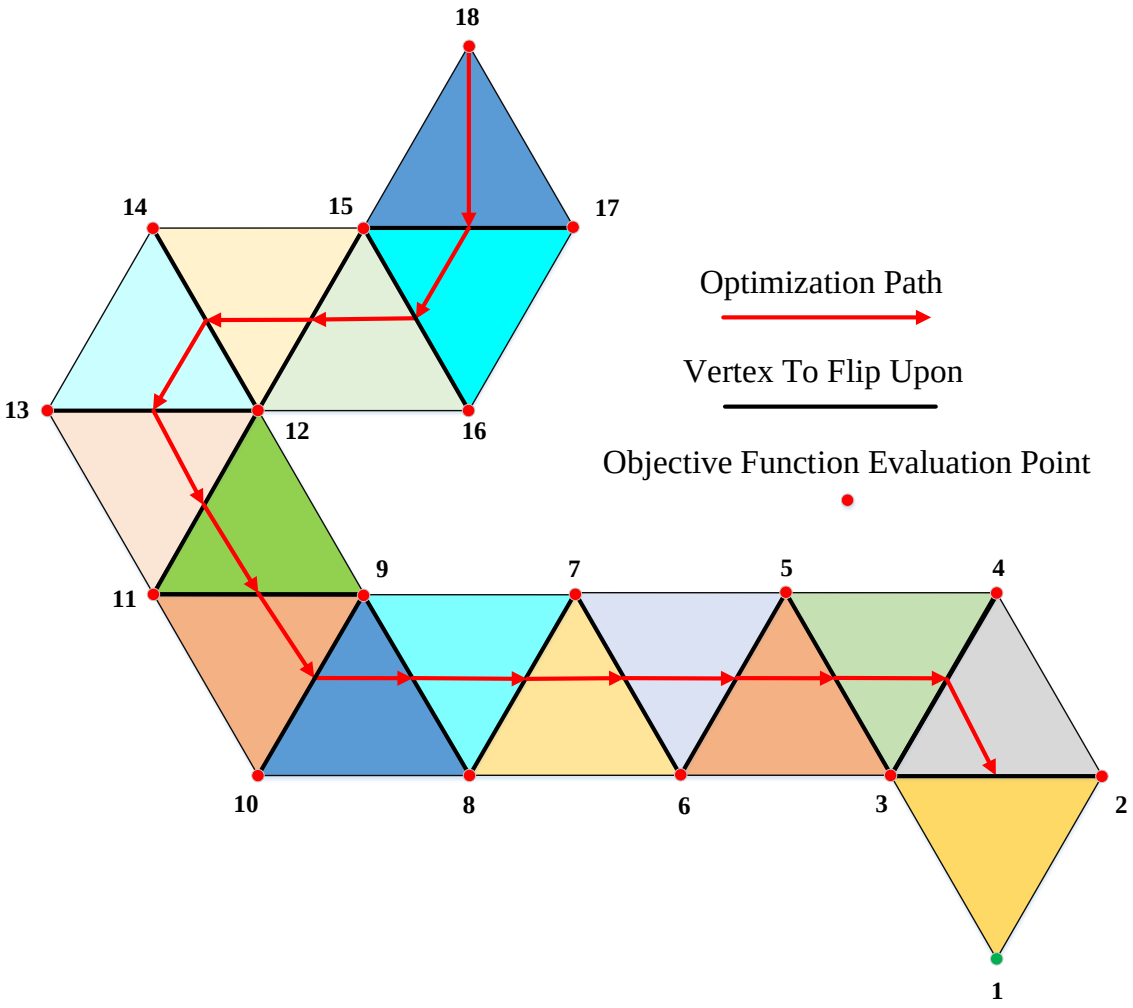

Figure 1.7: Simplex Optimization Variable Path

More generally, the n updated variables of the function in each loop of the simplex optimization are chosen by taking a comparison of the function values at $n+1$ points, and the vertex with the largest value is reflected upon itself and the new variable values are found and used in the next iteration.

Some of the recent research works for HVDC controller (to minimize switching losses) have shown that the simplex optimization process is best suited for functions with less than 10 variables [47]. Simplex optimization is computationally efficient and compact, keeping no information other than the results of the previous run. This nonlinear optimization process

works efficiently guiding the objective function towards a minimum [49].

Simplex optimization is more efficient than some conventional multi-run optimization routines such as Monte-Carlo simulation, which uses an exhaustive search to find an optimum point. Monte-Carlo optimization uses a random distribution of input variables, and as such accuracy of the optimization can only be assured if a nearly exhaustive search of the input range is performed. The simplex optimization has been found to require orders of magnitude less simulation runs than conventional methods, with higher levels of accuracy [50] Gole et al. have worked on developing an optimization process using the simplex algorithm tailored to HVDC design, this field is considerably different than the SSCI issues focused on in this thesis.

1.6 Objective of the Thesis

The main objective of this thesis is to:

1. Develop a method to damp the SSCI's that can develop on radially connected wind farms that are series compensated.
2. Develop a EMT simulation of the system model using PSCAD that demonstrates SSCI issues similar to the Zorillo wind farm when series compensation is added to the transmission line.
3. Investigate the frequency components within the oscillations that occur as stability is lost with the existence of series compensation.
4. Develop the multi-band damping controller to eliminate this instability.
5. Study the impact of the addition of the multi-mass rotor model to the system and modify the control system as necessary to maintain stability.
6. Optimize the MBSSDC for both the single mass and multi-mass rotor model systems using a nonlinear time domain simplex optimization approach.

1.7 Organization of the Thesis

This thesis is split into five chapters:

Chapter 1: Renewable Energy and the Power System

Chapter 2: Multi-Band Sub-Synchronous Damping Control with Single Mass Rotor Model

Chapter 3: Multi-Band Sub-Synchronous Damping Control with Multi-Mass Rotor Model

Chapter 4: Simplex Optimization of the MBSSDC

Chapter 5: Thesis Summary and Conclusions

Chapter 1 gives some background information on the current state of wind generation in North America and worldwide, discussing the growth rate and some challenges with the integration of this power into the grid. Three types of sub-synchronous oscillations that can affect power systems are discussed, with the main focus on sub-synchronous control interactions and their effects on type III DFIG wind generators. The use of series compensation on transmission lines is touched upon in relation to long radially connected systems. Specifications of the model system are covered followed by a literature review showing various techniques regarding sub-synchronous control interactions and wind generators.

Chapter 2 introduces the wind generation system used as the system model and discusses Type III Doubly Fed Induction Generators and their use in wind generation systems. A few comments on the concept of stability precede the introduction of the MBSSDC. The single mass rotor model system is shown operating under normal conditions showing stability, followed by some incidents to demonstrate the instability it can experience under certain conditions. Analysis of the instability that occurs leads into the development and design of the MBSSDC. Extensive testing results show the impact of the MBSSDC on the model system.

Chapter 3 focuses on the addition of a multi-mass rotor model to the generators in the system used in the previous chapter, with testing and verification of its operation. The con-

cept of the multi-mass rotor model will be discussed along with the details of implementing the multi-mass rotor model inside the system model. Development of the controller, and testing results will be shown in detail. A comparison of the results of the MBSSDC on the single mass and multi-mass rotor models is shown.

Chapter 4 details the Simplex optimization of the MBSSDC. The optimization is run on both the single mass and multi-mass system models using the 8 time constants in the lead-lag blocks of each damping band. The results from the testing of both systems responses to various levels of compensation and line faults is shown.

Chapter 5 summarizes the thesis, covering the research done and highlighting the results. Following the summary is a list of the contributions of the thesis, and some suggestions for future work conclude the document.

Chapter 2

Multi-Band Sub-Synchronous Damping Control with Single Mass Rotor Model

2.1 Introduction

This chapter will focus on the wind generation system used as the system model and will cover Type III Doubly Fed Induction Generators and their use in wind generation systems. The introduction of the Multi-Band Sub-Synchronous Damping Controller (MBSSDC) construct will follow a brief discussion of the concept of stability.

Testing of the single mass rotor model system to demonstrate the instability it can experience under certain conditions will be shown. Analysis of the instability that occurs will be shown.

The concept of the MBSSDC will be shown and the development of the controller will be documented in detail, showing the testing results of individual bands of the MBSSDC and the results obtained from the testing of the MBSSDC as a whole.

2.2 Induction Wind Generators

There are four main types of induction generators in use in the power industry, the Type I squirrel cage generator, the Type II wound rotor induction generator, the Type III doubly fed induction generator and the Type IV full converter induction generator. These are shown in Figure 2.1

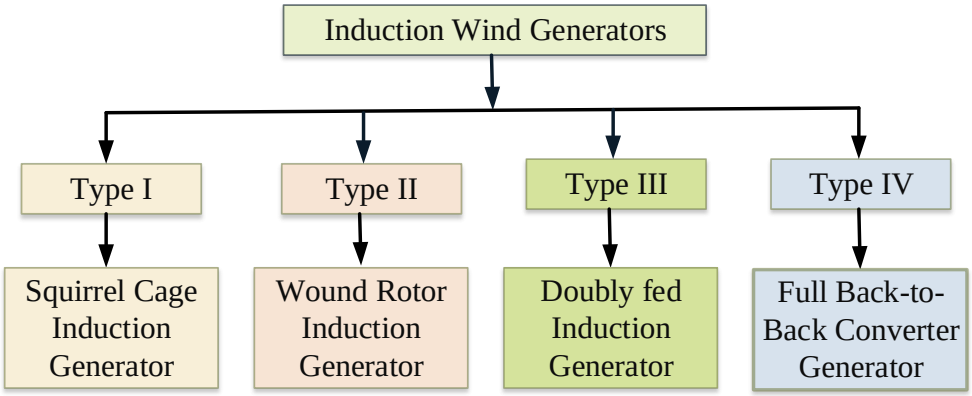

Figure 2.1: Common Wind Generator Types

The Type III generator is the most commonly used induction generator used in wind turbines at this time [18] [11]. The Type IV full converter turbine is shown to be gaining some popularity, perhaps due to the extremely wide range of wind speed it can operate in and the decreasing cost of the power electronics required for it. The Type I and Type II induction generators have been steadily declining in popularity, perhaps due to the limited operating range they possess. Figure 2.2 shows the trends the four types of induction generators have been following over the past 15 years [18].

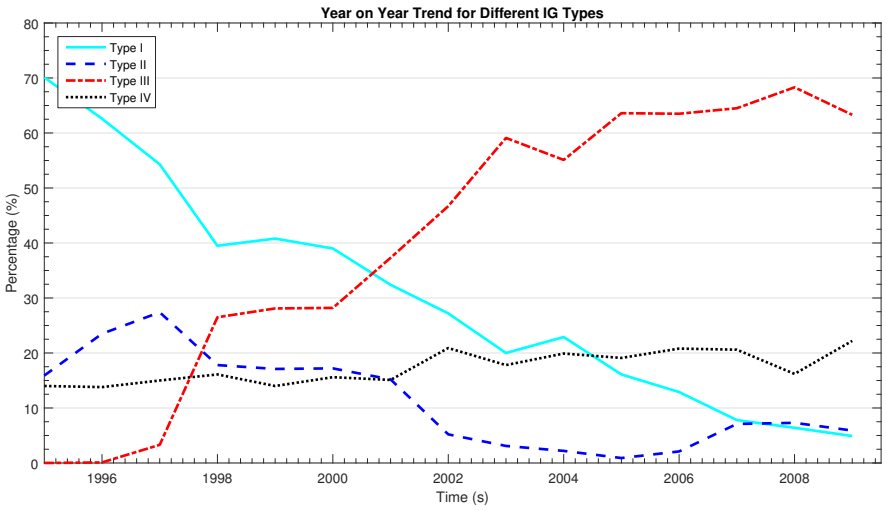

Figure 2.2: Induction Generator Type Market Penetration

Types I, II, and IV will be briefly covered here, while the Type III DFIG which is the focus of this research will be covered in more detail in the next Section.

2.2.1 Type I Induction Generators

Type I induction generators, also known as squirrel cage induction generators (SCIG) are the simplest (yet robust) type of induction generator. They are designed to be used at a constant speed, meaning that there is some inefficiencies created as the wind speed fluctuates.

As the wind speed changes the electrical power and mechanical torque on the generator also varies. Control of the pitch angle on the blades is used to regulate the speed of the turbine shaft to its designated value [19]. A diagram of a Type I induction generator is shown in Figure 2.3.

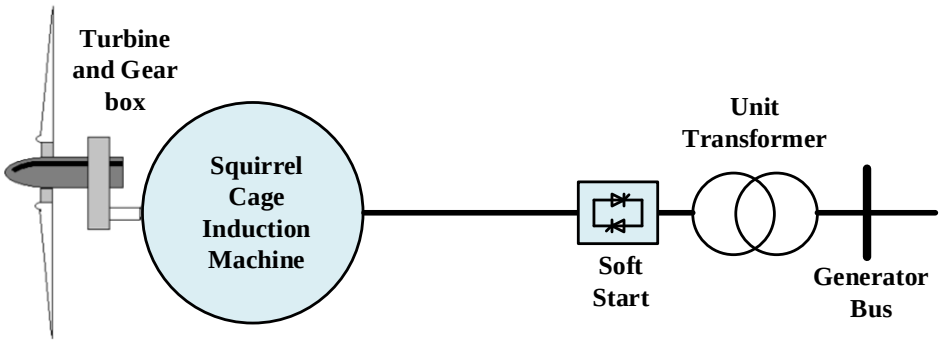

Figure 2.3: Type I Induction Generator

2.2.2 Type II Induction Generators

The Type II induction generator is also known as the wound rotor induction generator (WRIG), which allows better extraction of power from the wind than the previously mentioned Type I generator. This type of machine features a wound rotor winding, access to these windings is made through a slip-ring.

In addition to using pitch control similar to the Type I generators, they are also able to

use rotor resistance speed control to allow more efficient extraction of wind power at speeds over the machines rated speed. Rotor resistance speed control uses an external resistance connected to the rotor windings to allow some limited speed control. The range of slip the WRIG can operate at is around 10% [19] [18]. The external rotor resistance represents a non-trivial power loss when in use. A diagram of a typical Type II induction generator is shown in Figure 2.4.

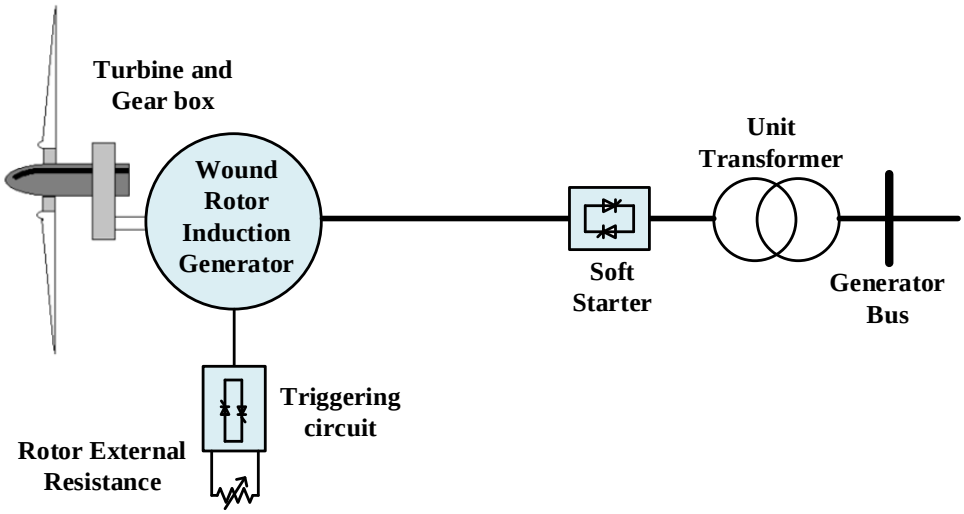

Figure 2.4: Type II Induction Generator

2.2.3 Type IV Generators

The Type IV induction generator is commonly known as a full converter induction generator, although a synchronous generator may be used in place of the induction generator. The generator is connected to the grid through a back-to-back converter that is rated for the full power of the generator, effectively isolating the grid and the generator from each other, therefore allowing the generator to run at any speed, potentially eliminating the need for a gear box as well [18]. Type IV IG's are the most costly due to this converted capable of carrying the rated power of the machine [19]. A diagram showing a typical Type IV induction generator is shown below in Figure 2.5.

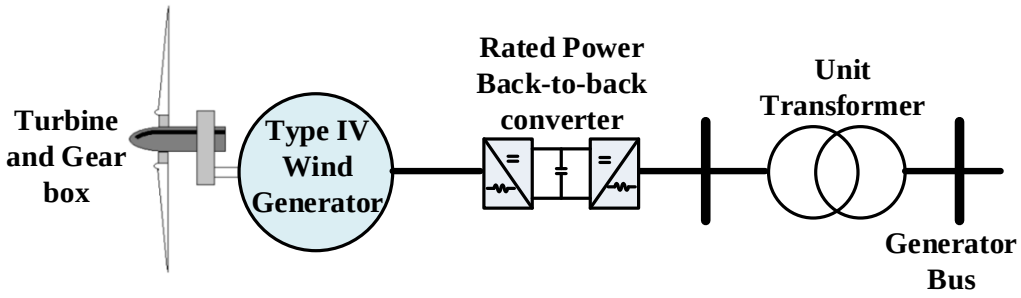

Figure 2.5: Type IV Induction Generator

2.3 Type III Doubly Fed Induction Generators

A high level view of a typical Type III DFIG wind system appears in Figure 2.6. The system consists of four main parts: wind turbine, induction generator, excitation control, and grid connection. The DFIG has two electrical connections, one through to the back-to-back converter to the rotor via slip-rings, and one directly to the stator windings, thus the 'doubly fed' moniker.

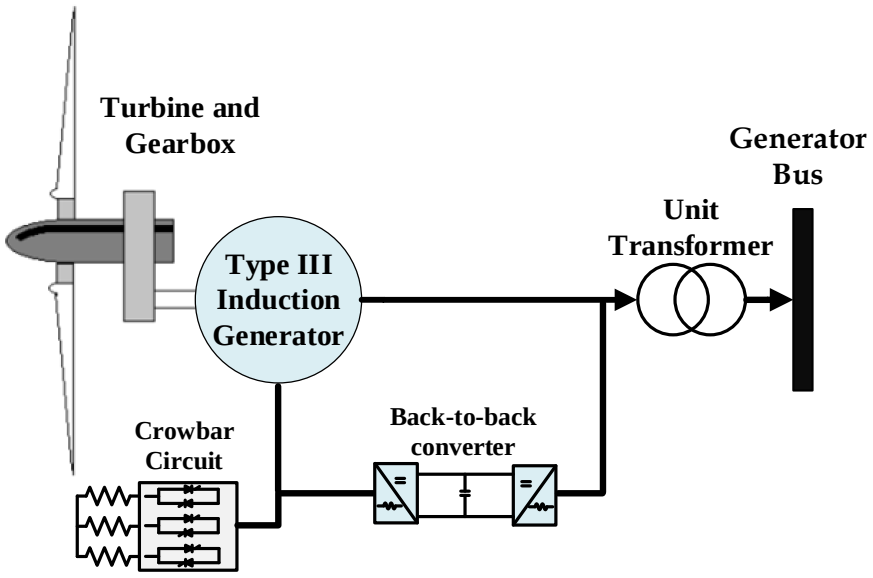

Figure 2.6: High level view of a Type III DFIG

The Type III generator is the most commonly used generator in the market due to the low-cost solution for the capture of wind power at variable wind speeds that it provides [11] [18]. The output power of a DFIG is proportional to the cube of the wind speed as shown in Equation 2.1 [51]. As the wind varies, the excitation of the generator must be altered to maintain operation of the machine at the desired set-point.

$$P_{extractable} = \frac{1}{2}\rho A v^3 C_P \tag{2.1}$$

Where $P_{extractable}$ is the power in the wind in Watts that can be extracted, ρ is the density of the air in $\frac{kg}{m^3}$, A is the swept area in m^2, v is the wind speed in $\frac{m}{s}$, and C_P is the turbine power coefficient.

The DFIG consists of a wound rotor induction machine that has the stator windings fed directly from the three phase voltage supply, while the rotor windings are fed through a back-to-back converter that is powered by the grid side connection feeding the stator. The back-to-back converter rectifies the grid voltage and uses an inverter to feed the rotor windings with a variable frequency AC voltage [19].

In comparison with the Type II WRIG which has its rotor windings excited by the same supply as the stator windings, the Type III DFIG has the rotor windings excited independently of the stator windings which allows for a large range of, up to around 30% which thus implies that the back-to-back converter must be rated for 30% of the machines rated power [19] [52]. While the DFIG is more complex than the SCIG, or the WRIG and thus more expensive, the DFIG offers some distinct advantages over its simpler counterparts [53] [52]:

- Large power extraction capability comparatively.
- Large range of rotor speeds allowed, increasing generation possibilities.
- Power factor adjustment through control of both real and reactive power.
- Smaller cost for back-to-back converter (compared to Type IV induction generator) due to converter only passing approximately $\frac{1}{4}$ to $\frac{1}{3}$ of the rated power.

- Mechanical stress on the turbine is reduced as the energy is stored in the inertia of the turbine reducing mechanical oscillations. Note: this is also true to some extent with WRIG, although the range of operation is much narrower for the WRIG.

DFIG's are designed to vary the excitation of the machine such that the excitation of the rotor is altered to allow the magnetic field within the machine to rotate at the machines synchronous speed [19]. To vary the excitation of the DFIG, a control system that independently alters the active and reactive output power through rotor winding governs these generators. When the system output varies from the set points for either the real or reactive power an error signal is generated which causes the control system to alter the generators excitation.

When the control system detects power or speed deviations, the control system alters the excitation of the generator to damp out the disturbance and attempt to bring the error signal back to zero; to put it in another manner, to bring the real and/or reactive power back to the steady state values.

The excitation control of the DFIG is facilitated by a series of semiconductor converters, known as a back-to-back converter, that are fed by a shunt transformer which is connected to the transmission line and to the rotor. A back-to-back converter is a power electronics based circuit that is connected to an alternating current (AC) power source rectifying this AC power to a direct current (DC) voltage that charges a capacitor bank. The DC link then feeds an AC inverter to convert the DC back to an AC signal. This back-to-back converter serves to isolate the two AC sources from each other in magnitude and frequency.

The connection to the grid is known as the grid side converter (GSC), while to converter connected to the rotor is referred to as the rotor side converter (RSC). The GSC maintains the voltage at the DC link between the two converters. The RSC controls the rotor voltage frequency and magnitude such that the maximum power can be extracted from the prevailing winds. The RSC also maintains the reactive power needs of the system.

The largest advantage of the back-to-back converter is that it allows the frequency and magnitude of the AC voltage on one side of the converter to be independent of the frequency

and amplitude of the AC voltage on the other side. This independence allows for a great deal of control over the operating conditions of the DFIG.

A high level block diagram of a back-to-back converter appears in Figure 2.7. Through the adjustment of the generator excitation, the back-to-back converter permits the phase angle and the magnitude of the rotor side voltage to be quickly adjusted and allows control over the output of real and reactive power of the generator.

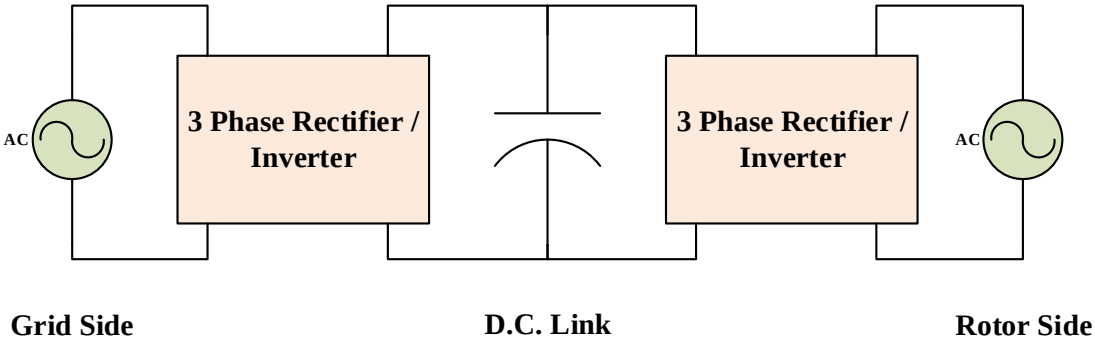

Figure 2.7: Back-to-Back Converter

The converters in the rotor circuit control system provide varying generator flux control facilitating a wide range of turbine speed. The control of the back-to-back converters is generally based on a pulse width modulation (PWM) voltage source converter (VSC) control scheme which allows for precise control of the excitation.

The firing signals of the converters are altered when the control system detects a variation in the speed or power from the set points. This error signal is generated through the comparison of the current operating levels to the desired level, and the difference between the respective levels is the error signal. The excitation is altered in an attempt to eliminate this error and maintain stable operation.

2.4 Stability

Stability as defined in 'Control Systems Engineering 6th Ed.' [54], is the condition which exists when for every bounded input signal, the system output will be stable. A bounded signal is a signal that does not tend towards infinity, having an upper or lower level that it does not exceed. This definition of stability is also referred to as Bounded Input - Bounded Output stability (BIBO).

Another way to characterize a stable system is one whose natural response tends to zero as time tends to infinity. Conversely then, an unstable system has a natural response that tends toward infinity as time tends toward infinity.

The total response of a system to an input signal is defined by the sum of the systems natural and forced response shown in equation 2.2.

$$Total\ Response\ =\ Forced\ Response\ +\ Natural\ Response \tag{2.2}$$

The natural response of the system is the way the system responds to a change in operating conditions and is determined by the time constants of the various components within the system. The natural response is sometimes referred to as the transient response of a system; transient response describes how the system receives or unloads energy. In a stable system the natural response decays to zero as time tends toward the infinite [54] as shown in equation 2.3.

$$\lim_{t\to\infty} f(t) = 0 \tag{2.3}$$

The forced response of a circuit is the systems response to some external force; a voltage source, a chemical reaction, a prime mover, for example. This response is dependent upon some type of input stimuli. The forced response in a stable system is represented by the steady state system conditions.

The total response, consisting of the natural and forced response, for the current in an

RL circuit is shown below in equation 2.4.

$$i(t) = Ae^{\frac{-Rt}{L}} + \frac{V_{forcing}(t)}{|R + jX_L|} \tag{2.4}$$

It is clear that as time tends toward the infinite, the natural response, the $Ae^{\frac{-Rt}{L}}$ portion of the equation, will tend toward zero as R, L, and t must all be positive terms (negative quantities of resistance, inductance, or time do not exist), classifying this response as a decaying exponential. The effect of this decaying exponential term is transient in nature. Figure 2.8-(a) shows the graph of the function e^{-t}, which is a decaying exponential function. Initially the output is at its maximum value, quickly decaying to a negligible value, this is a decaying transient that will have little to no effect on the operation of a system after five time constants have elapsed. This response is representative of a stable system. The forcing function, the $\frac{V_{forcing}(t)}{|R+jX_L|}$ portion of the equation, will thus be the dominant term for a stable system.

In a different situation where the exponential term is not negative, but is positive i.e. Ae^{Kt}, as shown in Figure 2.8-(b) with the function e^{Kt}, the magnitude of the exponential term will increase with time causing the system output to increase until the magnitude is limited by the physical characteristics of the system. This is a growing exponential function. This response is an example of an unstable system.

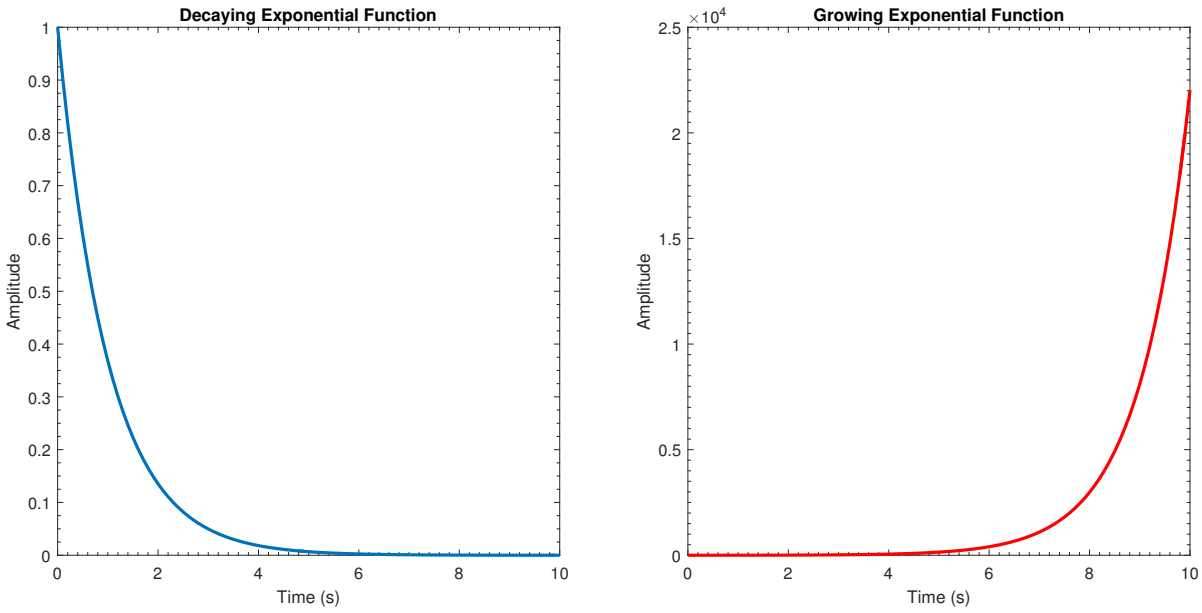

(a) Decaying Exponential Curve

(b) Growing Exponential Curve

Figure 2.8: Decaying and Growing Exponential Functions

The goal of this research is to ensure that when the generation system experiences an event that could trigger oscillations, the multi-band control system damps out this disturbance, ensuring the generation system remains stable.

2.5 Multi-Band Sub-Synchronous Damping Controller Concept

The focus of this thesis is a construct known as the Multi-band Sub-Synchronous Damping Controller (MBSSDC). The MBSSDC, the main contribution of my research, is a supplementary control system with frequency specific band(s) designed to damp out specific oscillations that have lead to system instability, in a Type III DFIG based wind farm.

These bands are placed in parallel with the existing excitation control of a Type III DFIG wind generator in order to remove the instability in the system, instability that can develop when series compensation is inserted on the connecting transmission line.

The MBSSDC works by using the supplementary control system to alter the excitation of the DFIG, damping out the oscillations encountered during an SSCI event, and allowing system stability to be maintained. A high level view of the MBSSDC concept is shown in Figure 2.9.

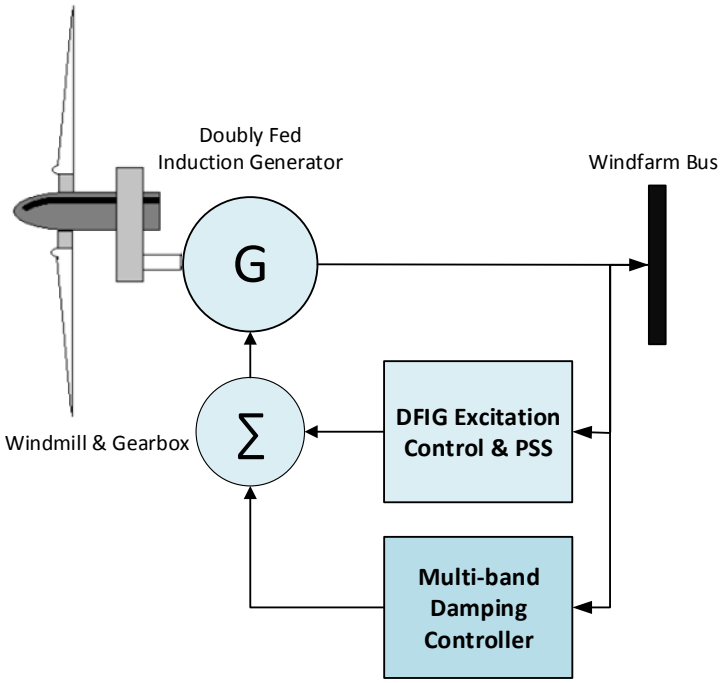

Figure 2.9: Multi-Band Sub-Synchronous Damping Controller

The diagram is the same as seen in Figure 2.6 aside from the addition of the supplementary control loop which is summed with the existing excitation control. The frequency of the supplementary control band(s) of the MBSSDC is determined through a frequency analysis of the system which will be described in Section 2.8.2.

The MBSSDC solution is a control system level scheme that alters the generator excitation signal in response to the oscillations that can develop as series compensation is attached to the system. As the MBSSDC is a control level construct, the MBSSDC has a much lower power level than the generator which it is exciting produces. This has the effect of lowering the cost of components used as a result of their lower power rating. This is a compelling

feature when compared with the some of the possible solutions discussed in the literature review (Section 1.5).

The MBSSDC is a supplemental control loop placed in parallel with the existing control system. As a shunt loop, there is no new element placed in series with the existing control system.

2.6 Model Wind-Farm and SSCI Issues Encountered

A discussion of the model wind-farm and its operation will precede an in-depth consideration of the design and results of the MBSSDC. The wind-farm model will be used to demonstrate the SSCI issues that Type III DFIG installations can experience; the model will serve as a benchmark by which to judge the success of the MBSSDC concept.

Electromagnetic Transient programs (EMT, or EMTP) are a type of program that solves the short term behaviour of a power system. Time domain differential equations are solved using numerical methods as the program executes. EMT programs solve the system in small time steps for great detail and accuracy in the model and as such are computationally intensive. EMT programs primarily use the trapezoid method for solving the differential equations as it will function properly even with larger time steps in the simulation, some other methods will fail if a time step is too large [55].

The wind-farm is modeled using the PSCAD/EMTDC software package. PSCAD/EMTDC is a graphical electro-magnetic transient (EMT) simulation program developed by the Manitoba HVDC research center. This tool allows complete simulation of electric power systems. Models for common power system and control level devices are provided, and users are able to design custom device models as necessary [56].

2.6.1 Model Wind-Farm

An over-view of the wind-farm model developed in PSCAD/EMTDC appears in Figure 2.10. The wind-farm connecting to the generator bus is shown as a lumped mass, representing 150-3 MW Type III DFIG machines. Each turbine is rated at 0.69 kV and is connected to 3.4 MVA 0.69:33 kV unit transformer. The values of the generator constants can be found in appendix A. The system is then connected to the generator bus through a 600 MVA station transformer. The generator bus is then connected to a 240 km (150 mile) transmission line that has a series capacitor placed inline with it. This transmission line is then connected to the 'infinite bus' at the receiving end.

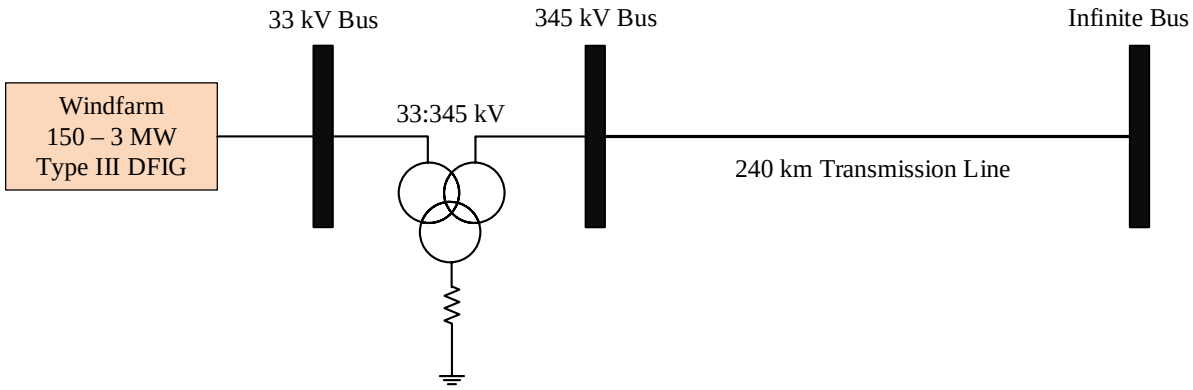

Figure 2.10: Model Wind-Farm

The value of the series capacitor can be varied within the PSCAD/EMTDC model to provide any desired level of compensation. The capacitance is normally shorted out by a breaker that is opened up to insert the capacitor in series with the transmission line after the system has reached steady state and series compensation of the transmission line is desired.

The far end of the transmission line, the receiving end, is connected to a voltage source with a large damping angle (85^o), which is used to represent the 'infinite bus'. This stiff voltage source simulating the 'infinite bus' models the population centers which would ultimately receive the power generated by the wind-farm.

A lower-level view of the generators appears in Figure 2.11, as does the station transformer connecting the generators to the generator bus. Also of note is the placement of a controllable fault on the 345 kV bus. This fault allows any type of line fault (3 phase, line to line, line to line to ground, single line to ground) to be applied to the system directly after the transformer bus.

The duration of the fault is adjustable as well; the fault duration was set to 200 ms for all the fault testing done with the MBSSDC. This number was chosen based on the assumption that after 200 ms had elapsed either the fault would be somehow cleared or the protection would be tripped. Older style mechanical relays would still be expected to trip within this time-frame.

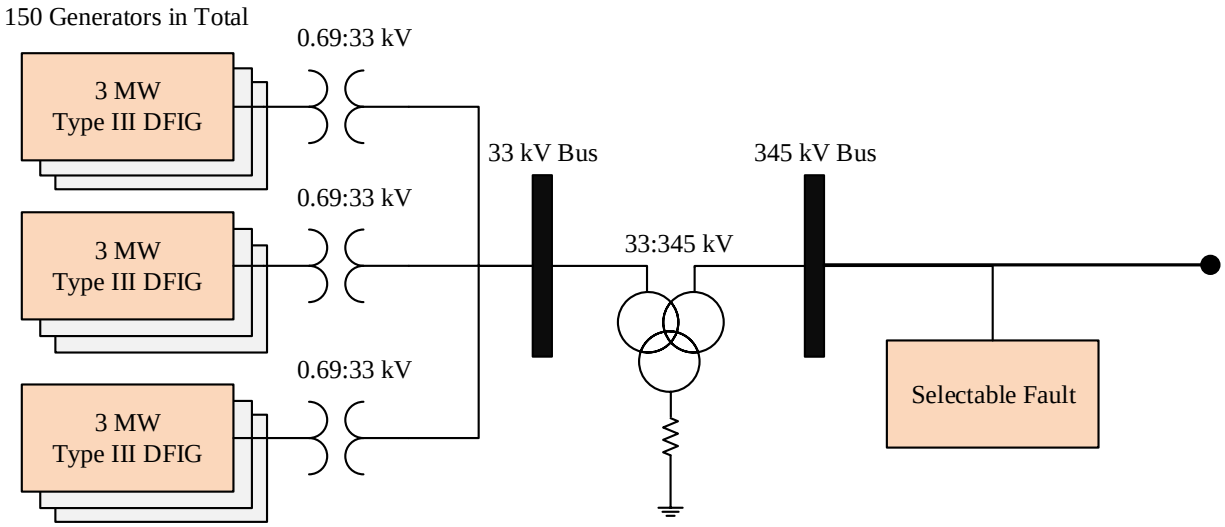

Figure 2.11: Wind-Farm Generators

The generator main control loop appears in Figure 2.12. This is the direct-quadrature-zero (dq0) control loop. The MBSSDC will be place inside the dq0 control loop of the generator excitation control.

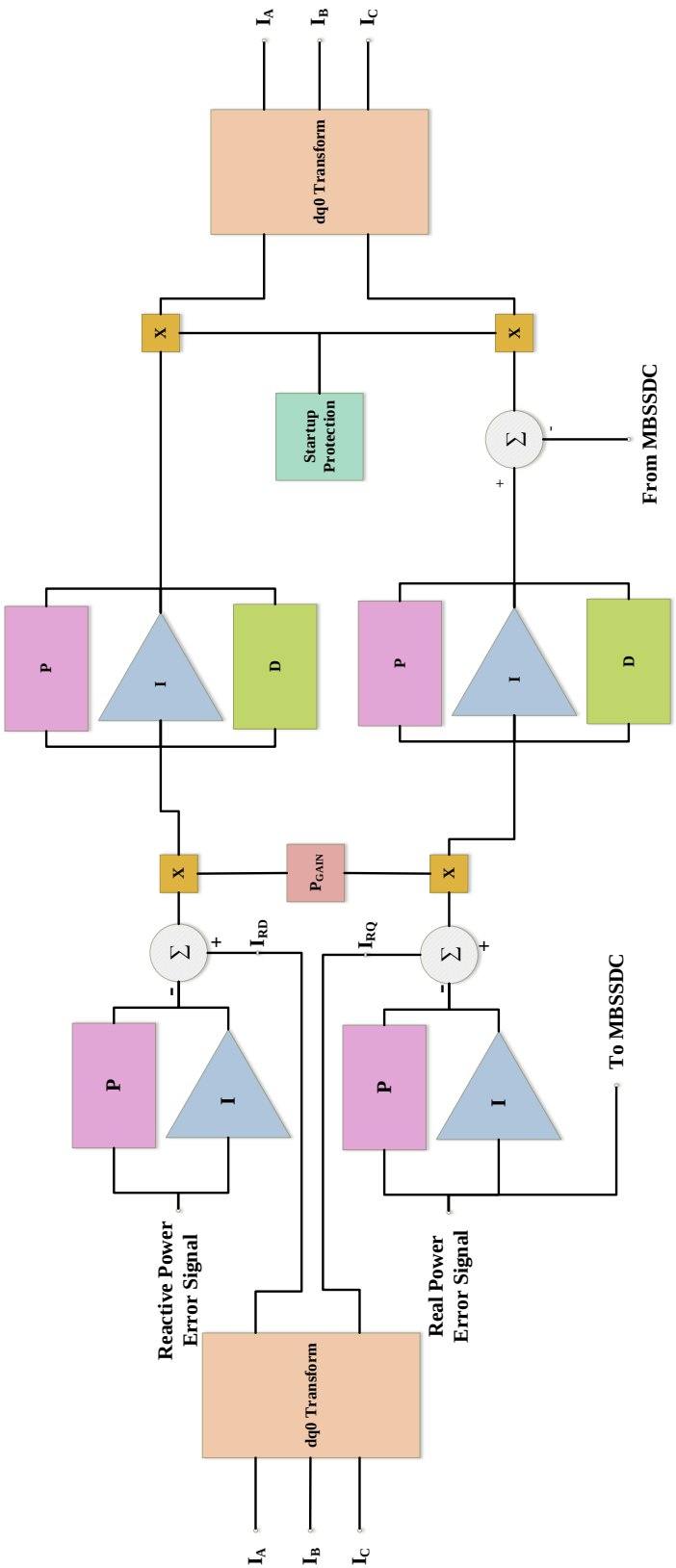

Figure 2.12: Generator Control Loop

The dq0 transformation is a standard method of modeling machine behavior by converting 3 phase AC signals into three DC quantities. This transformation is also known as the Park transform, and as the Blondel two-reaction method based off the work of Andre Blondel. The Park transforms facilitates the ease of manipulations and calculations in the control loop, compared to working with three phase AC phasors. The transformed quantities effectively rotate with the rotor and as such are presented with a constant magnetic path [57].

Additionally if the three phase system is balanced the 0 signal is zero, simplifying the control further. The dq0 method of control is used extensively in the control of three phase electric machines. The transform allows the control of AC power by DC control circuits through alteration of the d and q quantities. The method to convert three phase AC signals to dq0 is shown in the equation below.

$$\begin{bmatrix} i_d \\ i_q \\ i_0 \end{bmatrix} = \sqrt{\frac{2}{3}} \begin{bmatrix} \cos(\theta) & \cos(\theta - \frac{2}{3}\pi) & \cos(\theta + \frac{2}{3}\pi) \\ \sin(\theta) & \sin(\theta - \frac{2}{3}\pi) & \sin(\theta + \frac{2}{3}\pi) \\ \frac{1}{\sqrt{2}} & \frac{1}{\sqrt{2}} & \frac{1}{\sqrt{2}} \end{bmatrix} \begin{bmatrix} I_a \\ I_b \\ I_c \end{bmatrix} \tag{2.5}$$

Where i_d, i_q, and i_0 are the currents in the dq0 section, I_a, I_b, and I_c are the three phase currents and θ is the angular displacement of the Park reference frame.

Running the wind-farm simulation shows that the system is stable in normal operation provided that the connecting transmission line does not have any series compensation inserted. The system start-up transients within the EMT program are shown, followed by the steady state output power of the base wind-farm model running with no series compensation is seen in Figure 2.13.

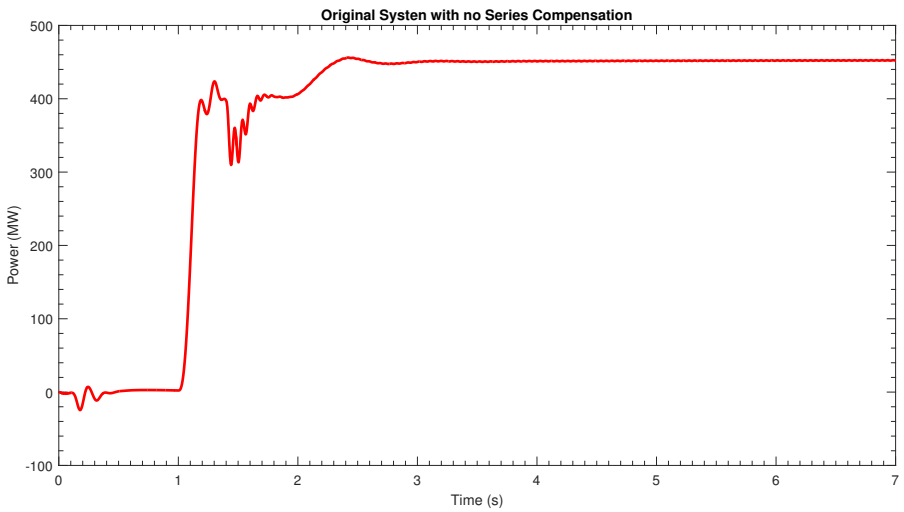

Figure 2.13: Base Wind-Farm Operation Without Series Compensation

Figure 2.13 demonstrates that the model system is stable and is delivering its rated output to the transmission line. The initial oscillations are the start-up transients, and steady state operation is commenced around three seconds. The aggregrated wind farm model is used and it is assumed that all turbine are seeing the same wind [16].

Numerous faults were applied to the generator bus at seven seconds for a 200 ms duration after the model was running at its steady state operation. A three phase fault, a line-to-line fault, a double line to ground, and a single line to ground fault were all simulated. The response of the base wind-farm model running with no series compensation connected in the line to these faults is seen in Figure 2.14.

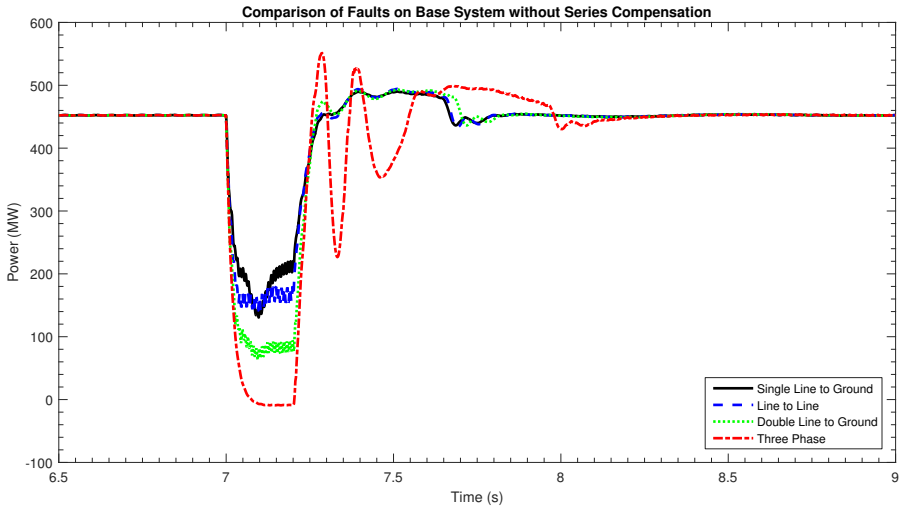

Figure 2.14: Base Wind-Farm Operation Response to Faults

Figure 2.14 shows the base-wind-farm riding through the 4 different 200 ms faults that were applied and returning to normal system operation in less than one second. It is evident that the response of the system to the faults is somewhat dependent upon the type of fault occurring but the response is generally similar for all cases. The base wind-farm maintained stability in all four fault events.

The connection of 3% compensation to the system at the time of 5 seconds demonstrated that the system was still stable with very small amounts of compensation. The output waveform showing the results of the addition of 0%, 3% is shown in Figure 2.15. An excahnge of energy between the windfarm and the transmission system is shown by the oscillations. The system was stable up to a 3% compensation level, although the limits of stability for the base system are evidently approaching.

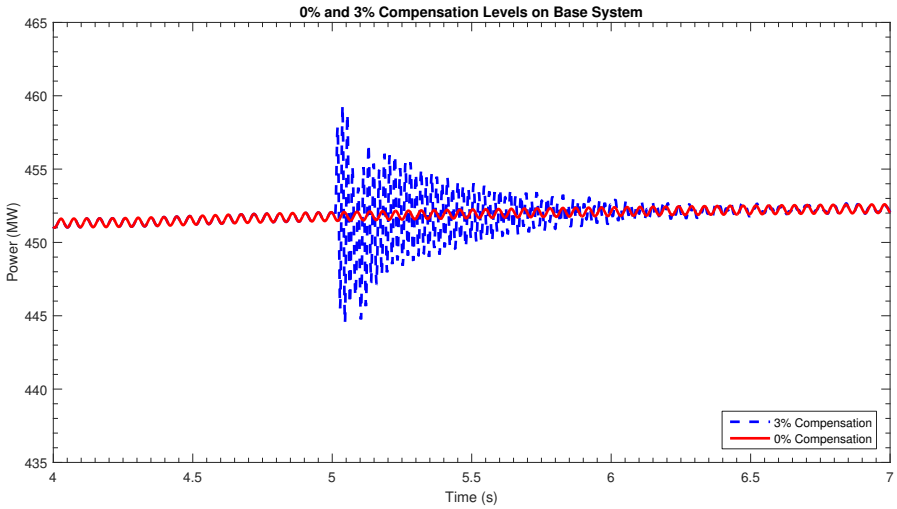

Figure 2.15: Base Wind-Farm Operation with 3% Series Compensation

Fault testing was performed with 3% series compensation attached and the system was able to maintain stability through the same 4 fault situations as the model system; the faults were again 200 ms in duration. Figure 2.16 shows the response of the wind farm to these events.

The addition of larger values of series compensation resulted in the system losing stability. This system instability is discussed in the next Section 2.7.

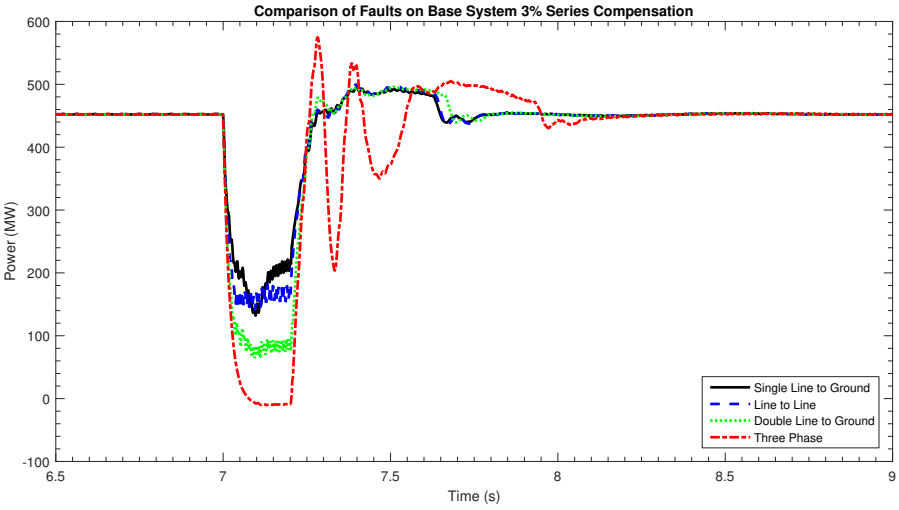

Figure 2.16: Base Wind-Farm Operation with 3% Series Compensation Fault Response

2.7 Instability From the Addition of Series Compensation

The addition of series compensation to the model wind-farm triggers system instability. Compensation levels of 5% are able to trigger oscillations in the output power of the wind-farm as shown in Figure 2.17. These oscillations show the windfarm has lost stability and would have to be tripped from the system or risk damaging the turbines.

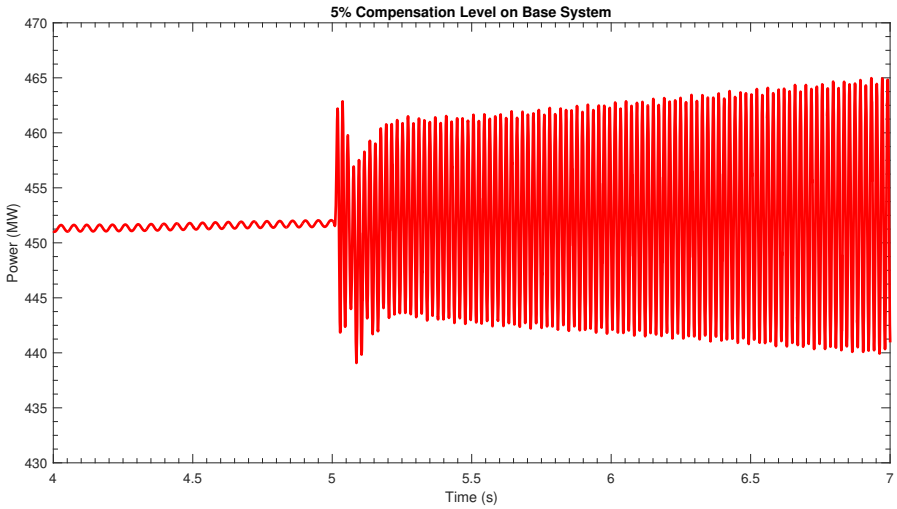

Figure 2.17: Base Wind-Farm Operation with 5% Series Compensation

The series compensated radial transmission line and the DFIG control system interact in a manner that quickly generates large oscillations in the output power and voltage. Clearly the system cannot be run in a safe manner with these oscillations present.

2.7.1 SSCI Issues

Figure 2.18 shows the response of the model wind-farm to the insertion of 8% series compensation in the line at a time of five seconds. Prior to the five second mark, the system was running in a stable fashion. Once the compensation is inserted in the line, an SSCI event is triggered and the oscillations begin immediately and grow to dangerous levels. Figure 2.19 shows the magnitude of the output voltage (line to line) of the wind-farm during this same

event. A detailed analysis of the frequencies within the oscillations is performed in Section 2.8.3.

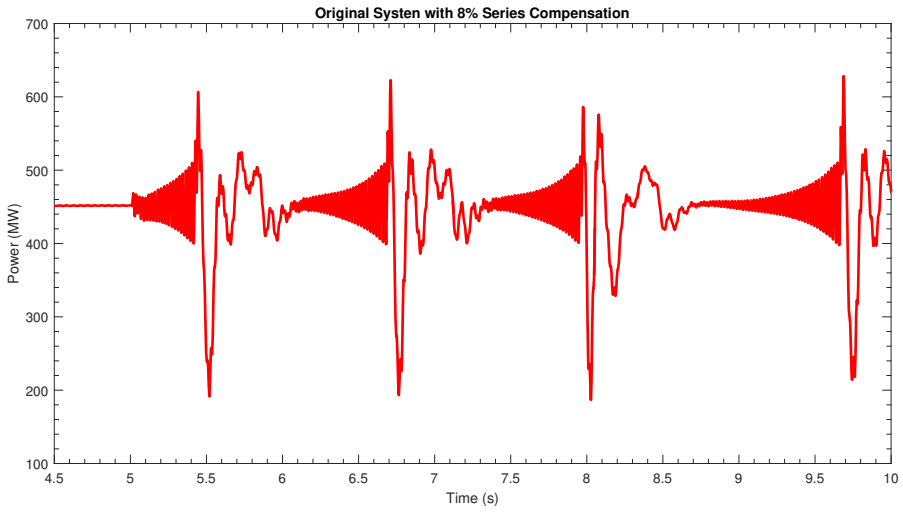

Figure 2.18: Base Wind-farm Output Power Response to Application of 8% Compensation

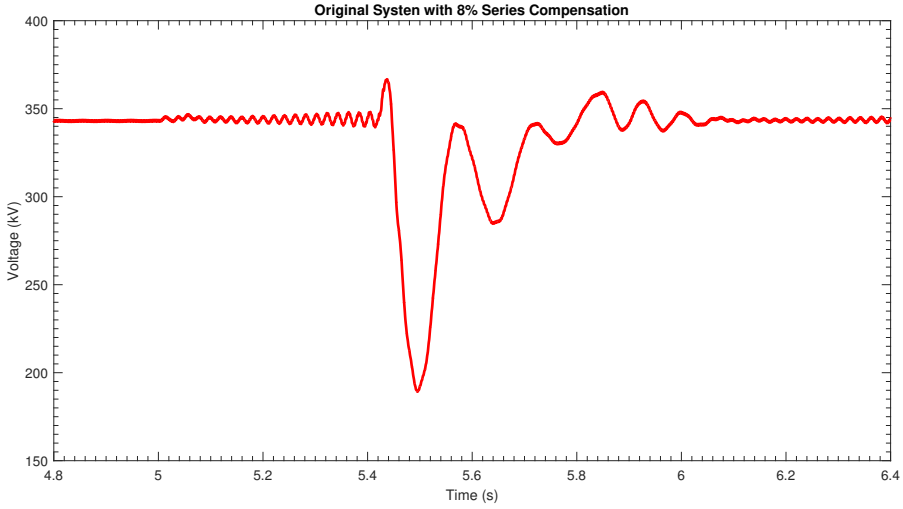

Figure 2.19: Base Wind-farm Output Voltage Response to Application of 8% Compensation

A feature of note in Figure 2.18 is the two sections of the output power oscillation: a higher frequency sinusoid that is growing in the initial section, followed by a larger magnitude but lower frequency component. These two sections proceed to repeat in a periodic fashion as the oscillations continue. A tighter view of these two sections in the oscillation is shown in 2.20.

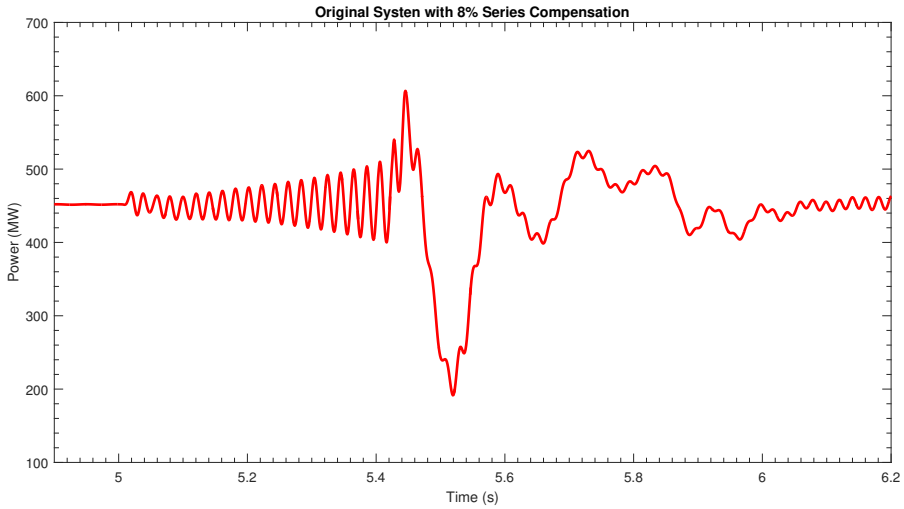

Figure 2.20: Closer View of Base Wind-farm Output Power Response to Application of 8% Compensation

Figure 2.21 shows the response of the model wind-farm to the insertion of 50% series compensation in the line at a time of five seconds. The oscillations begin immediately and quickly exceed levels that can damage the associated equipment.

Figure 2.22 shows the magnitude of the output voltage (line to line) of the wind-farm during this same 50% compensation event. The piece-wise appearance of Figure 2.18 is not nearly as evident in the Figure 2.21.

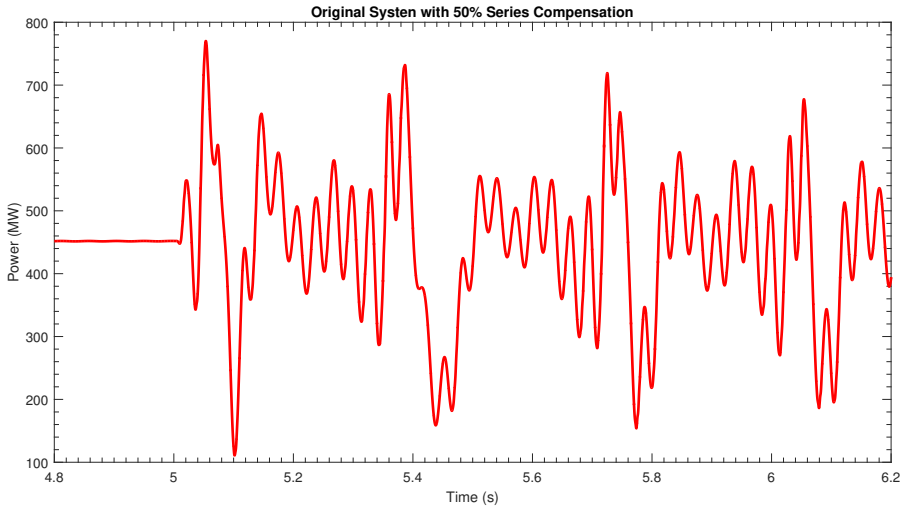

Figure 2.21: Base Wind-farm Output Power Response to Application of 50% Compensation

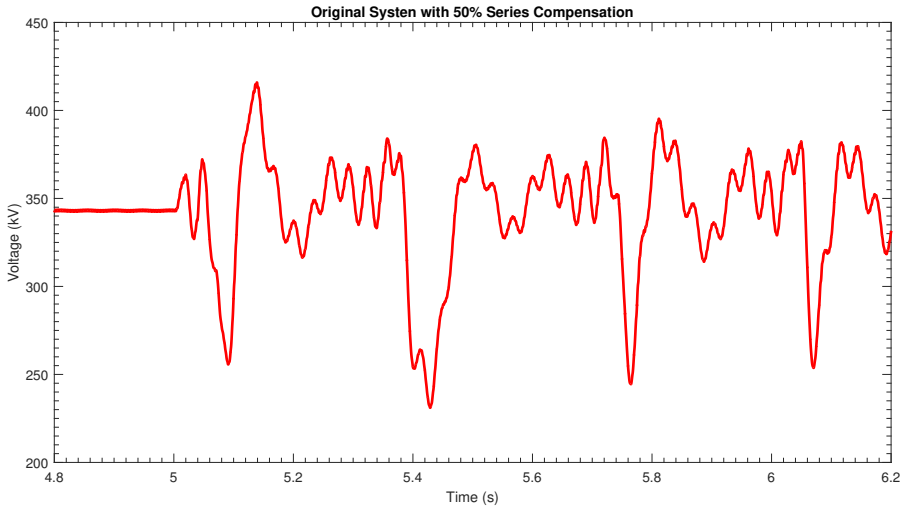

Figure 2.22: Base Wind-farm Output Voltage Response to Application of 50% Compensation

Figure 2.23 shows the response of the model wind-farm to the insertion of 80% series compensation in the line at a time of five seconds. The oscillations begin immediately and quickly reach dangerous levels. Figure 2.24 shows the magnitude of the output voltage (line to line) of the wind-farm during this same event. As with the 50% compensation event shown in Figure 2.21, the piece-wise appearance of Figure 2.18 is not nearly as evident during the 80% compensation event shown in Figure 2.23.

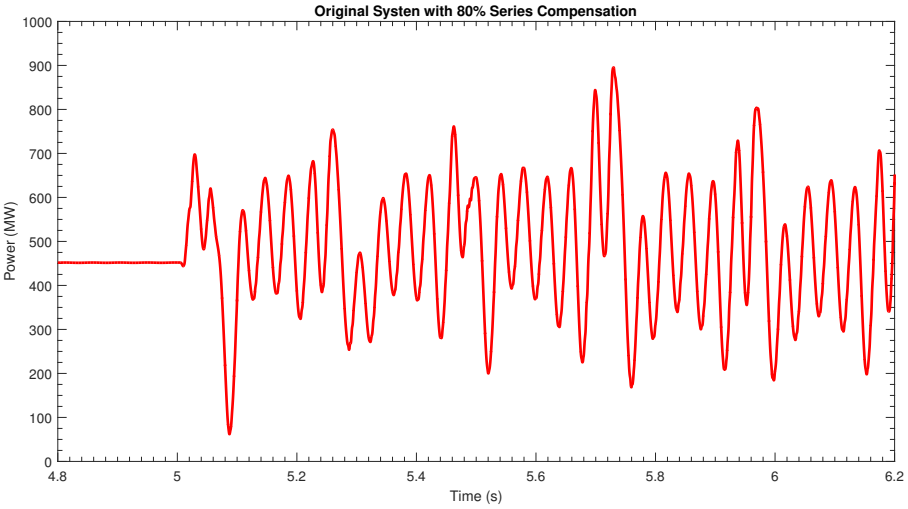

Figure 2.23: Base Wind-farm Output Power Response to Application of 80% Compensation

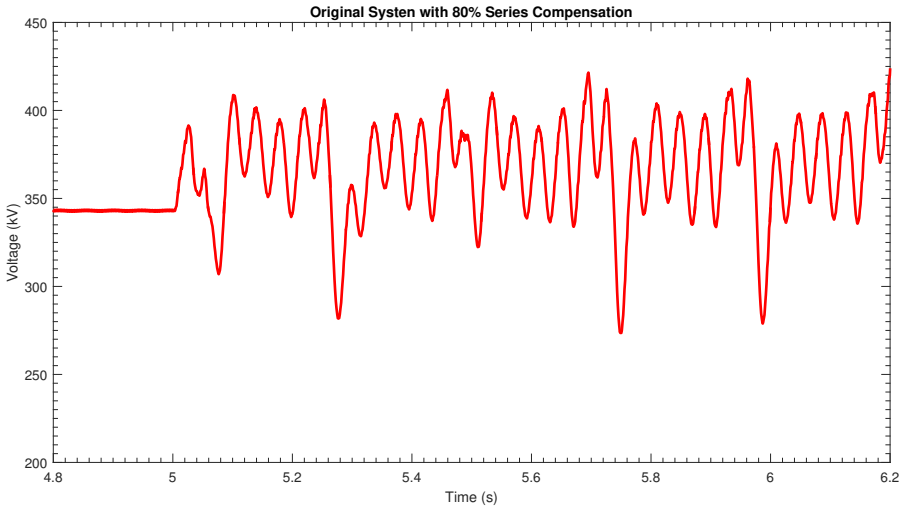

Figure 2.24: Base Wind-farm Output Voltage Response to Application of 80% Compensation

Overlaying the three power output wave-forms for the three different series compensation events, it becomes evident that the frequencies of oscillation within these wave-forms are different from each other. This difference is shown in Figure 2.25.

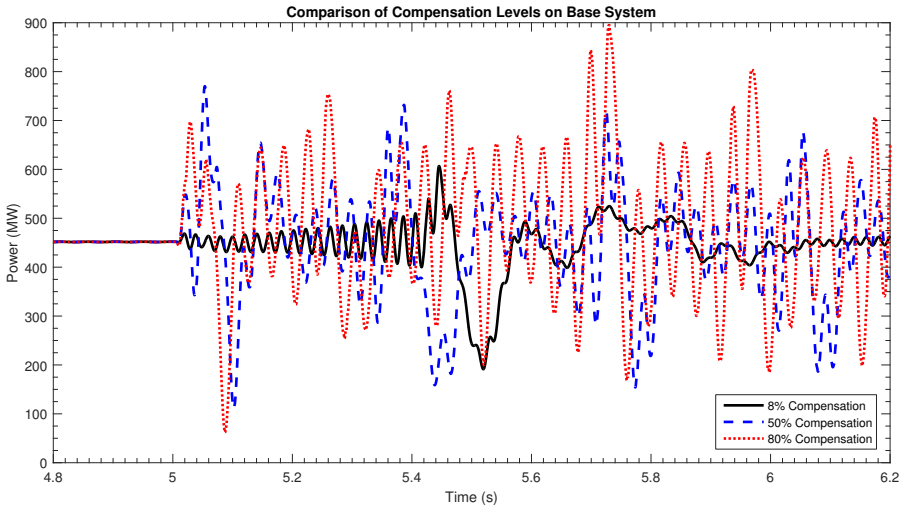

Figure 2.25: Base Wind-farm Response to Application of Various Levels of Compensation

It is evident from the graph overlaying the three power output wave-forms for 8%, 50%, and 80% compensation, that the frequency content of the oscillations are changing as the level of compensation changes. Only the level of series compensation was changed to develop Figures 2.18, 2.21, and 2.23; the rest of the system was identical in all three cases. Section

2.8.3 discusses the analysis and spectral content of the oscillations.

2.7.1.1 Instability During Faults

Stability testing of the series compensated model wind-farm during faults was not undertaken for compensation levels of more than 3%. The system was not stable at those levels of series compensation as shown in Figures 2.18, 2.21, and 2.23, and as such fault testing would be meaningless.

2.8 Multi-Band Sub-Synchronous Damping Controller Design

The problem of multiple sub-synchronous oscillations was discussed by Grondin et al [58] in relation to the very low frequency oscillations Hydro-Quebec experienced with their hydro generators connected to long transmission lines.

The Hydro-Quebec problem discussed in [58] represents a different problem than the SSCI events this thesis attempts to eliminate, but does provide some insight into solving the problem of multiple sub-synchronous oscillation frequencies on a long transmission line. The generation equipment used by Hydro-Quebec was a conventional hydro-power generation system, much different than the power electronics based type III DFIG system being modeled in this research.

The oscillations experienced by Hydro-Quebec were in three different ranges, 0.05 Hz, 0.2 - 1 Hz, and 1 - 4 Hz. A cursory analysis of the oscillations experienced by the model wind-farm shows that the oscillation frequencies are significantly higher than the Hydro-Quebec issues. SSCI issues cover a much broader spectrum of frequencies than the relatively tight range of frequencies (4 Hz) in the Hydro-Quebec oscillations.

2.8.1 Low Level System Analysis

The main component in each band of the MBSSDC is the lead-lag block or lead-lag compensator. A lead lag-block introduces additional pole and zero pairs into the open-loop response of the control system. The lead-lag compensator is essentially a lead compensator cascaded with a lag compensator.

Lead compensation is a method of improving the transient response of a system by providing a phase lead in the system response. A lead compensator adds a pole and a zero to the system response, with the pole placed above the frequency of the additional zero [54].

The lag compensator improves the steady state response of the system but at the cost of increasing the settling time, providing a phase lag in the system output relative to the input. The lag compensator also adds a pole-zero pair the system response, but in this case the pole is placed below the zero frequency [54].

A lead-lag compensator provides the functions of both the lead compensator and the lag compensator by cascading the two compensators in series. The transfer function of a lead block or lag block can be written as shown below, with the difference between lead response and lag response being the relative placement of the pole zero pair [54]. The transfer function of a lead-lag compensator appears in equation 2.6

$$T(s) = \frac{s - Z_1}{s - P_1} \tag{2.6}$$

The basic building block of the PSS is shown in Figure 2.26. This differential block consists of a gain stage and a lead-lag compensator for the positive and negative sides of the differential block followed by a summing block that sums the differential signals. This is adapted from the IEEE PSS4B stabilizer.

The MBSSDC takes its input from the dq0 control loop of the DFIG. The MBSSDC uses the Δ_P signal.

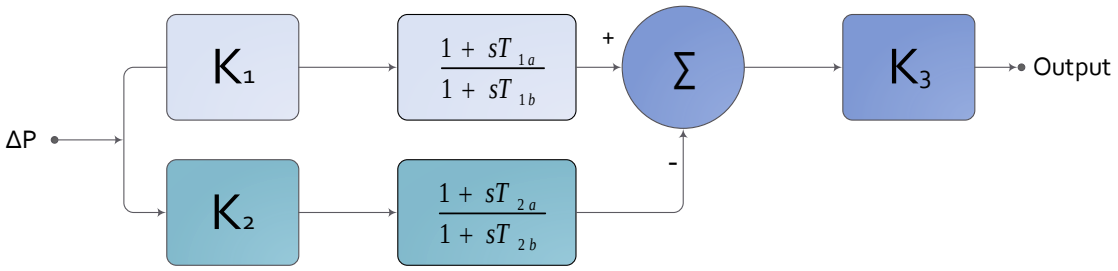

Figure 2.26: Differential Lead-Lag Control Block

This summed signal is run through an additional gain stage before the signal reaches the MBSSDC output. The initial value of the time constants and gain blocks for the system were set using the formulas in equations 2.7, 2.8, 2.9, and 2.10 as noted in the IEEE PSS4B standard [58].

$$T_{1_a} = \frac{T_{1_b}}{R} \tag{2.7}$$

$$T_{2_a} = T_{1_a} = \frac{1}{2\pi * F_{Band} * \sqrt{R}} \tag{2.8}$$

$$T_{2_b} = T_{1_b} * R \tag{2.9}$$

$$K_1 = K_2 = \frac{R^2 + R}{R^2 - 2R + 1} \tag{2.10}$$

The value R is known as the constant ratio, and as a result of the way the equations are constructed, R acts as a ratio between the time constants of the numerator and denominator of the lead-lag blocks and the positive and negative loops of the differential block. This constant ratio keeps all the time constant values tied to each other. This value is typically set to 1.2 as per IEEE PSS4B [58], but an R value of 2 was used in the MBSSDC due to the wider frequency ranges in comparison to the much lower frequency that the IEEE PSS4B was designed for (0.1 - 4 Hz region)

Equations 2.7, 2.8, 2.9, and 2.10 work together to set the overall gain of the entire differential block to unity. The unity gain of the differential block means the overall gain of each band is controlled by K_T, the final block of Figure 2.26. The output of this block is returned to the dq0 control loop of the Type III DFIG.

The transfer function of this supplementary control loop is shown in equation 2.11.

$$Out(s) = K_3 \left(K_1 \frac{sT_{1_a} + 1}{sT_{1_b} + 1} - K_2 \frac{sT_{2_a} + 1}{sT_{2_b} + 1} \right) \tag{2.11}$$

2.8.2 Frequency Analysis of Power Oscillations

In order to determine the frequencies that the bands must be tuned to, analysis of the output power oscillations must be performed. By inspection it is clear that the frequencies within the oscillations of the 8% compensation, 50% compensation, and 80% compensation events (shown in Figures 2.18, 2.21, and 2.23) are at least somewhat different from each other.

To determine appropriate frequencies for the control band development, an analysis of the above wave-forms was performed to determine the dominant frequencies within the oscillations. This frequency analysis was performed using a Prony analysis within the Transient Security Assessment Tool (TSAT) program. TSAT is a non-linear time-domain simulator developed by Powertech Labs Inc. TSAT provides a large number of analysis tools specifically designed for power systems [59].

2.8.3 Prony Analysis

Prony analysis is a method of decomposing signals into constituent sinusoids similar to Fourier analysis; however Prony's method allows the sinusoid to be modified by a growing or decaying exponential term. Prony's method was developed by Gaspard Riche de Prony in the late 1700's. The Prony method is shown below in equation 2.12. Prony analysis samples the output waveform and fits this waveform to the sum of a set of complex damped sinusoid

components $y(t)$, which is given by

$$y(t) = \sum_{i=1}^{N} A_i e^{\sigma_i t} cos(2\pi f_i t + \phi_i), \tag{2.12}$$

where A_i is the magnitude, σ_i is the damping coefficient, f_i is the sinusoid frequency and ϕ_i is the phase angle of the i^{th} frequency sinusoid component. N is the total number of damped sinusoid components [60].

2.8.3.1 Prony Analysis of the 8% Compensation Waveform

The Prony analysis was first performed on the waveform recorded when the system lost stability as 8% series compensation was connected to the line. This waveform appears in Figure 2.27.

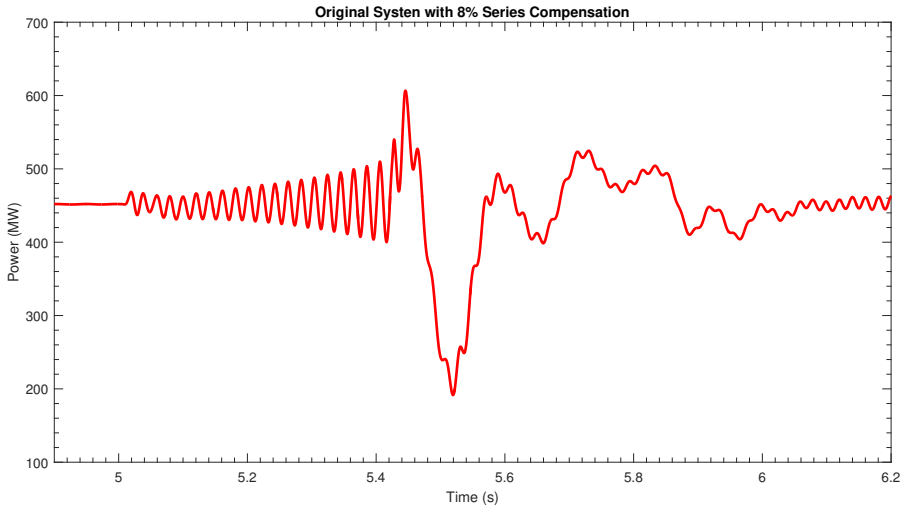

Figure 2.27: Waveform of Base Wind-farm Stability Loss in Response to Application of 8% Compensation

The Prony analysis yielded the following data for the 8% compensation waveform as listed in Table 2.1. Table 2.1 demonstrates that the waveform contains many damped sinusoidal components to completely recreate the original waveform.

Table 2.1: Results From The Prony Analysis Of The 8% Instability Waveform

Magnitude (MW)	***Phase (deg)***	***Frequency (Hz)***	***Damping (%)***
611.2148	-155.298	3.579	30.159
511.0027	-98.991	54.881	3.210
465.2447	165.725	50.142	3.096
435.8179	178.257	53.307	3.496
404.0118	0.000	0.000	-100.000
332.0217	-88.141	5.303	11.598
321.1628	-34.068	56.504	2.686
302.1179	53.455	48.953	1.779
244.6546	-56.056	7.086	6.569
185.5730	30.455	58.034	2.631
173.2023	-97.780	31.337	12.745
173.1895	-29.246	16.339	17.862
135.5252	25.037	46.767	2.393
133.1203	-51.444	86.311	2.568
131.9422	5.175	8.501	4.343
129.8252	127.876	2.169	9.232
99.8046	19.048	88.098	2.266
81.7346	-4.992	44.586	3.134
68.4253	55.614	90.176	2.096
65.9638	-43.516	79.394	2.392

As is shown in Figure 2.27, the 8% compensation waveform contains two distinct portions, an initial high frequency section, followed by a lower frequency section. Figure 2.28 shows the 8% compensation waveform split into the two mentioned sections.The analysis of the 8% compensation event was therefore split into these two sections. This pattern of oscillation is

repetitive for the 8% compensation event, as previously shown in Figure 2.18.

While it is possible to use the Prony analysis to synthesize a waveform matching both sections of the waveform at one time, dividing the waveform into its two constituent pieces allows the use of a smaller value of N. This smaller value of N means fewer sinusoids required to compose the signal allowing a more targeted damping of the oscillations.

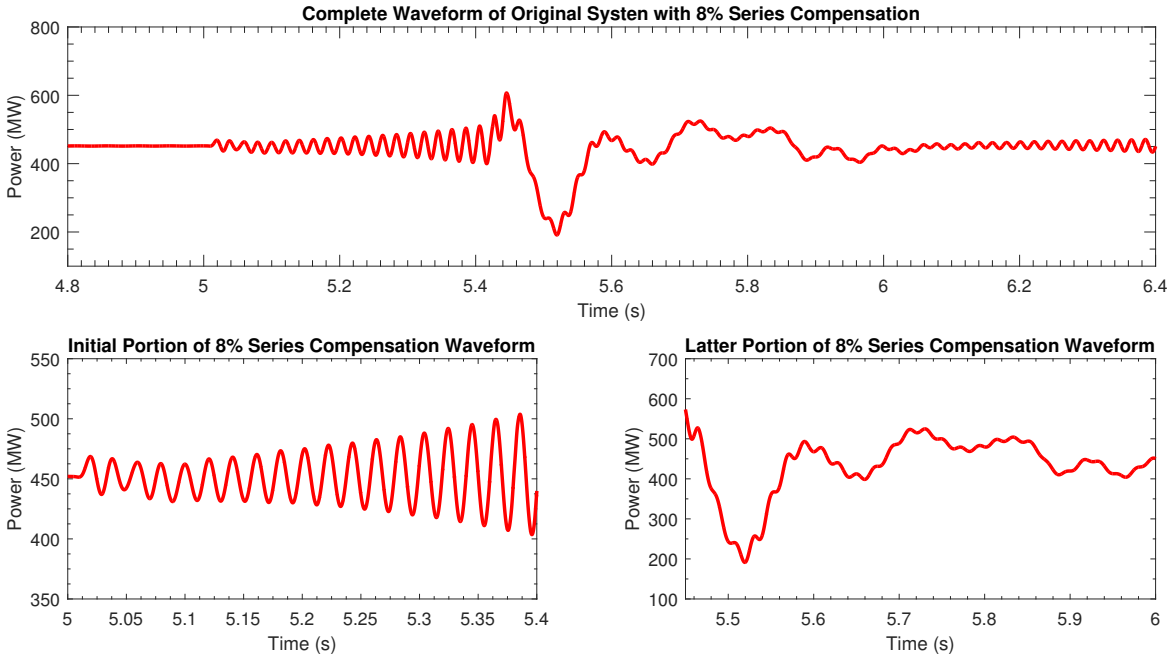

Figure 2.28: 8% Compensation Waveform Split into Two Main Sections

The Prony analysis was performed on both these sections separately. The results of the Prony analysis for the initial high frequency portion (from 5 seconds to 5.45 seconds) are shown in Table 2.2.

Table 2.2: Prony Composition of Initial High Frequency Portion of 8% Instability Waveform

Magnitude (MW)	***Phase (deg)***	***Frequency (Hz)***	***Damping (%)***
29.2728	-63.035	16.644	36.196
27.1701	147.144	13.156	37.902
11.1118	38.368	48.979	-1.135
10.6363	14.740	3.957	47.138
5.9004	162.820	70.344	4.395
1.9321	-102.624	77.080	27.489
0.6931	-120.044	36.960	13.747
0.1383	126.995	70.314	0.610
0.1305	-69.938	22.917	-2.364
0.0676	-61.694	40.532	4.022
0.0543	-19.222	104.422	7.934
0.0539	-47.521	49.673	-4.023
0.0511	-74.813	116.598	2.277
0.0402	135.931	97.881	-1.207
0.0172	66.805	82.298	2.221
0.0111	-119.785	146.862	1.936
0.0102	-75.814	62.162	-0.521
0.0050	151.844	94.389	-0.428
0.0033	-83.755	25.079	-8.200

Again it is clear that there are many components in waveform, but analyzing the Prony output it can be shown that the waveform can be replicated closely by the damped sinusoid listed in Table 2.3.

Table 2.3: Reduced Prony Composition of Initial High Frequency Portion of 8% Instability Waveform

Magnitude (MW)	***Phase (deg)***	***Frequency (Hz)***	***Damping (%)***
11.1118	38.368	48.979	-1.135

Figure 2.29 shows the initial high frequency of the original 8% waveform with the single negatively damped sinusoid of picked from the Prony analysis overlayed in top of it. Figure 2.29 shows that the signal is approximated very well by a negatively damped sinusoid of 49 Hz. This 49 Hz sinusoid is consistent with the initial observations of the high frequency component from Figure 2.18. Splitting the waveform into two parts has allowed the replication of the initial portion of the waveform with a single sinusoid ($N = 1$).

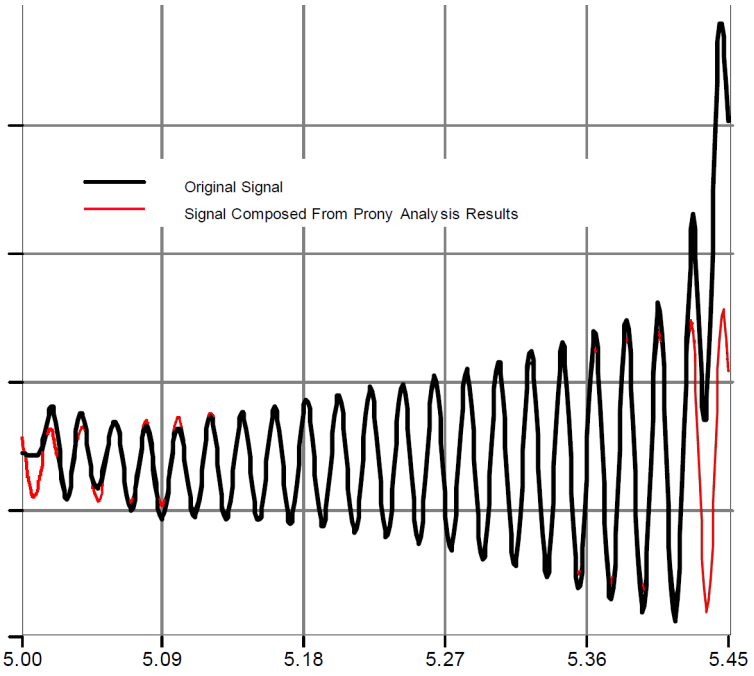

Figure 2.29: 8% Compensation Waveform Compared With Prony Output Waveform

The equation for the waveform representing the reduced Prony composition of the initial

high frequency portion of the 8% series compensation stability loss waveform is shown in equation 2.13.

$$y(t) = 11.118e^{+1.135*t}cos(2\pi * 48.979 * t + 38.368^{\circ}) \tag{2.13}$$

The results of the Prony analysis for the latter low frequency portion (from 5.45 seconds to 6.1 seconds) are shown in Table 2.4.

Table 2.4: Prony Composition of Low Frequency Portion of 8% Instability Waveform

Magnitude (MW)	***Phase (deg)***	***Frequency (Hz)***	***Damping (%)***
253.4313	50.309	55.749	51.694
216.9940	168.872	84.219	56.862
166.7641	80.904	4.874	30.850
134.8716	-28.174	7.803	10.636
90.6672	87.903	2.409	13.072
36.4643	8.193	50.071	3.346
19.3520	-116.332	44.393	9.279
13.3174	89.179	56.941	4.178
4.7674	49.786	49.086	0.030
3.3612	180.000	172.690	12.886
3.0205	37.073	10.325	-5.006
2.3397	79.136	16.353	0.050
2.3159	171.321	70.663	2.275
1.4850	127.760	14.085	-4.878
1.4179	99.658	51.795	1.588
0.8030	33.033	60.283	1.226
0.6229	-68.331	77.450	2.727
0.3835	-85.655	75.286	2.534
0.3452	23.941	19.188	-3.061

Again it is clear that there are many components in waveform, but analyzing the Prony output it can be shown that the waveform can be replicated closely by the damped sinusoids listed in Table 2.5. The waveform requires more components to adequately reconstruct it in comparison to the initial HF frequency portion that was able to be replicated with a single negatively damped sinusoid.

Table 2.5: Reduced Prony Composition of Low Frequency Portion of 8% Instability Waveform

Magnitude (MW)	***Phase (deg)***	***Frequency (Hz)***	***Damping (%)***
134.8716	-28.174	7.803	10.636
90.6672	87.903	2.409	13.072
36.4643	8.193	50.071	3.346
4.7674	49.786	49.086	0.030

Figure 2.29 shows the latter portion of the original 8% waveform with the single negatively damped sinusoid picked from the Prony analysis overlayed in top of it.

Analysis of the lower frequency component shows that in this case the original signal is reasonably approximated by a combination of two 10 Hz sinusoids and several sinusoids clustered around 50 Hz, similar to the 49 Hz component observed in Figure 2.30.

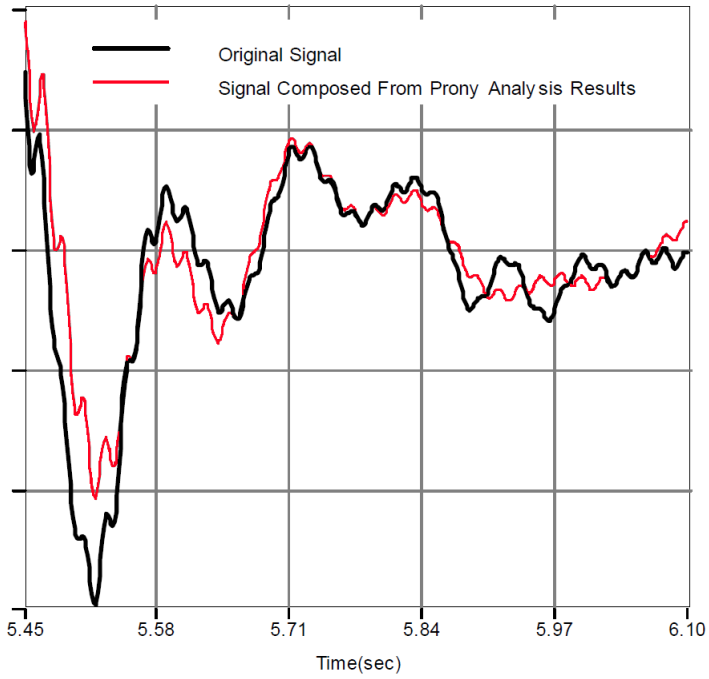

Figure 2.30: 8% Compensation Waveform Compared With Prony Output Waveform

The equation for the waveform representing the reduced Prony composition of the latter lower frequency portion of the 8% series compensation stability loss waveform is shown in equation 2.14.

$$\begin{aligned} y(t) = 134.8716e^{-10.636*t}cos(2\pi * 7.803 * t - 28.174°) \\ +90.6672e^{-13.072*t}cos(2\pi * 2.409 * t + 87.903°) \\ +36.4643e^{-3.346*t}cos(2\pi * 50.071 * t + 8.193°) \\ +4.7674e^{-0.03*t}cos(2\pi * 49.086 * t + 49.786°) \end{aligned} \tag{2.14}$$

Analysis of the power output oscillations during the 8% series compensation event demonstrates the need for a control band around 50 Hz to be integrated into the MBSSDC.

2.8.3.2 Prony Analysis of the 50% Compensation Waveform

Similar analysis was done on the output power wave-forms for the 50% compensation event. Table 2.6 shows the results of the Prony analysis.

Table 2.6: Prony Composition of 50% Instability Waveform

Magnitude (MW)	***Phase (deg)***	***Frequency (Hz)***	***Damping (%)***
296.3672	143.752	6.018	47.550
53.5134	-32.847	33.300	-0.813
20.6368	-13.734	36.661	1.062
10.5408	-156.765	8.587	-16.035
2.3845	-145.756	30.390	-4.932
2.3749	0.000	166.282	28.667
0.6219	-103.830	14.728	-16.931
0.4850	-25.068	89.453	0.456
0.4755	26.433	68.531	0.052
0.3914	-80.941	41.402	-5.482
0.3371	15.859	106.187	3.368
0.2388	-18.452	65.378	-1.801
0.2354	-134.200	136.028	3.947
0.1818	151.302	23.436	-10.729
0.1276	-132.083	156.049	2.909
0.0477	107.953	90.394	-2.277
0.0407	135.064	123.619	0.782
0.0308	138.896	19.537	-18.364

The dominant component in this oscillation were several sinusoids with negative damping

in the 30 Hz range, along with negatively damped sinusoid at 8.5 Hz. Table 2.7 shows the values of these constituent waveforms.

Table 2.7: Reduced Prony Composition of 50% Instability Waveform

Magnitude (MW)	***Phase (deg)***	***Frequency (Hz)***	***Damping (%)***
10.5408	-156.765	8.587	-16.035
2.3845	-145.756	30.390	-4.932
53.5134	-32.847	33.300	-0.813

The equation for the waveform representing the reduced Prony composition of the 50% series compensation stability loss waveform is shown in equation 2.15.

$$\begin{aligned} y(t) = 10.5408e^{+16.035*t}cos(2\pi * 8.587 * t - 156.765^\circ) \\ +2.3845e^{+4.932*t}cos(2\pi * 30.39 * t - 145.756^\circ) \\ +53.5134e^{+0.813*t}cos(2\pi * 33.3 * t - 32.847^\circ) \end{aligned} \tag{2.15}$$

Figure 2.31 shows the original 50% waveform with the sinusoids extracted from the Prony analysis overlayed on top of it.

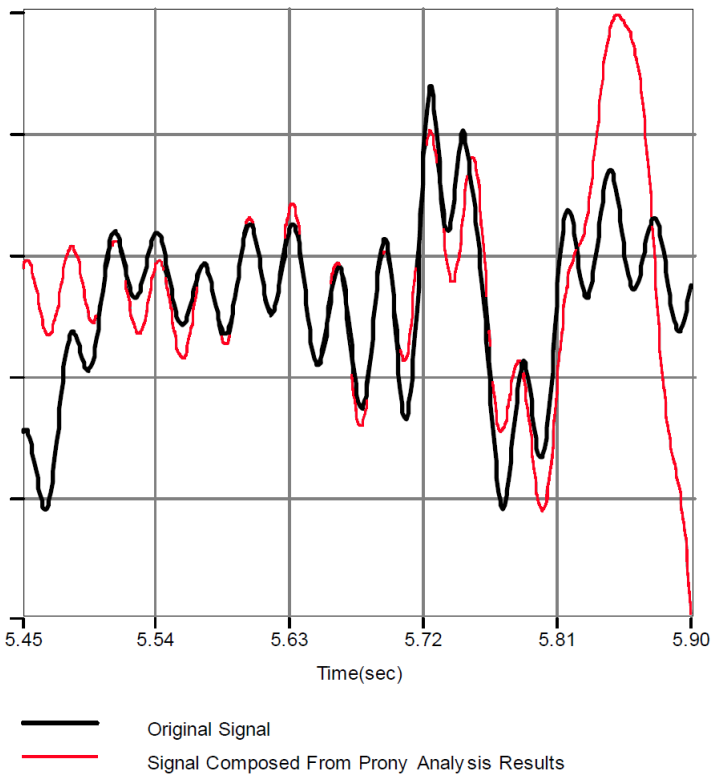

Figure 2.31: 50% Compensation Waveform Compared With Prony Output Waveform

Analysis of the 50% compensation waveform shows that in this case the original signal is reasonably approximated by a combination of one 10 Hz sinusoids and several sinusoids clustered around 32 Hz. The analysis conducted on the 50% compensation event indicates the need for a damping band in the 32 Hz range on the MBSSDC.

2.8.3.3 Prony Analysis of the 80% Compensation Waveform

The Prony analysis for an 80% compensation event is shown in Table 2.8. Analysis of the 80% waveform indicates the presence of multiple modes of oscillation, and no distinct single band.

Table 2.8: Prony Composition of the 80% Compensation Instability Waveform

Magnitude (MW)	***Phase (deg)***	***Frequency (Hz)***	***Damping (%)***
754.8580	-90.753	23.113	59.080
151.0391	103.178	25.410	0.064
131.8064	126.928	13.980	5.413
82.4259	30.195	4.370	3.287
80.8731	-135.687	9.929	-1.111
48.8878	32.232	54.314	6.615
33.8136	0.000	224.534	20.663
29.0961	79.323	34.485	1.010
26.5045	59.932	65.212	5.901
23.0131	137.841	29.813	0.901
21.4897	-19.550	39.456	1.056
18.7820	-70.051	19.622	-0.708
18.7816	162.570	9.277	-8.725
12.7767	9.724	105.050	3.906
6.5544	55.344	51.005	0.402
6.3915	-148.700	44.759	-0.399
6.3475	-13.966	158.105	2.872
6.3198	-117.327	151.407	4.070
3.7003	127.193	94.081	1.091

The largest magnitude components of the reconstituted waveform are around 25 Hz. There is also relatively large components in the 5 - 8 Hz range and in the 40 - 50 Hz range. Reconstruction of the 80% compensation waveform was not as clean as with the 8% and 50% waveforms, there was not a defined frequency range dominating the oscillation. The reduced Prony waveform constituent sinusoids is shown in Table 2.9. Figure 2.32 shows these

components overlayed on the original waveform.

Table 2.9: Reduced Prony Composition of the 80% Compensation Instability Waveform

Magnitude (MW)	***Phase (deg)***	***Frequency (Hz)***	***Damping (%)***
132.2048	107.864	25.364	-0.246
116.8885	-177.385	13.170	3.868
24.3098	73.653	12.179	-1.634
21.5723	-66.646	5.688	-1.419
16.3156	-50.699	16.736	-0.823
11.1047	-146.694	37.763	-0.261

The equation for the waveform representing the reduced Prony composition of the 80% series compensation stability loss waveform is shown in equation 2.16.

$$\begin{aligned} y(t) = 132.2048e^{+0.2465*t}cos(2\pi * 25.364 * t + 107.864^\circ) \\ +116.8885e^{-3.868*t}cos(2\pi * 13.170 * t - 177.385^\circ) \\ +24.3098e^{+1.634*t}cos(2\pi * 12.179 * t + 73.653^\circ) \\ +21.5723e^{+1.419*t}cos(2\pi * 5.688 * t - 66.646^\circ) \\ +16.3156e^{+0.823*t}cos(2\pi * 16.736 * t - 50.699^\circ) \\ +11.1047e^{+0.261*t}cos(2\pi * 37.763 * t - 146.694^\circ) \end{aligned} \tag{2.16}$$

Analysis of the 80% compensation waveforms did not yield a clear band of frequencies to integrate into the MBSSDC, a result that is significantly different than the results seen in the analysis of the 8% and the 50% cases.

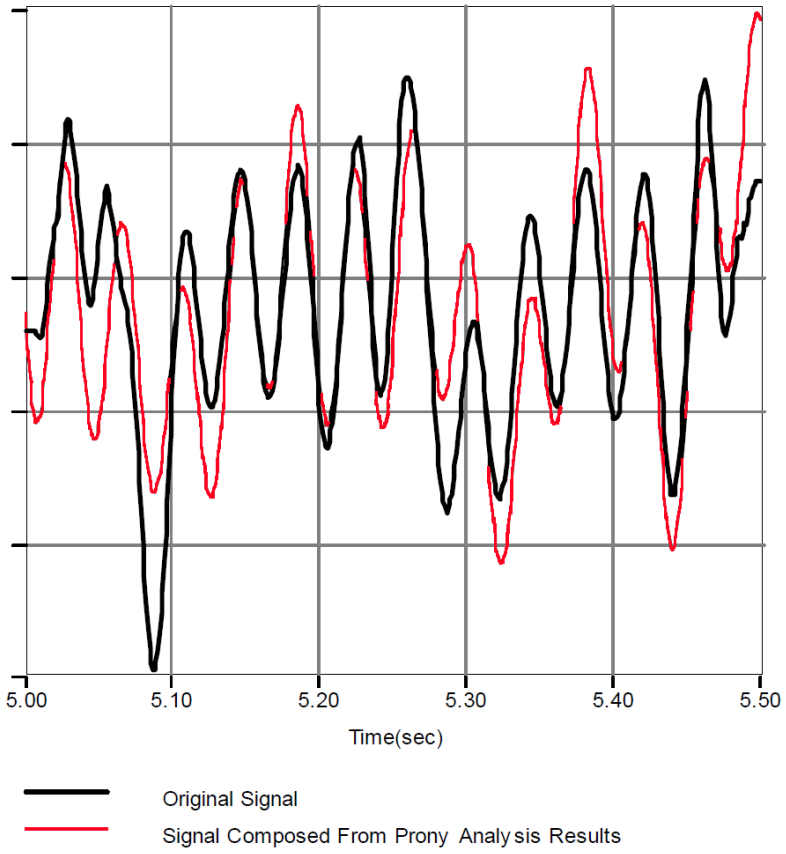

Figure 2.32: 80% Compensation Waveform Compared With Prony Output Waveform

2.8.3.4 Results of the Prony Analysis on the 8%, 50%, and 80% Compensation Waveform

The results of the Prony analysis on the three different oscillation events suggest the need for a supplementary control band centered around 50 Hz and another centered at 30 Hz. While there are many frequencies composing the wave-forms, the dominant frequencies found during the Prony analysis are around 30 Hz and 50 Hz.

During the Prony analysis, the time window for the analysis made a significant difference in the results in terms of the magnitude and damping of specific sinusoids, but the frequency components stayed consistent within a few Hz.

Table 2.10 shows the frequencies of interest from the numerous Prony analysis tests

that were used to reconstruct the oscillation waveforms. It is seen that there are multiple oscillation frequencies around 50 Hz and 30 Hz that are either poorly or negatively damped (increasing), this prompting the decision to design two supplementary control bands for these two frequencies.

Table 2.10: Frequencies of Note From The Multiple Prony Analysis Tests

Magnitude (MW)	***Phase (deg)***	***Frequency (Hz)***	***Damping (%)***
11.1118	38.368	48.979	-1.135
134.8716	-28.174	7.803	10.636
90.6672	87.903	2.409	13.072
36.4643	8.193	50.071	3.346
4.7674	49.786	49.086	0.030
10.5408	-156.765	8.587	-16.035
2.3845	-145.756	30.390	-4.932
53.5134	-32.847	33.300	-0.813
132.2048	107.864	25.364	-0.246
116.8885	-177.385	13.170	3.868
24.3098	73.653	12.179	-1.634
21.5723	-66.646	5.688	-1.419
16.3156	-50.699	16.736	-0.823
11.1047	-146.694	37.763	-0.261

Removing the low frequency components that would normally be damped by the power system stabilizer reveals that most of the problematic sinusoids have frequencies in the 30 Hz or 50 Hz ranges. This is shown in Table 2.11

Table 2.11: Poorly or Negatively Damped Frequencies of Note From The Multiple Prony Analysis Tests

Magnitude (MW)	***Phase (deg)***	***Frequency (Hz)***	***Damping (%)***
11.1118	38.368	48.979	-1.135
36.4643	8.193	50.071	3.346
4.7674	49.786	49.086	0.030
2.3845	-145.756	30.390	-4.932
53.5134	-32.847	33.300	-0.813
132.2048	107.864	25.364	-0.246
16.3156	-50.699	16.736	-0.823
11.1047	-146.694	37.763	-0.261

2.9 Design and Implementation of the 50 Hz Damping Band

Using the information gleaned from the Prony analysis, research of the MBSSDC was undertaken. The initial step was to observe the results of adding a single additional stabilizer loop to the system. As both the 8% and 50% compensation events contained a 49 - 50 Hz component, the initial band was centered at 50 Hz.

Equations 2.7, 2.8, 2.9, and 2.10 were used to set the initial values of the time constants in the lead-lag blocks of the differential band. Equations 2.7, 2.8, 2.9, and 2.10 above set the overall gain of the differential block to unity, this means the overall gain of each band is set by the value of K_T as shown in Figure 2.26. The values used for the time constants and gains are shown in table 2.12.

Table 2.12: Initial Values for 50 Hz Damping Band

T_1	T_2	T_7	T_8	R	K_{H_1}	K_{H_2}	K_T
0.001125	0.00225	0.00225	0.0045	2	6	6	1

The transfer function for this control block is shown in equation 2.17.

$$Y(s) = \frac{6.75 \times 10^{-3} s}{1.012 \times 10^{-5} s^2 + 6.75 \times 10^{-3} s + 1} \tag{2.17}$$

A single control band was implemented into the dq0 control loop of the generator model. The gain on the PID controllers in the dq0 loop was slightly decreased and the time constant on the integrator increased to reduce the sensitivity of the response. This band is shown in Figure 2.33. The frequency of the band was centered at 50 Hz as both the 8% and 50% compensation oscillations contained 50 Hz content. The output of the windfarm was observed for various compensation levels and four different 200 ms faults on the generator bus.

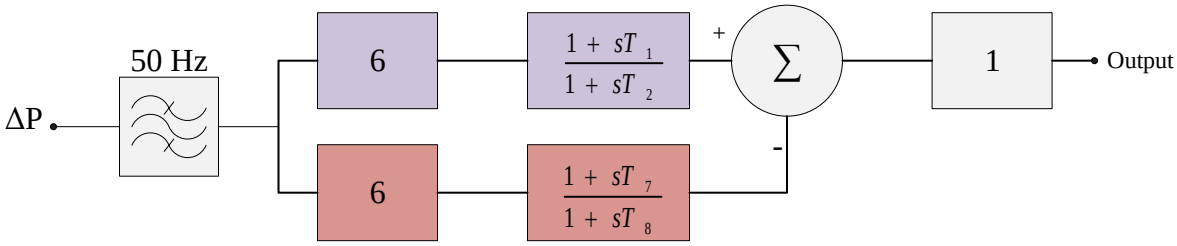

Figure 2.33: 50 Hz Control Band

The results of the analysis for the single band of the damping controller show that while system stability is maintained during most compensation events, the result is not entirely satisfying. There is a decreasing oscillation similar to a ringing that is present in the windfarm output when there is no series compensation present. While this oscillation damps

out by itself eventually, and quickly dissipates when compensation is added to the line, its existence is unsatisfactory.

2.9.1 Testing the Response of the 50 Hz Band to the Connection of 8% Series Compensation

An initial compensation value of 8% was added to the line at a time of five seconds. The system was able to maintain stability as shown in Figure 2.34. From approximately three seconds on, until the compensation is inserted into the line, a damped oscillation is seen. This is undesirable. Recall from Figure 2.18 that the base wind-farm was not stable with an 8% series compensation applied.

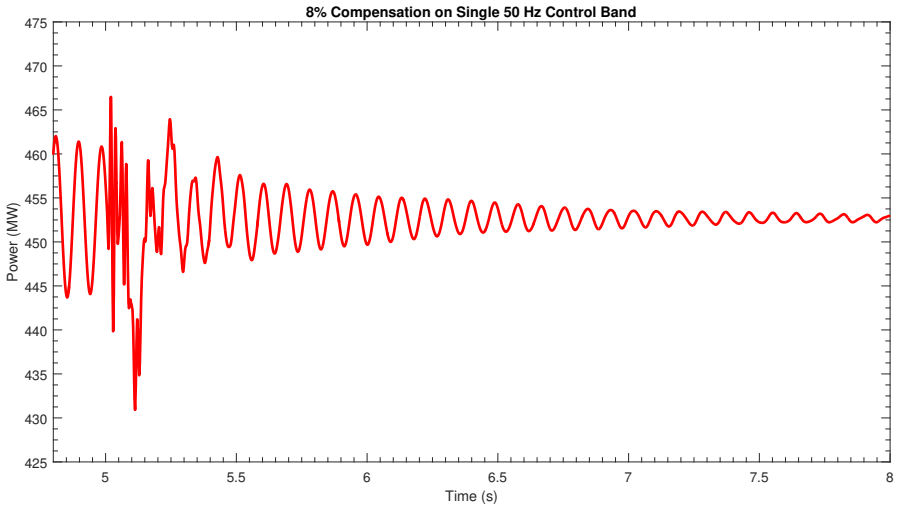

Figure 2.34: 8% Compensation on Single 50 Hz Control Band

2.9.2 Testing the Response of the 50 Hz Band to Faults Occurring While Line is Compensated to 8%

The system was subjected to four different faults on the generator bus while the system was series compensated at 8%: a single line to ground fault, a line to line fault, a double line to ground fault, and a three phase fault. The results of this are shown in Figure 2.35. System stability was maintained throughout all the faults, and steady state operation

resumed approximately 500 ms after the fault was cleared.

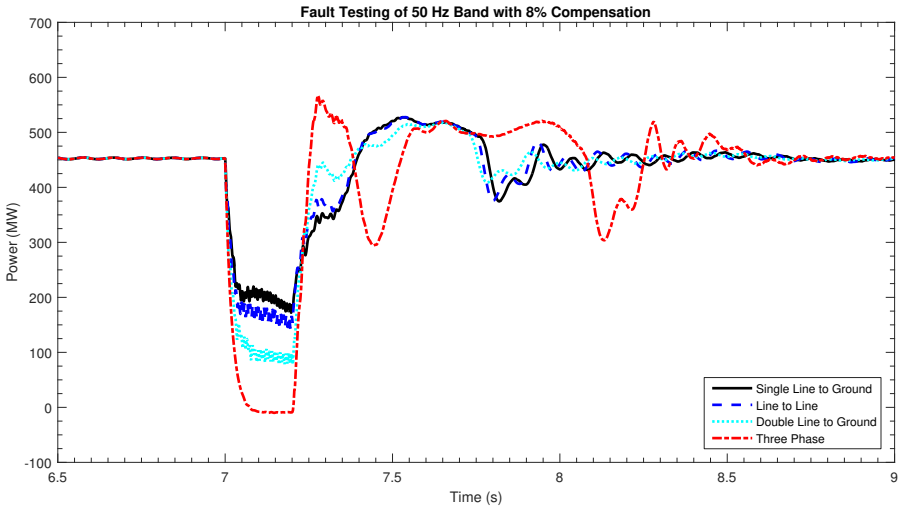

Figure 2.35: Faults with 8% Compensation on Single 50 Hz Control Band

2.9.3 Testing the Response of the 50 Hz Band to the Connection of 50% Series Compensation

Next a compensation value of 50% was added to the line at a time of five seconds. The system was able to maintain stability as shown in Figure 2.36. From approximately three seconds on, until the compensation is inserted into the line, a damped oscillation is again seen. This is undesirable. Recall from Figure 2.21 that the base wind-farm was not stable with 50% series compensation applied.

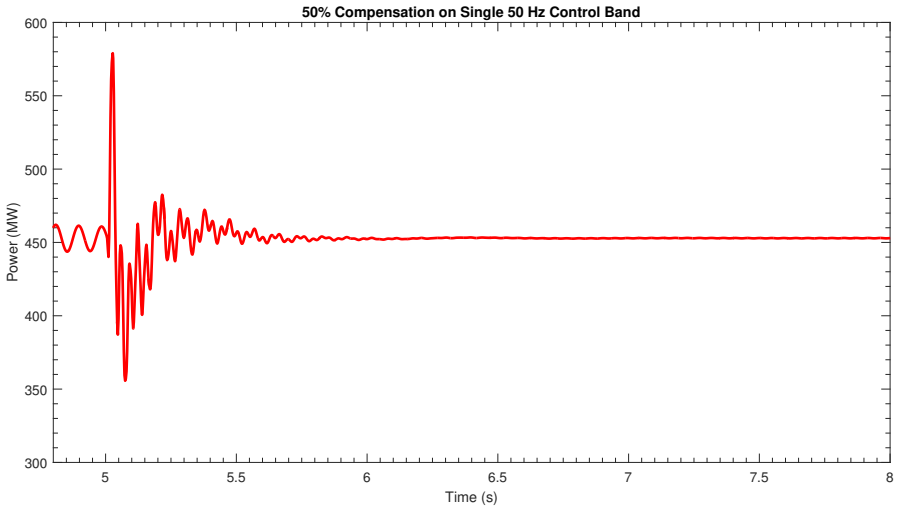

Figure 2.36: 50% Compensation on Single 50 Hz Control Band

2.9.4 Testing the Response of the 50 Hz Band to Faults Occurring While Line is Compensated to 50%

The system was subjected to four different faults on the generator bus while the system was series compensated at 50%: a single line to ground fault, a line to line fault, a double line to ground fault, and a three phase fault. The results of this fault exposure are shown in Figure 2.37. System stability was maintained throughout all the faults.

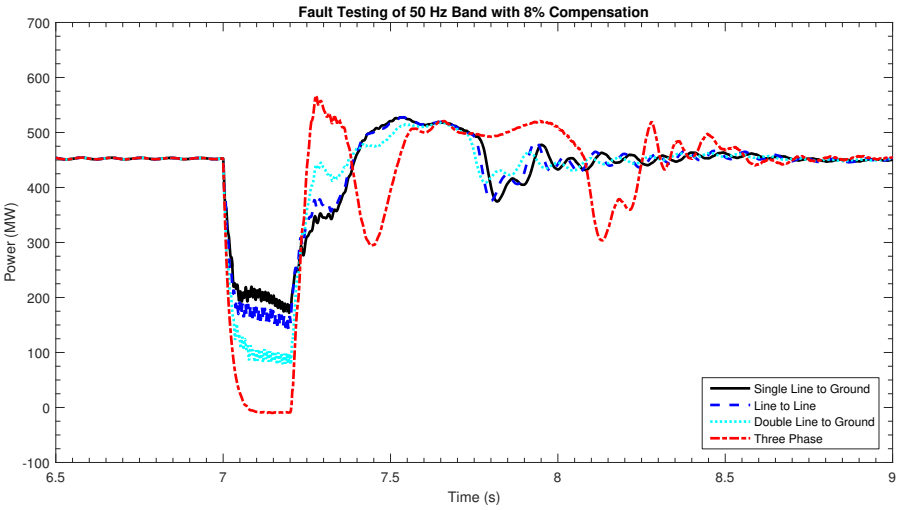

Figure 2.37: Faults with 50% Compensation on Single 50 Hz Control Band

2.9.5 Testing the Response of the 50 Hz Band to the Connection of 80% Series Compensation

Finally a compensation value of 80% was added to the line at a time of five seconds. The system was unable to maintain stability as shown in Figure 2.38. Once the capacitor was placed in series with the line to achieve 80% compensation, the output power began to oscillate, losing stability at about seven seconds. Recall from Figure 2.23 that the base wind-farm was not stable with 80% series compensation applied.

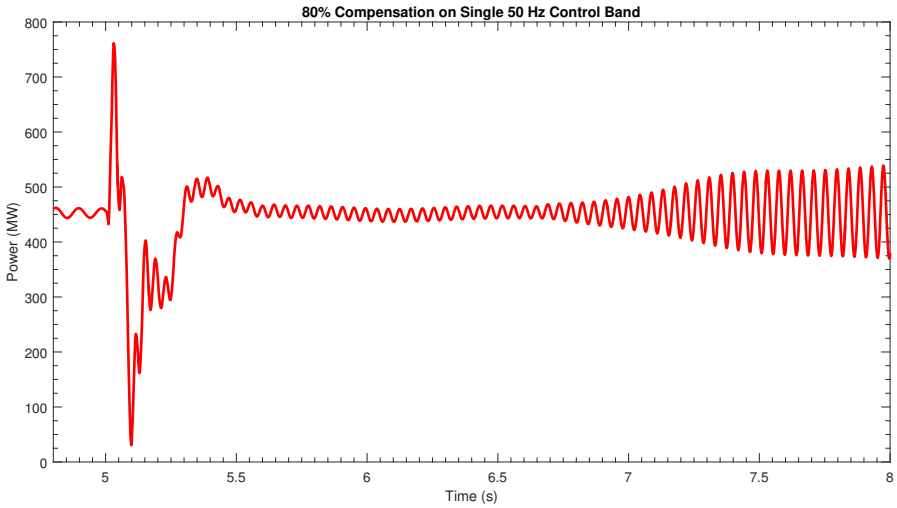

Figure 2.38: 80% Compensation on Single 50 Hz Control Band

Fault testing on the 80% compensated line was not undertaken due to the lack of stability after the compensation was applied.

Subsequent testing has revealed the system is able to maintain stability up to a level of 73% compensation with the single 50 Hz damping band added to the base model. Higher levels of compensation resulted in an increasing oscillation in the output power as shown in the 80% series compensation waveform (Figure 2.38). Fault testing was not performed at this high end level of compensation.

The results of the testing the single 50 Hz damping band demonstrate that the system stability has been greatly improved. Recall the original system would lose stability at levels of 5% series compensation, while stability is now maintained to levels in excess of 70% series

compensation.

2.10 Design and Implementation of the 30 Hz Damping Band

After the implementation of the 50 Hz damping controller and analysis of the results, the implementation of a single band at 30 Hz was begun. The 50 Hz band was removed from the system at this point. The Prony analysis performed earlier showed the dominant frequencies in the oscillations to be centered around 30 Hz and 50 Hz.

As before, equations 2.7, 2.8, 2.9, and 2.10 were used to set the initial values of the time constants in the lead-lag blocks of the differential band. Equations 2.7, 2.8, 2.9, and 2.10 above set the overall gain of the differential block to unity, this means the overall gain of each band is set by the value of K_T as shown in Figure 2.26. The values used for the time constants and gains are shown in table 2.13.

Table 2.13: Initial Values for 30 Hz Damping Band

T_1	T_2	T_7	T_8	R	K_{H_1}	K_{H_2}	K_T
0.001876	0.003751	0.003751	0.007503	2	6	6	1

The transfer function for this control block is shown in equation 2.18.

$$Y(s) = \frac{11.26 \times 10^{-3} s}{2.816 \times 10^{-5} s^2 + 11.26 \times 10^{-3} s + 1} \tag{2.18}$$

A single control band was implemented in the model. This band is shown in Figure 2.39. The frequency of the band was centered at 30 Hz as analysis of the oscillation wave-forms indicated a dominant mode centered around this frequency. The output of the windfarm

was observed for three different compensation levels and four different 200 ms faults on the generator bus.

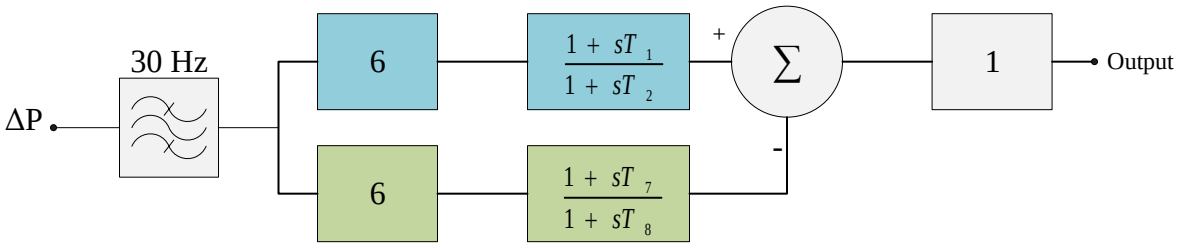

Figure 2.39: 30 Hz Control Band

The results of the analysis for the single band of the damping controller show that while system stability is maintained during most compensation events, the result is again not entirely satisfying. The settling time for series compensation events is excessively long, as is shown in the Figures 2.40, 2.42, and 2.44, with the system taking several seconds to damp out the minor oscillations.

2.10.1 Testing the Response of the 30 Hz Band to the Connection of 8% Series Compensation

An initial compensation value of 8% was added to the line at a time of five seconds. The system was able to maintain stability as shown in Figure 2.40. This is undesirable. Recall from Figure 2.18 that the base wind-farm was not stable with an 8% series compensation applied.

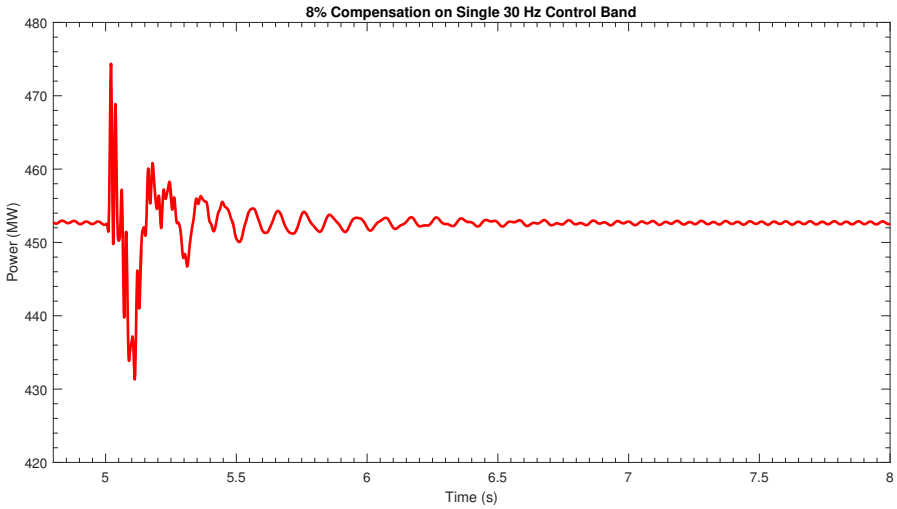

Figure 2.40: 8% Compensation on Single 30 Hz Control Band

2.10.2 Testing the Response of the 30 Hz Band to Faults Occurring While Line is Compensated to 80%

The system was subjected to four different faults on the generator bus while the system was series compensated at 8%; a single line to ground fault, a line to line fault, a double line to ground fault, and a three phase fault. The results of this fault exposure are shown in Figure 2.41. System stability was maintained throughout all the faults, and steady state operation resumed approximately 500 ms after the fault was cleared.

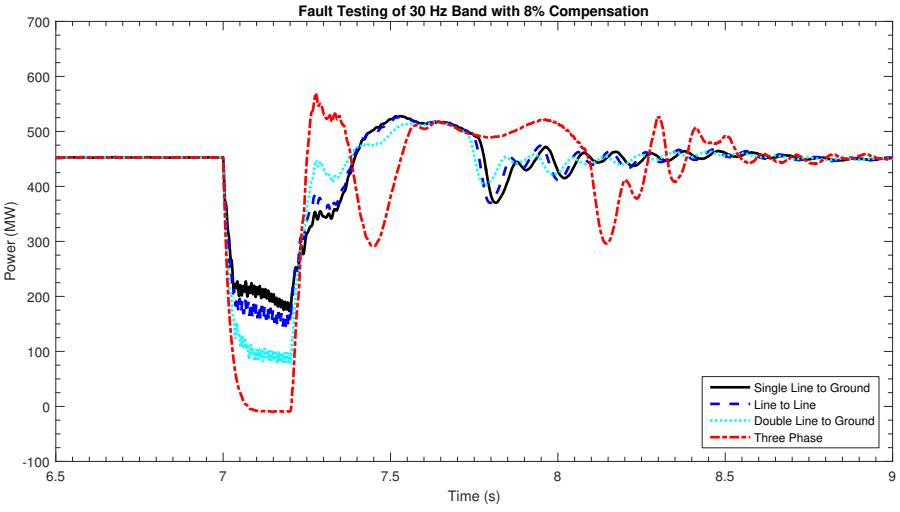

Figure 2.41: Faults with 8% Compensation on Single 30 Hz Control Band

This is a very favorable result, as the original system was not stable at 5% series compensation, while the system now maintains stability during faults conducted with 80% series compensation on the line.

2.10.3 Testing the Response of the 30 Hz Band to the Connection of 50% Series Compensation

Next a compensation value of 50% was added to the line at a time of five seconds. The system was able to maintain stability as shown in Figure 2.42. Recall from Figure 2.21 that the base wind-farm was not stable with 50% series compensation applied.

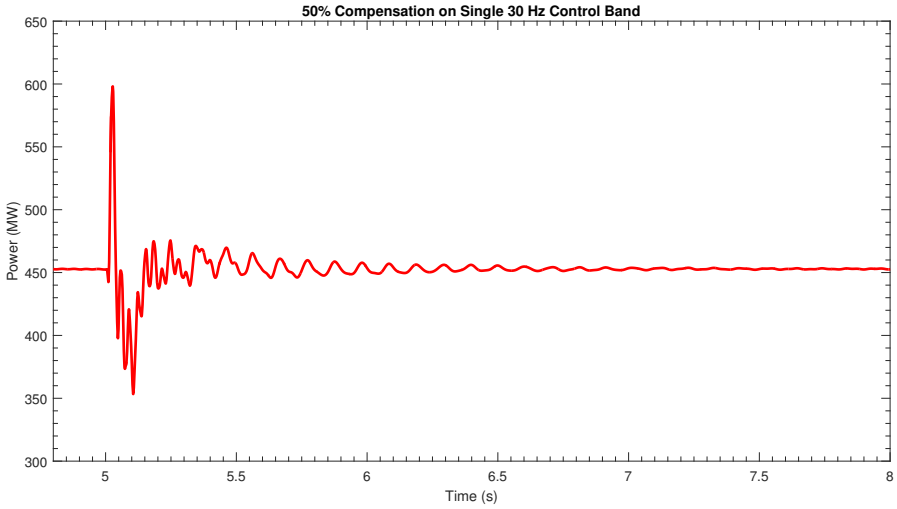

Figure 2.42: 50% Compensation on Single 30 Hz Control Band

2.10.4 Testing the Response of the 30 Hz Band to Faults Occurring While Line is Compensated to 50%

The system was subjected to four different faults on the generator bus while the system was series compensated at 50%: a single line to ground fault, a line to line fault, a double line to ground fault, and a three phase fault. The results of this fault testing are shown in Figure 2.43. System stability was maintained throughout all the faults.

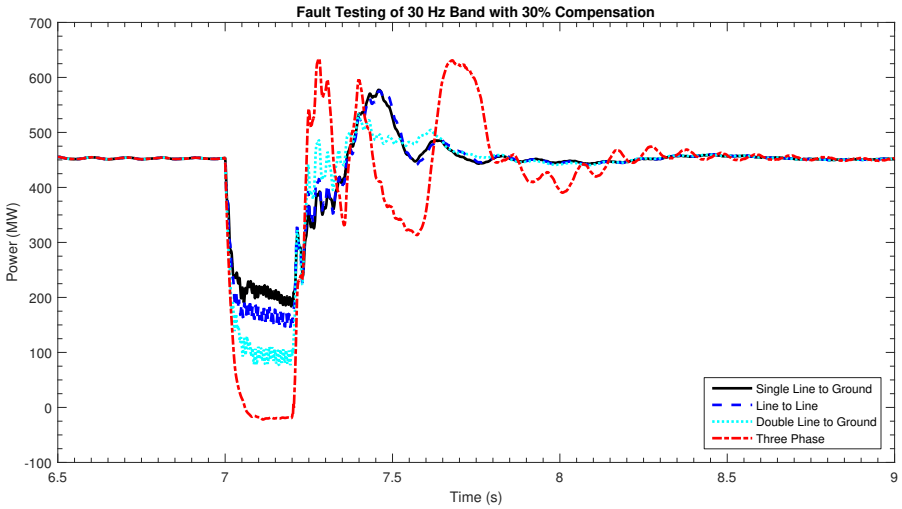

Figure 2.43: Faults with 50% Compensation on Single 30 Hz Control Band

2.10.5 Testing the Response of the 30 Hz Band to the Connection of 80% Series Compensation

Finally, a compensation value of 80% was added to the line at a time of five seconds. The system was able to maintain stability as shown in Figure 2.44. Recall from Figure 2.23 that the base wind-farm was not stable with 80% series compensation applied. Also recall from Figure 2.38 that the system with the single 50 Hz damping controller was also unstable with 80% series compensation applied.

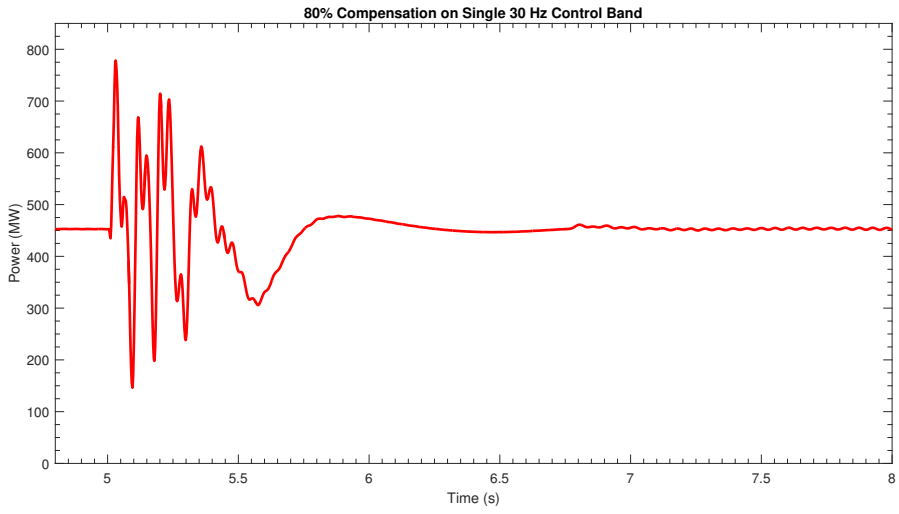

Figure 2.44: 80% Compensation on Single 30 Hz Control Band

2.10.6 Testing the Response of the 30 Hz Band to Faults Occurring While Line is Compensated to 80%

The system was subjected to four different faults on the generator bus while the system was series compensated at 80%: a single line to ground fault, a line to line fault, a double line to ground fault, and a three phase fault. The results of this fault testing are shown in Figure 2.45. System stability was maintained throughout all the faults.

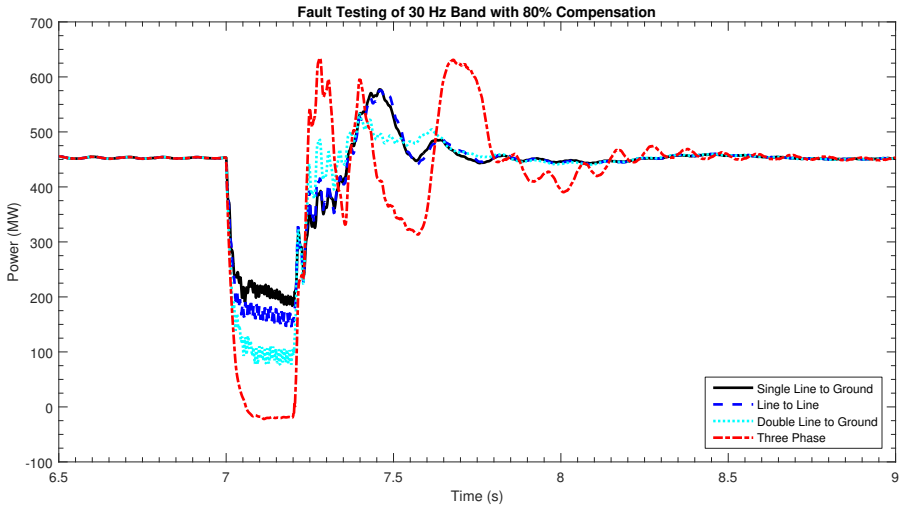

Figure 2.45: Faults with 80% Compensation on Single 30 Hz Control Band

Subsequent testing has revealed the system is able to maintain stability up to a level of 92% compensation with the single 30 Hz damping band added to the base model. With a level of 92% compensation on the line, the settling time is around three seconds, a significant length of time.

The testing in Section 2.10 and Section 2.9 shows that either of the bands makes an improvement to the system stability individually, but overall there is still an opportunity to further improve the design by decreasing the settling time and minimizing ringing.

2.11 Addition of Second Control Band to the Multi-Band Sub-Synchronous Damping Controller Design

With the design and testing of both the 50 Hz & 30 Hz damping controllers completed, both bands were placed in the system and run together in parallel with each other and the main control loop. The two supplementary bands of the controller are illustrated in Figure B.5.

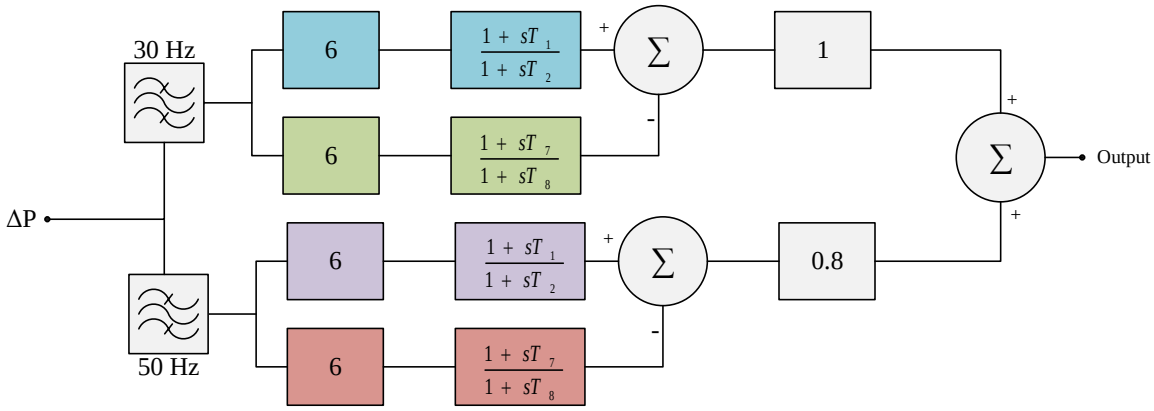

Figure 2.46: Multi-Band Sub-Synchronous Damping Controller Implementation

The values used for the time constants and gains of the 50 Hz and 30 Hz bands are listed in table 2.14.

Table 2.14: Initial Values for 50 Hz & 30 Hz Damping Bands

$Freq$	T_1	T_2	T_7	T_8	R	K_{H_1}	K_{H_2}	K_T
50 Hz	0.001125	0.00225	0.00225	0.0045	2	6	6	1
30 Hz	0.001876	0.003751	0.003751	0.007503	2	6	6	1

The transfer function for dual band damping controller is shown in equation 2.19.

$$Y(s) = \frac{2.66 \times 10^{-7}s^3 + 1.368 \times 10^{-4}s^2 + 16.66 \times 10^{-3}s}{2.851 \times 10^{-10}s^4 + 3.04 \times 10^{-7}s^3 + 1.143 \times 10^{-4}s^2 + 17.86 \times 10^{-3}s + 1} \tag{2.19}$$

The results of the analysis for the multiple bands of the damping controller show that system stability is maintained during all realistic compensation events. The decreasing oscillation (ringing) that was present on the wind-farm output with the single 50 Hz damping band present has been eliminated, and the settling time has been greatly improved in comparison to the single 30 Hz band.

Additionally, it was found that by decreasing the gain on the 50 Hz control band from 1 to 0.8 a quicker settling time resulted. The values used for the time constants and gains of the 50 Hz and 30 Hz bands are shown in table 2.15. The results of the testing use the dual band MBSSDC are discussed below.

Table 2.15: Updated Values for 50 Hz & 30 Hz Damping Bands

$\boldsymbol{Freq}$	$\boldsymbol{T_1}$	$\boldsymbol{T_2}$	$\boldsymbol{T_7}$	$\boldsymbol{T_8}$	$\boldsymbol{R}$	$\boldsymbol{K_{H_1}}$	$\boldsymbol{K_{H_2}}$	$\boldsymbol{K_T}$
50 Hz	0.001125	0.00225	0.00225	0.0045	2	6	6	0.8
30 Hz	0.001876	0.003751	0.003751	0.007503	2	6	6	1

Figure 2.47 shows the MBSSDC connected into the dq0 control loop.

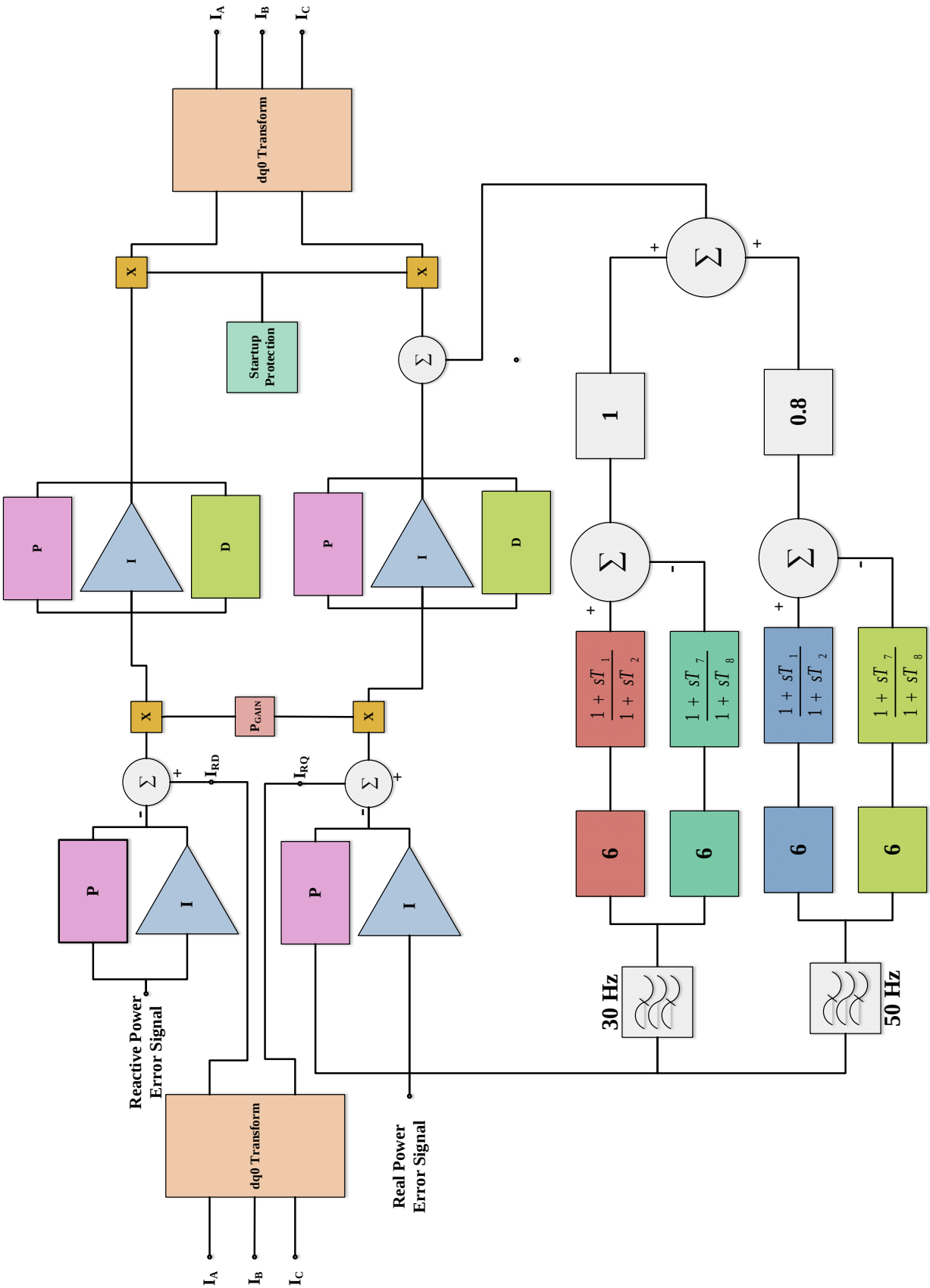

Figure 2.47: MBSSDC Placed in dq0 Control Loop

2.11.1 Testing the Response of the Two Band MBSSDC to the Connection of 8% Series Compensation

An initial compensation value of 8% was added to the line at a time of five seconds. The system was able to maintain stability as shown in Figure 2.48. The system maintains stability and steady state operation is quickly resumed. Recall from Figure 2.18 that the base wind-farm was not stable with an 8% series compensation applied.

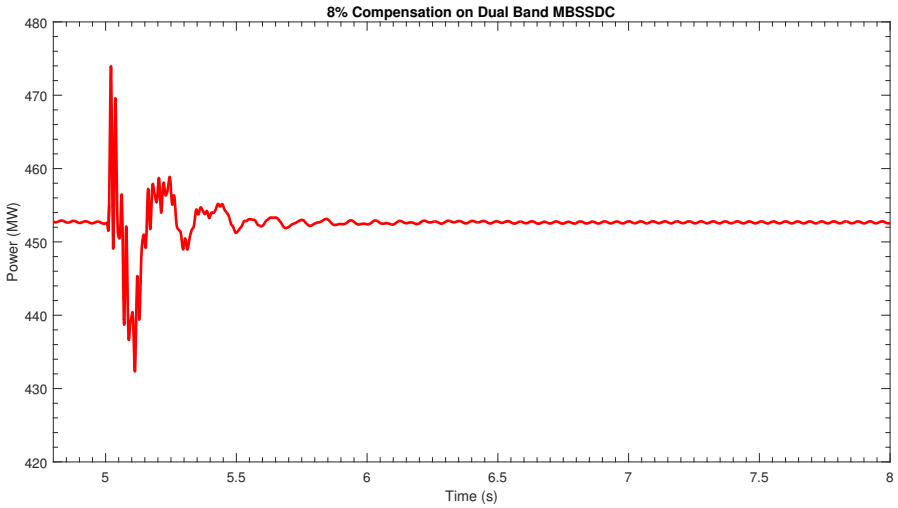

Figure 2.48: 8% Compensation on Dual Band Controller

2.11.2 Testing the Response of the Two Band MBSSDC to Faults Occurring While Line is Compensated to 8%

The system was then subjected to four different faults on the generator bus while the system was series compensated at 8%: a single line to ground fault, a line to line fault, a double line to ground fault, and a three phase fault. The results of this fault testing are shown in Figure 2.49. System stability was maintained throughout all the faults, and steady state operation resumed approximately 500 ms after the fault was cleared.

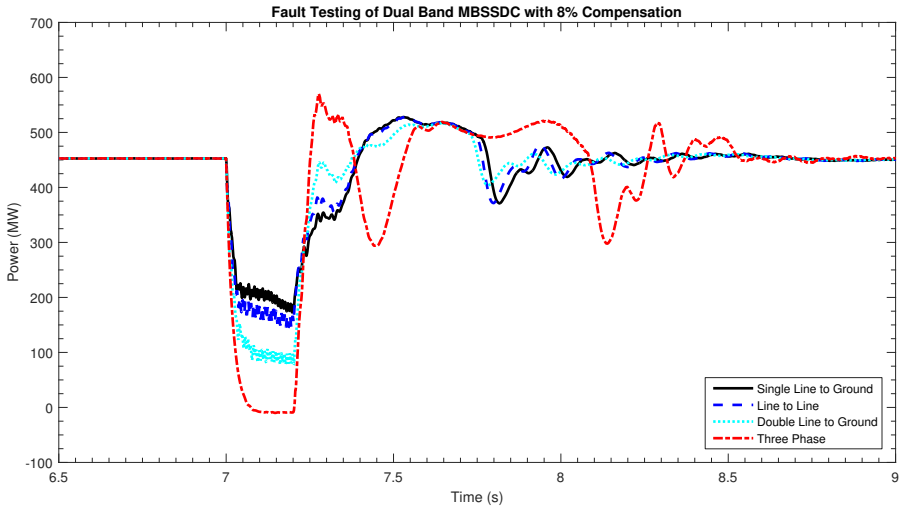

Figure 2.49: Faults with 8% Compensation on Dual Band Controller

2.11.3 Testing the Response of the Two Band MBSSDC to the Connection of 50% Series Compensation

Next a compensation value of 50% was added to the line at a time of five seconds. The system was able to maintain stability as shown in Figure 2.50. The system maintains stability and steady state operation is quickly resumed. Recall from Figure 2.21 that the base wind-farm was not stable with 50% series compensation applied.

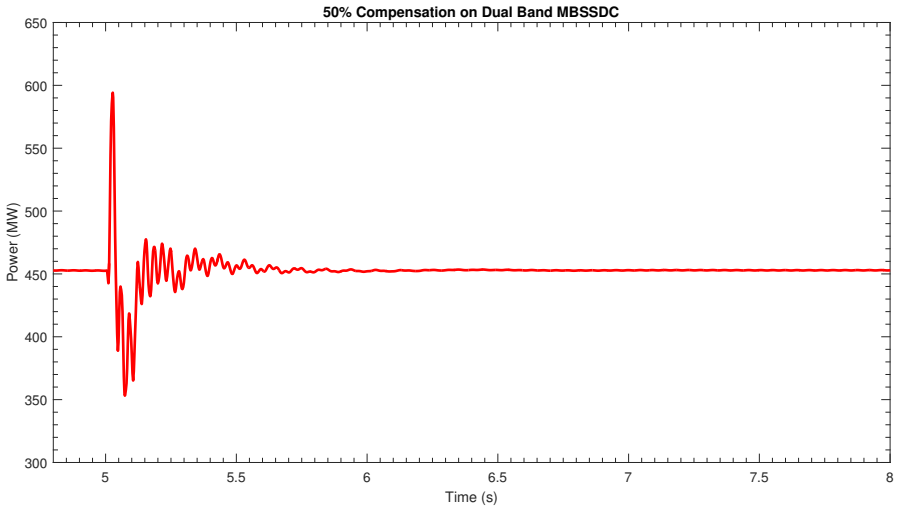

Figure 2.50: 50% Compensation on Dual Band Controller

2.11.4 Testing the Response of the Two Band MBSSDC to Faults Occurring While Line is Compensated to 80%

The system was subjected to four different faults on the generator bus while the system was series compensated at 50%: a single line to ground fault, a line to line fault, a double line to ground fault, and a three phase fault. The results of this fault testing are shown in Figure 2.51. System stability was maintained throughout all the faults.

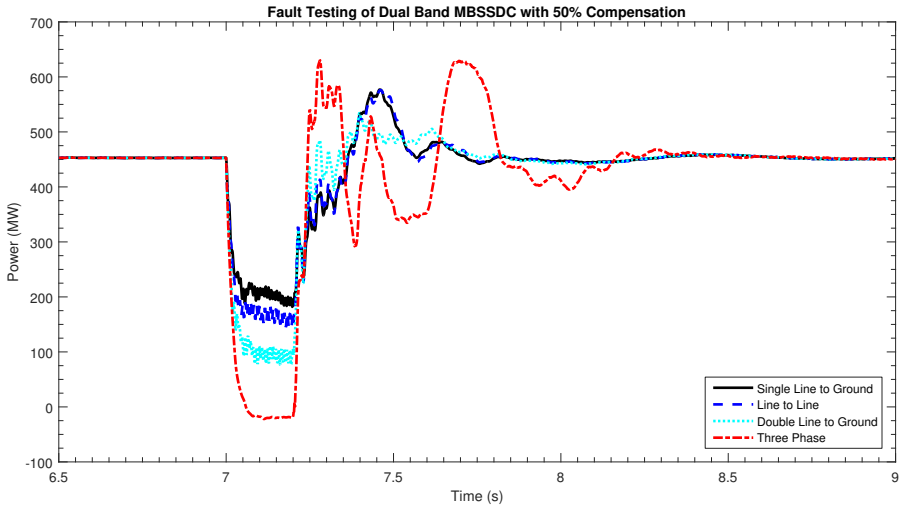

Figure 2.51: Faults with 50% Compensation on Dual Band Controller

2.11.5 Testing the Response of the Two Band MBSSDC to the Connection of 80% Series Compensation

Finally, a compensation value of 80% was added to the line at a time of five seconds. The system was able to maintain stability as shown in Figure 2.52 with the additional damping band in place. Recall from Figure 2.23 that the base wind-farm was not stable with 80% series compensation applied, nor was the system stable in the presence of these conditions with only the 50 Hz damping band in place (Figure 2.38). The system maintains stability and steady state operation is quickly resumed.

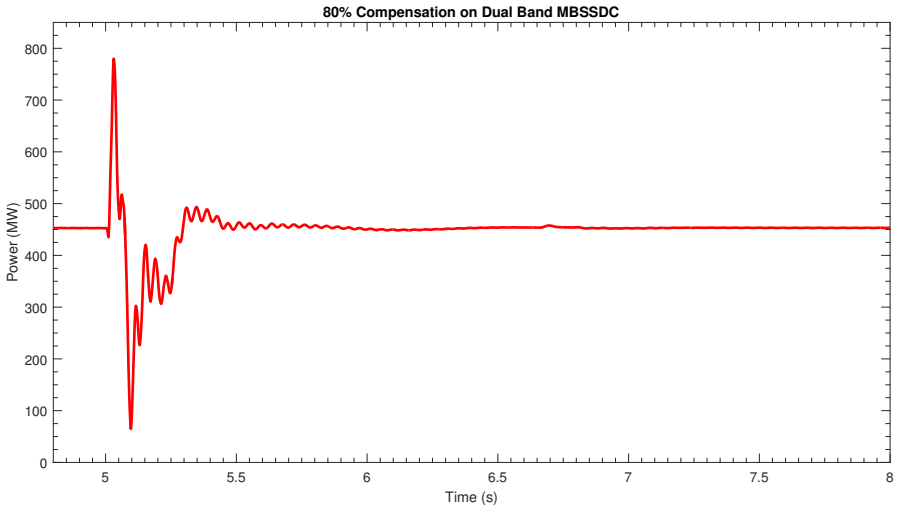

Figure 2.52: 80% Compensation on Dual Band Controller

2.11.6 Testing the Response of the Two Band MBSSDC to Faults Occurring While Line is Compensated to 8%

Fault testing on the 80% compensated line was now undertaken due to the stability gained from the additional damping controller band. The system was subjected to four different faults on the generator bus while the system was series compensated at 50%; a single line to ground fault, a line to line fault, a double line to ground fault, and a three phase fault. The results of this fault testing are shown in Figure 2.53. System stability was maintained throughout all the faults.

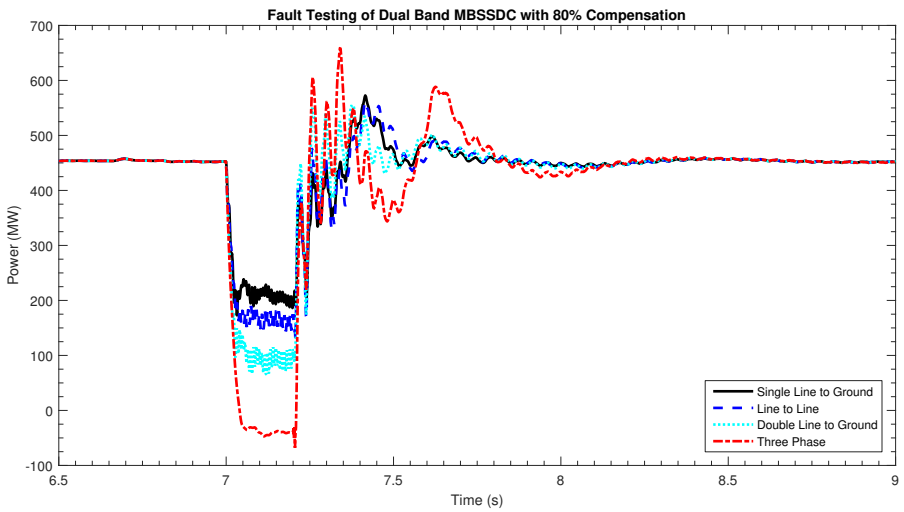

Figure 2.53: Faults with 80% Compensation on Dual Band Controller

2.12 Summary of the Implementation of the MBSSDC on a Model System with a Single Mass Rotor Model

Subsequent testing has revealed the system is able to maintain stability up to a level of 94% compensation with the 30 Hz and the 50 Hz damping band (dual band MBSSDC) added to the base model. Higher levels of compensation resulted in an increasing oscillation in the output power. The system response to the addition of 94% series compensation to the line is shown in Figure 2.54. The system response to four faults (SLG, L-L, DLG, and three phase) is shown in Figure 2.55.

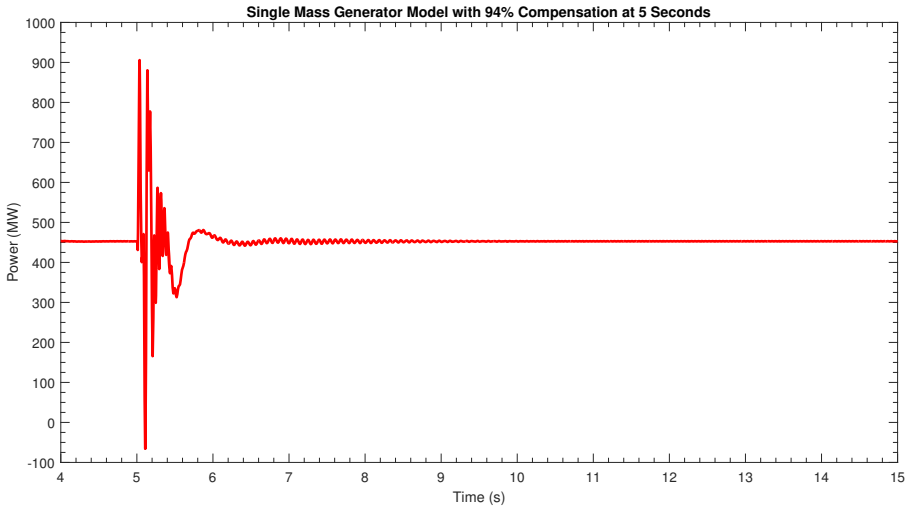

Figure 2.54: Response of the MBSSDC to 94% Series Compensation

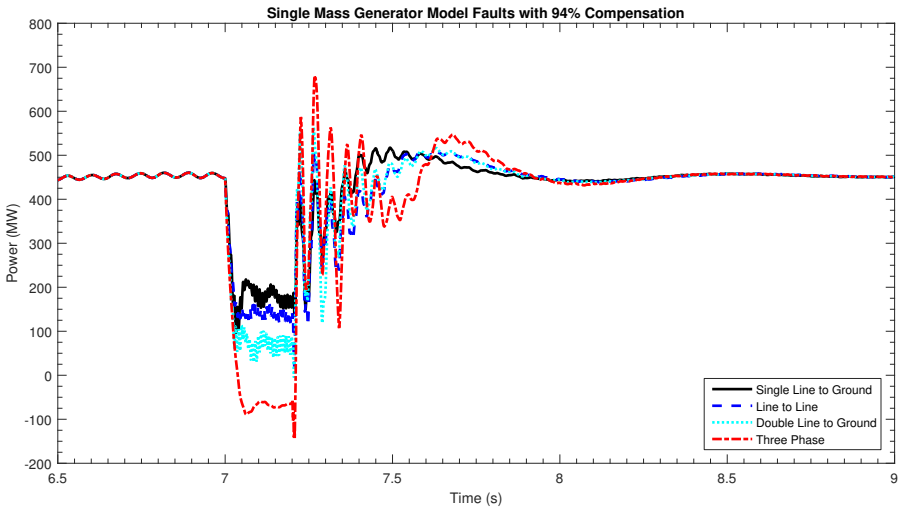

Figure 2.55: Response of the MBSSDC to Various Faults with 94% Series Compensation

The use of both bands in the system has greatly improved the stability of the system. Extremely high values of compensation, much higher than would normally be used in practice, can be inserted in the line and system stability is maintained.

The response of the four different systems (base system model, system with only the 50 Hz damping band, system with only the 30 Hz damping band, and the dual band MBSSDC) to the application of 50% series compensation is shown in Figure 2.56. Figure 2.56 shows that the each of the single bands was able to maintain system stability, the dual band MBSSDC

provides the best response.

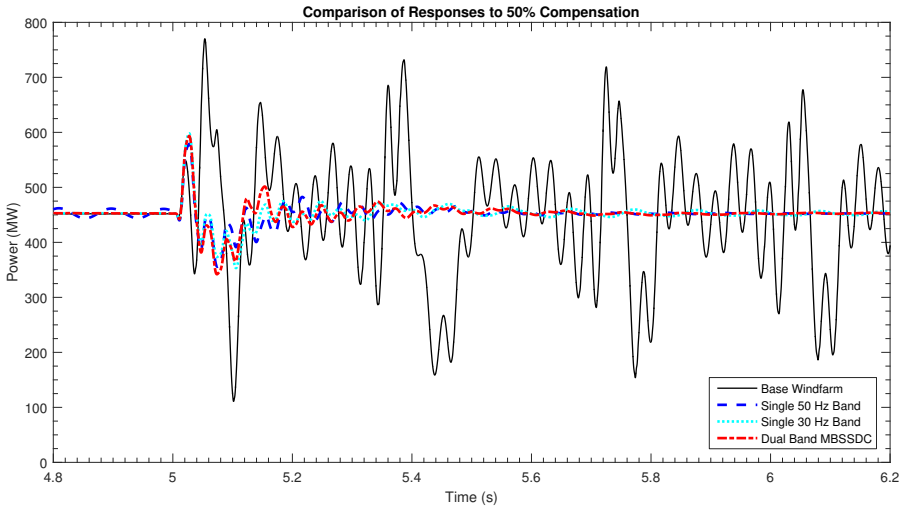

Figure 2.56: Response of Different Systems to 50% Series Compensation

While adding just a single band to the system does increase the stability, it is evident that the addition of a second band greatly improves the stability and response of the system.

Figure 2.57 shows the response to the addition of 50% compensation of the 50 Hz band and the 30 Hz band overlayed on each other. While the 30 Hz band is more effective, both bands do maintain stability.

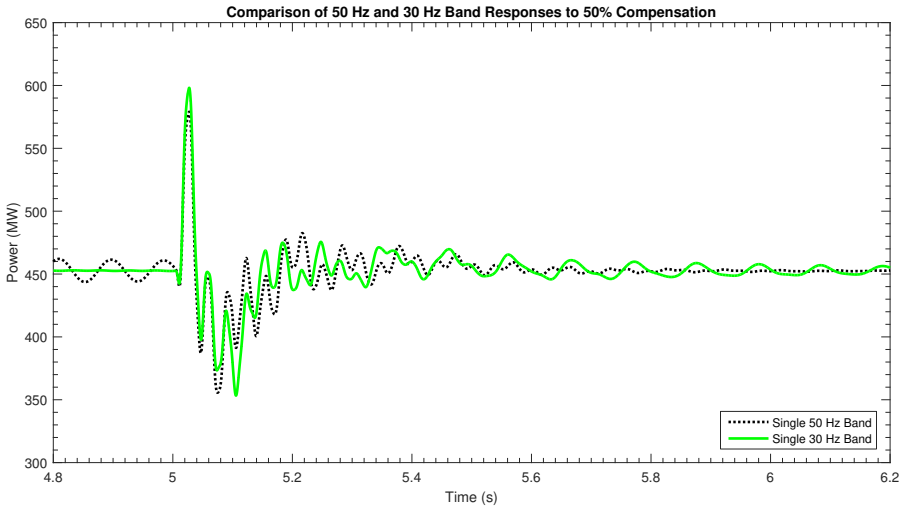

Figure 2.57: Response of 50 Hz Band and 50 Hz Band to 50% Series Compensation

Figures 2.58 and 2.59 show the responses of the dual band MBSSDC and each individual band to the addition of 50% compensation to the system.

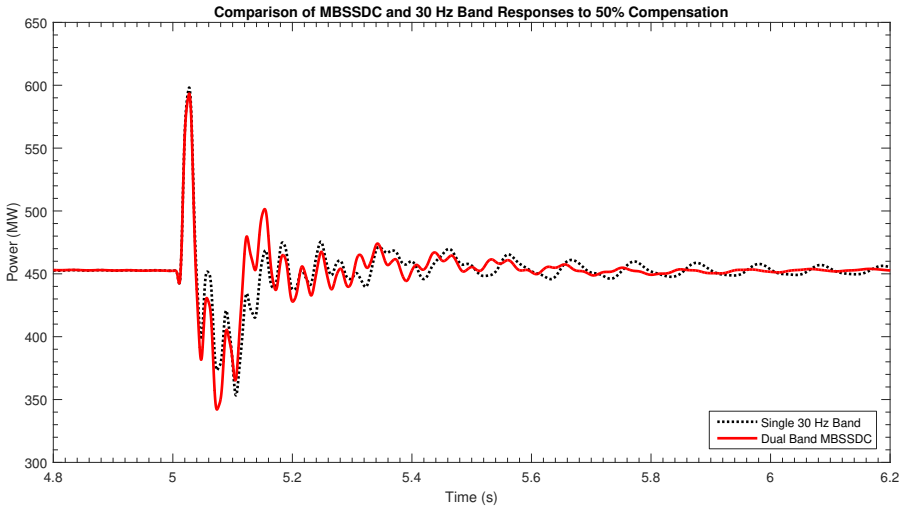

Figure 2.58: Response of MBSSDC and 30 Hz Band to 50% Series Compensation

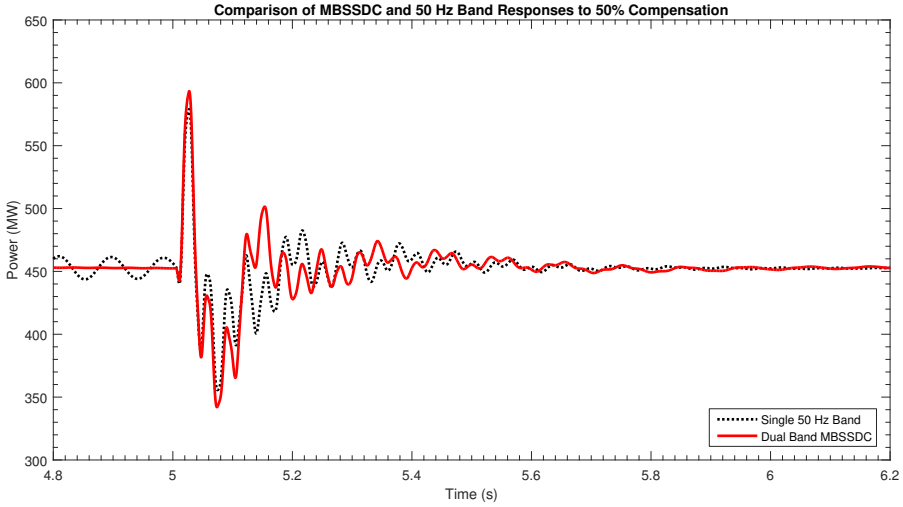

Figure 2.59: Response of MBSSDC and 50 Hz Band to 50% Series Compensation

It is clear from Figures 2.58 and 2.59 that the MBSSDC shown in the red line in each of the figures produces a superior result in eliminating the SSCI's that plagued the original system when series compensation was added.

The stability improvement from the base system is very significant, the original system was unstable at levels of compensation of 5% and greater, while the single mass rotor MB-

SSDC model is stable up to levels of 94% series compensation. A comparison of the original system and the single mass rotor model MBSSDC for series compensation levels of 8%, 50%, and 80% is shown in Figure 2.60.

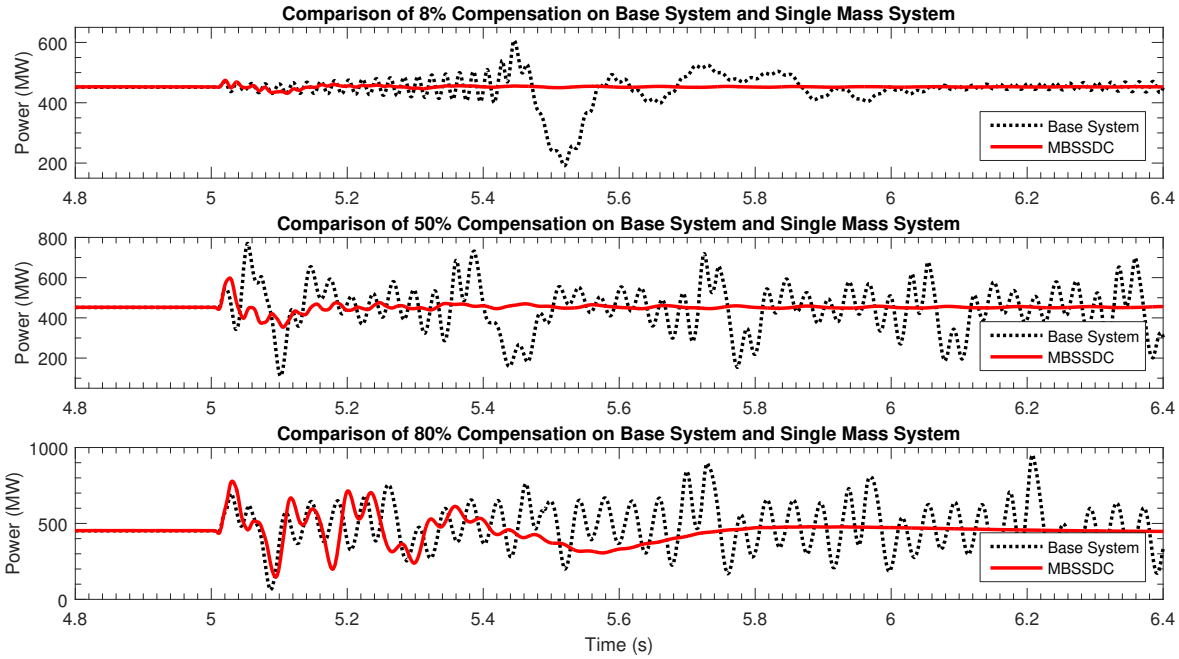

Figure 2.60: Comparison of the Base System to the Single Mass MBSSDC at Various Compensation Levels

Chapter 3

Multi-Band Sub-Synchronous Damping Control with Multi-Mass Rotor Model

3.1 Introduction

This chapter will focus on the addition of a multi-mass rotor model to the system used in the previous chapter and the testing and verification of its operation. The concept of the multi-mass rotor model will precede a discussion of the multi-mass rotor model inside PSCAD.

The results of the addition of the multi-mass rotor model to the MBSSDC will be shown and the development of the controller will be documented in detail. Testing results showing the operation of the multi-mass MBSSDC under various compensation levels and fault situations will be shown along with a comparison of the results from the single mass MBSSDC used in chapter 2.

3.2 Multi-Mass Rotor Model

The Type III DFIG employed in the system model in Chapter 2 used a single mass rotor model. This means that the entire rotor is modeled as a single solid rotating mass with infinite stiffness, this provides a simplified model allowing easier analysis. This model provides a good representation of systems but is not as accurate as the more complex multi-mass rotor model. The single mass rotor model is most commonly used when analyzing the system for the sake of operations and planning. More in-depth studies for stability analysis need to

employ the multi-mass rotor model for greater accuracy [61].

The multi-mass rotor model represents the rotor as a number of rotating masses connected to each other through sections of the shaft with finite stiffness [61]. This model allows for some low frequency torsional oscillation to occur between the connected masses in the shaft, which, while realistic, will increase the fragility of the overall system [62]. A representation of a multi-mass rotor is shown in Figure 3.1.

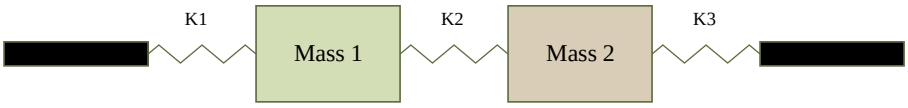

Figure 3.1: Multi-mass Rotor Model

The springs represent the torsional stiffness coefficients connecting the masses to each other. As the value of K connecting each section increases, the multi-mass rotor model begins to replicate the behavior of the the single mass rotor model as the sections are more stiffly connected to each other.

3.3 PSCAD Multi-Mass Rotor Model

The PSCAD model used in the previous chapter was modified for the implementation of a multi-mass rotor model into the DFIG's. The same initial values for the supplementary damping bands of the single mass rotor model system were used for the multi-mass rotor model system used in Chapter 2.

Implementing the multi-mass rotor model into the system required the addition of a multi-mass rotor control box to the generator model as well as the modification of the generator torque and speed signal connections. The new generator model is shown in Figure 3.2.

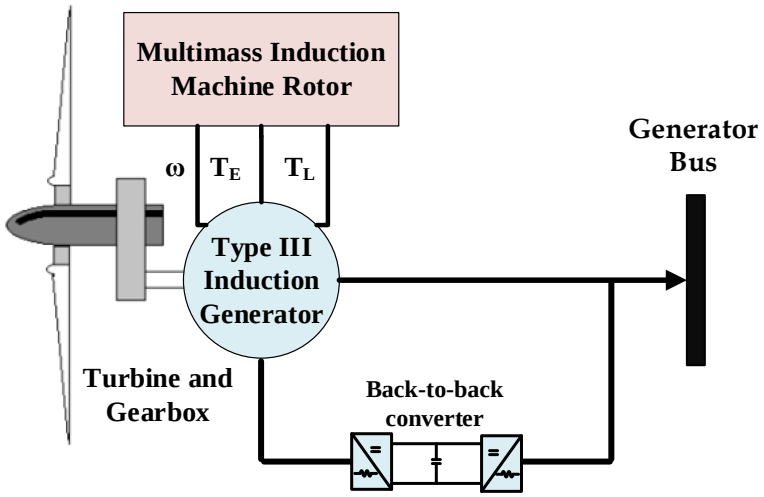

Figure 3.2: Multi-mass Generator Model

The values of the damping coefficients for the multi-mass model and the generator data are listed in appendix A.3.

3.4 Implementing the Multi-Mass Rotor Model in the MBSSDC

The multi-mass rotor model was implemented into the existing PSCAD model, replacing the single mass rotor with the multi-mass rotor; thereafter, testing similar to the work done in the Chapter 2 was done. Stability of the system was tested with various levels of compensation applied, and the fault response of the system at these various compensation levels was also tested.

As before, equations 2.7, 2.8, 2.9, and 2.10 were used to set the initial values of the time constants in the lead-lag blocks in each of the differential bands. Equations 2.7, 2.8, 2.9, and 2.10 set the overall gain of the differential block to unity; this means the overall gain of each band is set by the value of K_T as shown in Figure 2.26. The values for the time constants in

the lead-lag blocks of the damping controller were kept the same as the values used in the single mass rotor system tested in Chapter 2. These values are listed in Table 3.1.

Table 3.1: Initial Values for 50 Hz & 30 Hz Damping Bands in the Multi-Mass System

$Freq$	T_1	T_2	T_7	T_8	R	K_{H_1}	K_{H_2}	K_T
50 Hz	0.001125	0.00225	0.00225	0.0045	2	6	6	0.8
30 Hz	0.001876	0.003751	0.003751	0.007503	2	6	6	1

3.4.1 Testing the Response of the Two Band Multi-Mass MB-SSDC to the Connection of 8% Series Compensation

Preliminary testing was done with the multi-band MBSSDC and the it was found that the adjustment of the band gains yielded superior results. These adjusted parameters are shown in Table 3.2

Table 3.2: Time Constant and Gain Values for 50 Hz & 30 Hz Damping Bands in the Multi-Mass System

$Freq$	T_1	T_2	T_7	T_8	R	K_{H_1}	K_{H_2}	K_T
50 Hz	0.001125	0.00225	0.00225	0.0045	2	6	6	0.9
30 Hz	0.001876	0.003751	0.003751	0.007503	2	6	6	1.25

After stable operation was verified in the absence of series compensation, an initial compensation value of 8% was added to the line at a time of five seconds. The initial oscillations from approximately 0 - 3 seconds are the start-up transients of the system. The system was able to maintain stability as shown in Figure 3.3. The system maintains stability and steady

state operation is quickly resumed. Recall from Figure 2.18 that the base wind-farm was not stable with an 8% series compensation applied.

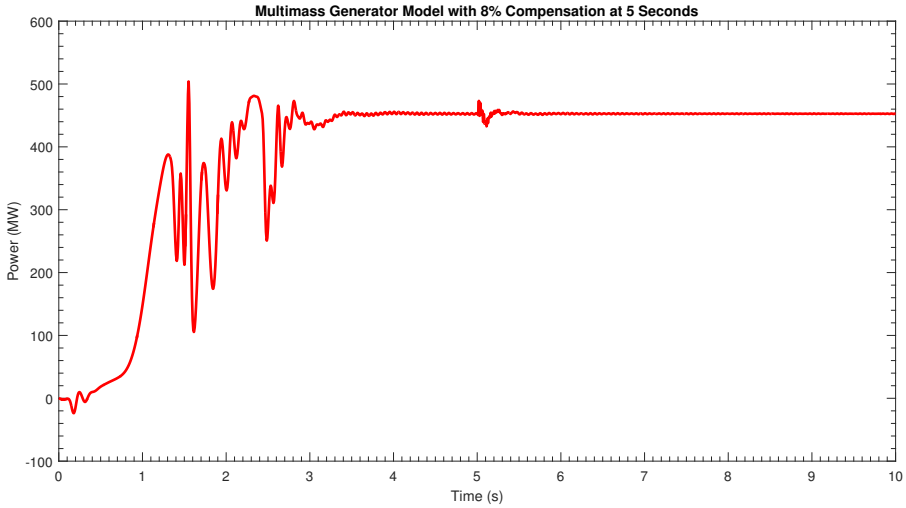

Figure 3.3: 8% Compensation Applied at 5 Seconds to the Multi-Mass System

It can be seen in Figure 3.3 that the response of the system is not as smooth as it was with the single mass rotor model used in Chapter 2 (see Figure 2.48). There is some increased ripple in the output of the multi-mass model, but the response of the two systems is substantially similar to each other. The multi-mass rotor model increases the fragility of the system due to the interaction of the masses shown in Figure 3.1, but it is a more realistic model of a generator shaft. A comparison of the single mass rotor model and multi-mass rotor model responses to the application of 8% compensation to the line is shown in Figure 3.4.

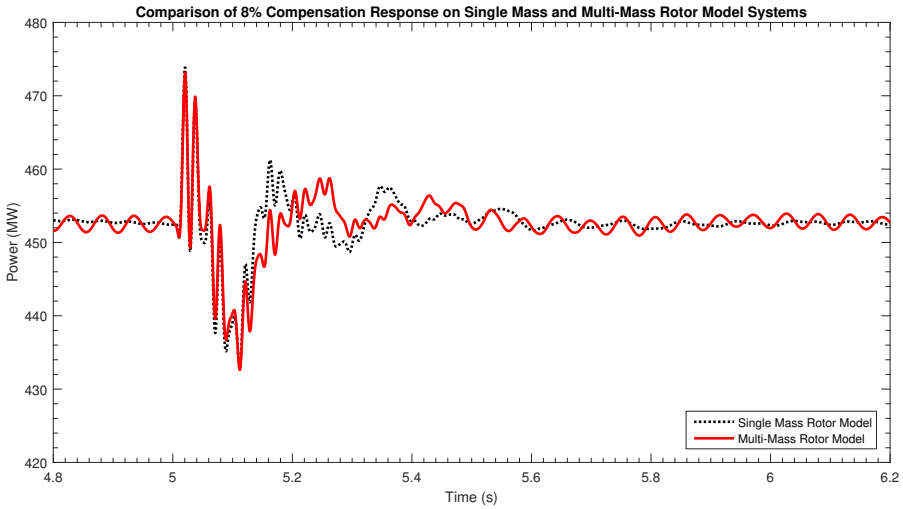

Figure 3.4: 8% Compensation Applied at 5 Seconds to Both the Single Mass Rotor System and the Multi-Mass Rotor System

3.4.2 Testing the Response of the Two Band Multi-Mass MB-SSDC to Faults Occurring While Line is Compensated to 8%

The multi-mass system was then subjected to four different faults applied on the generator bus while the system was series compensated at 8%: a single line to ground fault, a line to line fault, a double line to ground fault, and a three phase fault. The results of this fault testing are shown in Figures 3.5, 3.6, 3.7, 3.8, and 3.9. System stability was maintained throughout all the faults, and steady state operation resumed shortly after each of the faults was cleared. Recall that the original system model was unstable with the 8% compensation put in the line so fault testing was unable to be performed (see Figure 2.18).

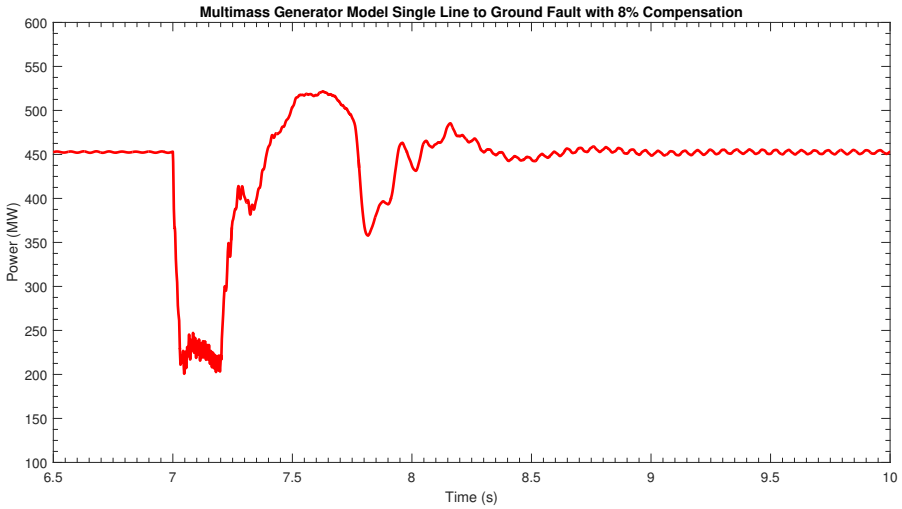

Figure 3.5: Single Line to Ground Fault Applied at 7 Seconds to the 8% Series Compensated Multi-mass System

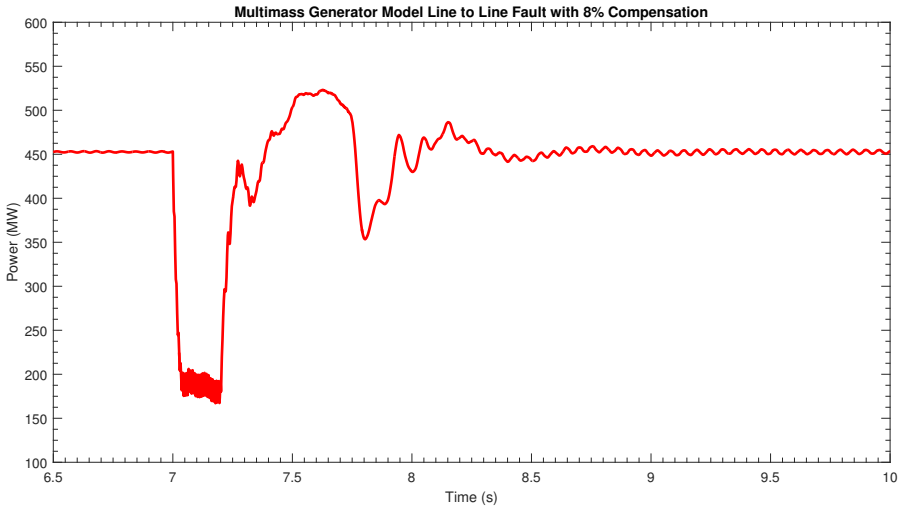

Figure 3.6: Line to Line Fault Applied at 7 Seconds to the 8% Series Compensated Multi-mass System

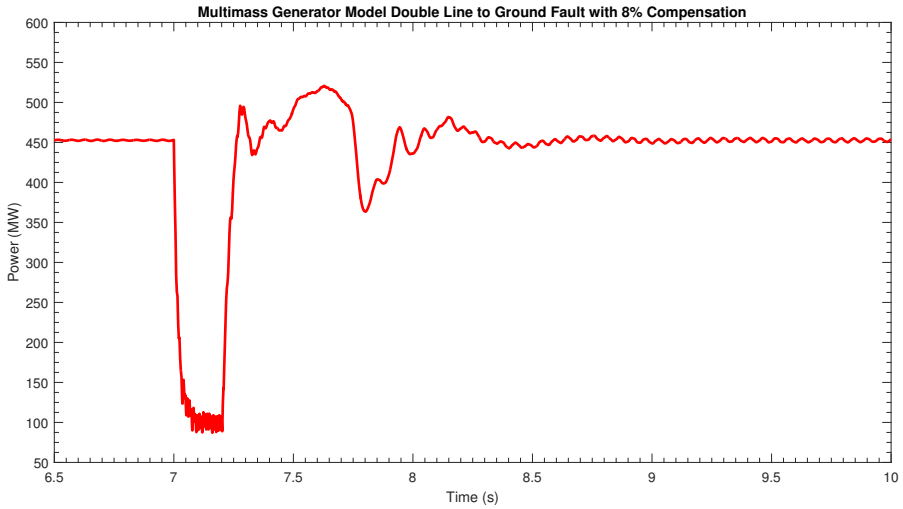

Figure 3.7: Double Line to Ground Fault Applied at 7 Seconds to the 8% Series Compensated Multi-mass System

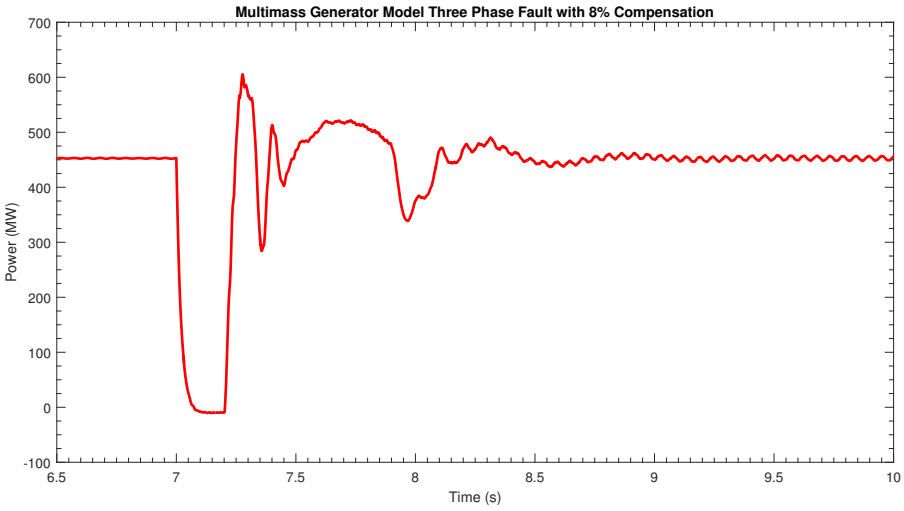

Figure 3.8: Three Phase Fault Applied at 7 Seconds to the 8% Series Compensated Multi-mass System

An overlay of all four faults occurring while the system is compensated to 8% appears in Figure 3.9.

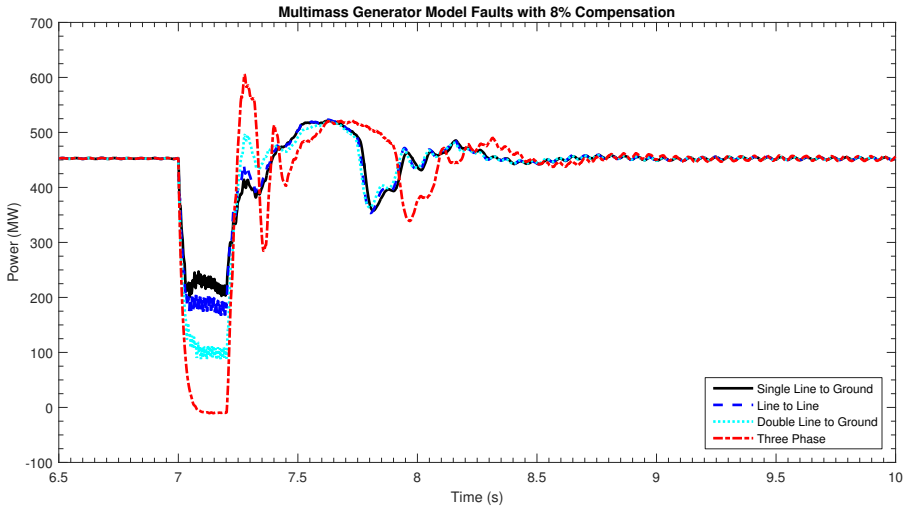

Figure 3.9: Comparison of 4 Fault Types Applied at 7 Seconds to the 8% Series Compensated Multi-mass System

3.4.3 Testing the Response of the Two Band Multi-Mass MB-SSDC to the Connection of 50% Series Compensation

Next a compensation value of 50% was added to the line at a time of five seconds and the system test was repeated. The system was able to maintain stability as shown in Figure 3.10. The system maintains stability and steady state operation is quickly resumed. Recall from Figure 2.21 that the base wind-farm was not stable with 50% series compensation applied.

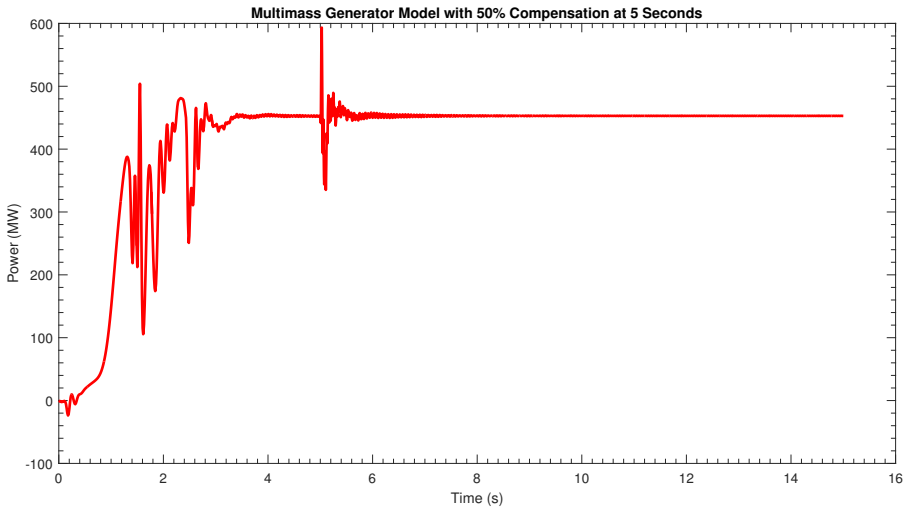

Figure 3.10: 50% Compensation Applied at 5 Seconds to the Multi-mass System

It can be seen that the response of the system is not as smooth as it was with the single mass rotor model used in Chapter 2 (see Figure 2.50) but the response of the two systems are again substantially similar to each other. A comparison of the responses is shown in Figure 3.11.

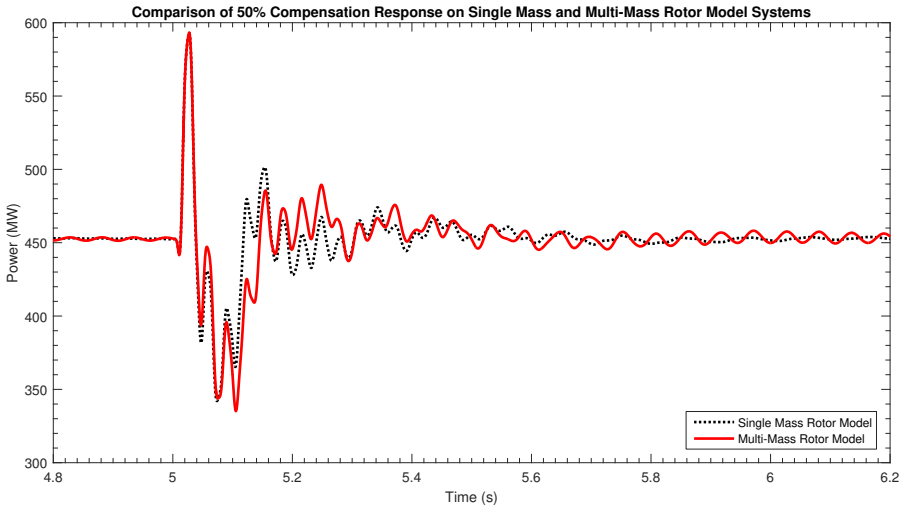

Figure 3.11: 50% Compensation Applied at 5 Seconds to Both the Single Mass Rotor System and the Multi-Mass Rotor System

3.4.4 Testing the Response of the Two Band Multi-Mass MB-SSDC to Faults Occurring While Line is Compensated to 50%

The system was again subjected to four different faults placed on the generator bus while the system was series compensated at 50%: a single line to ground fault, a line to line fault, a double line to ground fault, and a three phase fault. The results of this fault testing are shown in Figures 3.12, 3.13, 3.14, 3.15, and 3.16. System stability was maintained throughout all the faults, and steady state operation resumed shortly after the fault was cleared. Recall that the original system model was unstable with the 50% compensation put in the line so fault testing was unable to be performed (see Figure 2.21).

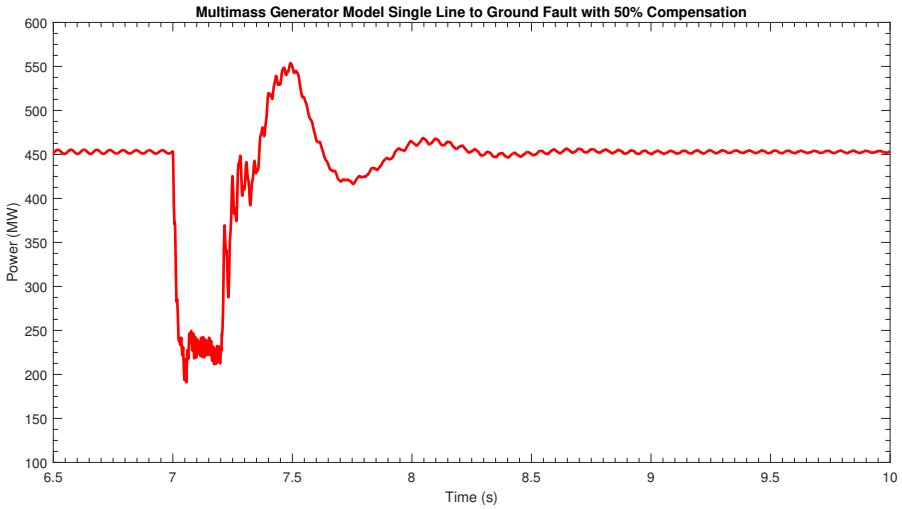

Figure 3.12: Single Line to Ground Fault Applied at 7 Seconds to the 50% Series Compensated Multi-mass System

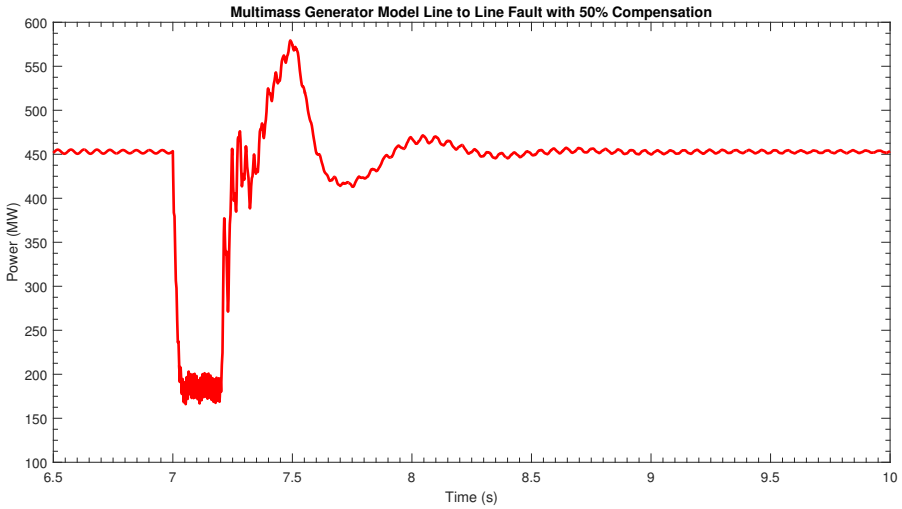

Figure 3.13: Line to Line Fault Applied at 7 Seconds to the 50% Series Compensated Multi-mass System

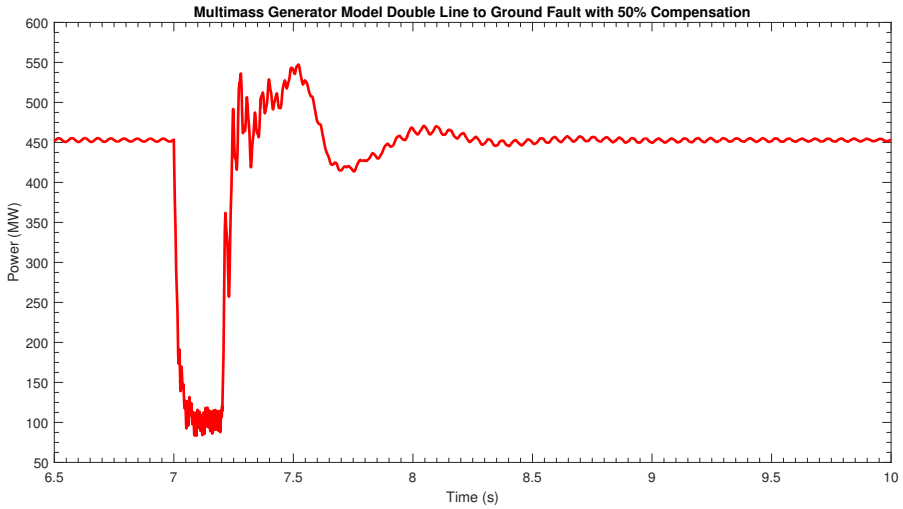

Figure 3.14: Double Line to Ground Fault Applied at 7 Seconds to the 50% Series Compensated Multi-mass System

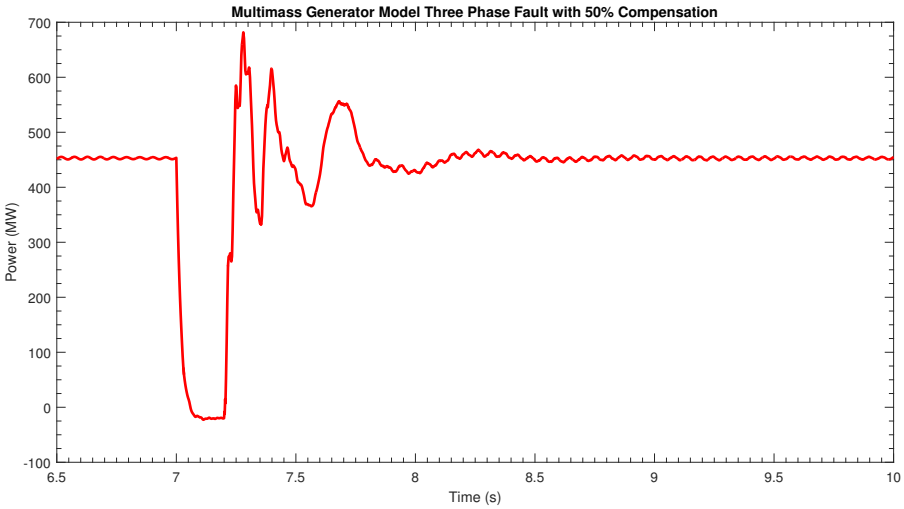

Figure 3.15: Three Phase Fault Applied at 7 Seconds to the 50% Series Compensated Multi-mass System

An overlay of all four faults occurring while the system is compensated to 50% appears in Figure 3.16.

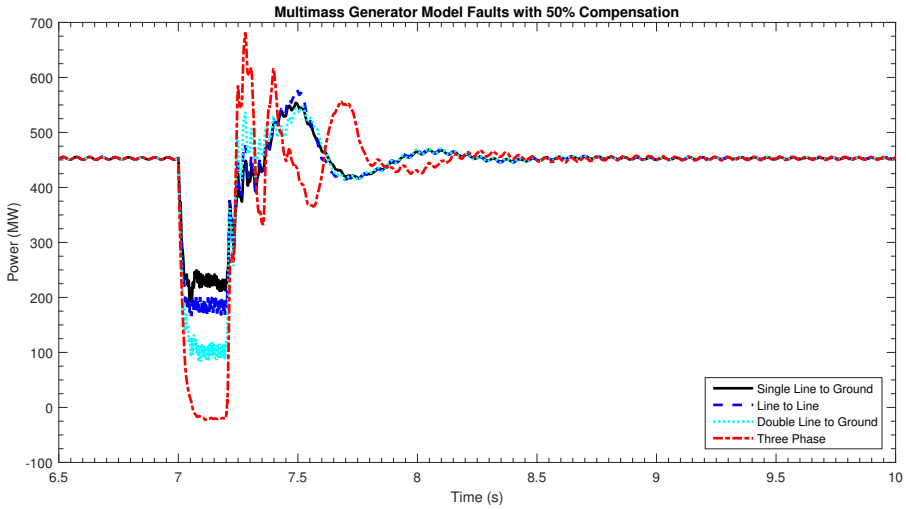

Figure 3.16: Comparison of 4 Fault Types Applied at 7 Seconds to the 50% Series Compensated Multi-mass System

Next a compensation value of 80% was added to the line at a time of five seconds. The system was able to maintain stability as shown in Figure 3.17. The system maintains stability and steady state operation is quickly resumed. Recall from Figure 2.23 that the base wind-farm was not stable with 80% series compensation applied.

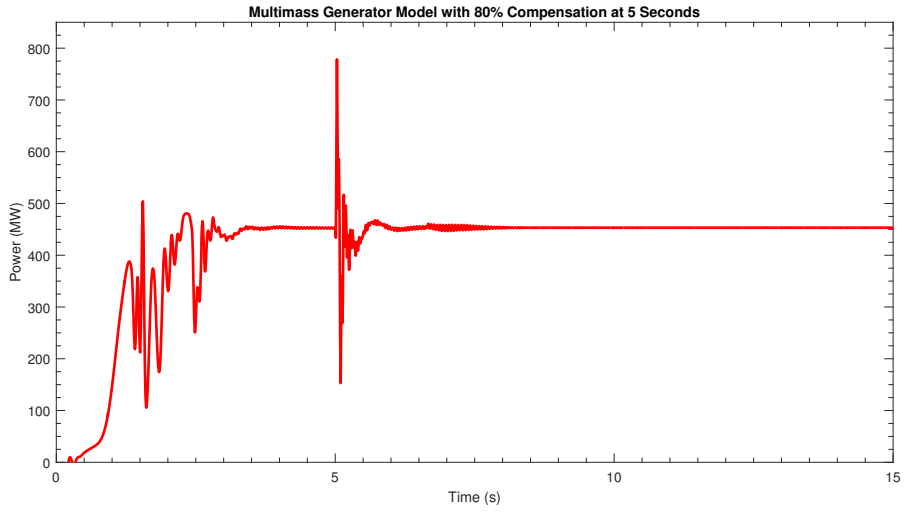

Figure 3.17: 80% Compensation Applied at 5 Seconds to the Multi-mass System

It can be seen that the response of the system is again not as smooth as it was with the single mass rotor model used in Chapter 2 (see Figure 2.52), but again the responses

between the two systems are substantially similar. A comparison of the responses is shown in Figure 3.18.

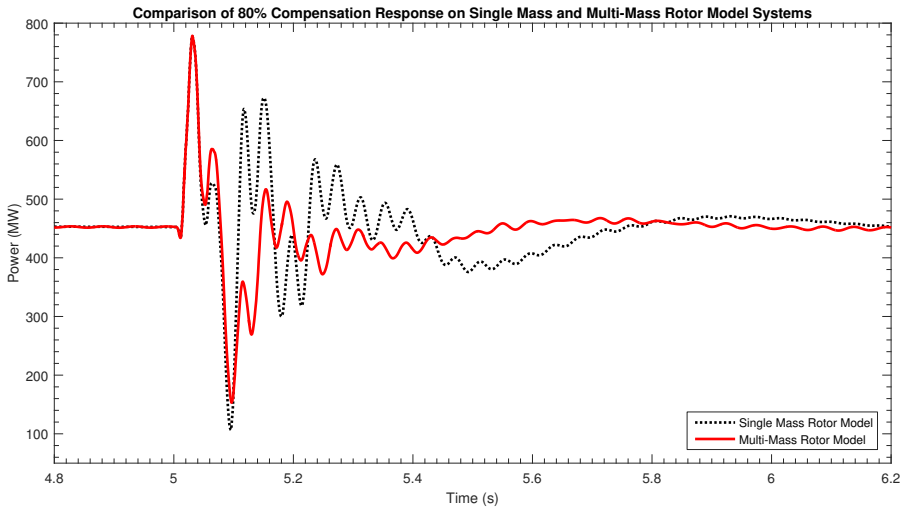

Figure 3.18: 80% Compensation Applied at 5 Seconds to Both the Single Mass Rotor System and the Multi-Mass Rotor System

3.4.5 Testing the Response of the Two Band Multi-Mass MB-SSDC to Faults Occurring While Line is Compensated to 80%

The system was then subjected to four different faults on the generator bus while the system was series compensated at 80%: a single line to ground fault, a line to line fault, a double line to ground fault, and a three phase fault. The results of this fault exposure are shown in Figures 3.19, 3.20, 3.21, 3.22, and 3.23. System stability was maintained throughout all the faults, and steady state operation resumed approximately 1500 ms after the fault was cleared. Recall that the original system model was unstable with the 80% compensation put in the line so fault testing was unable to be performed (see Figure 2.23).

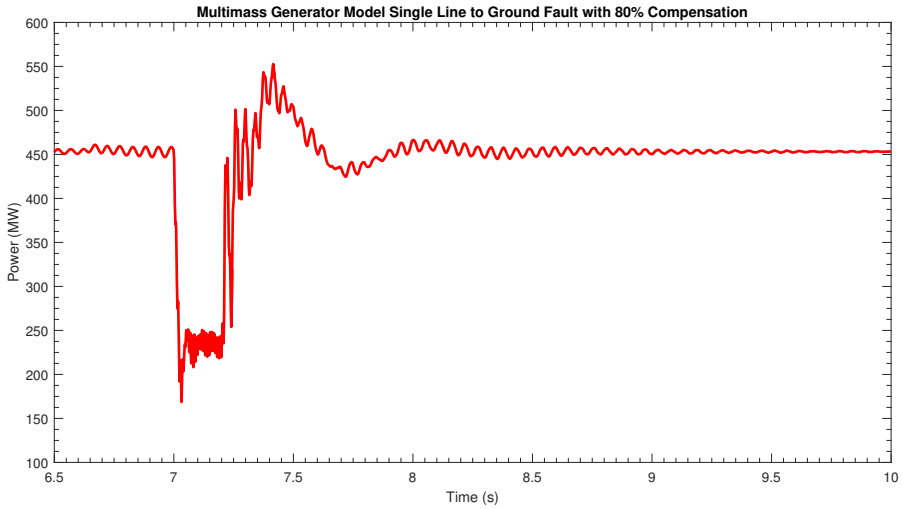

Figure 3.19: Single Line to Ground Fault Applied at 7 Seconds to the 80% Series Compensated Multi-mass System

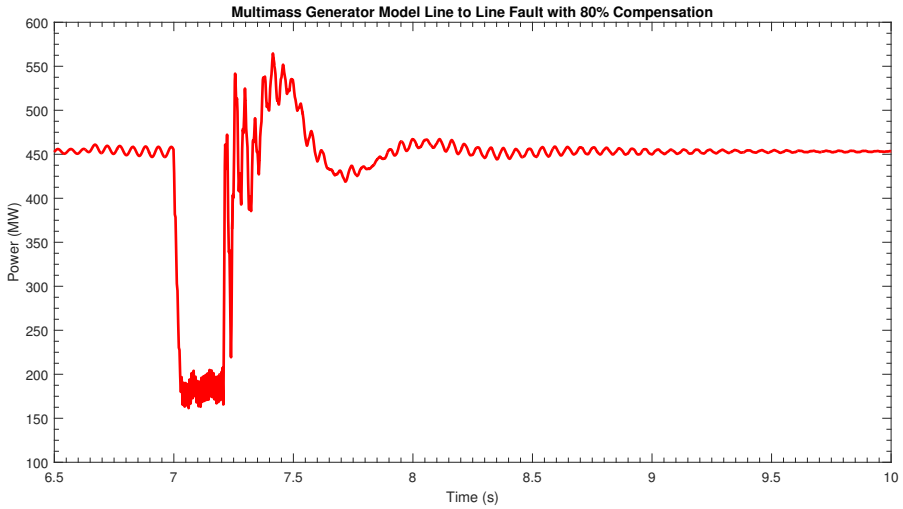

Figure 3.20: Line to Line Fault Applied at 7 Seconds to the 80% Series Compensated Multi-mass System

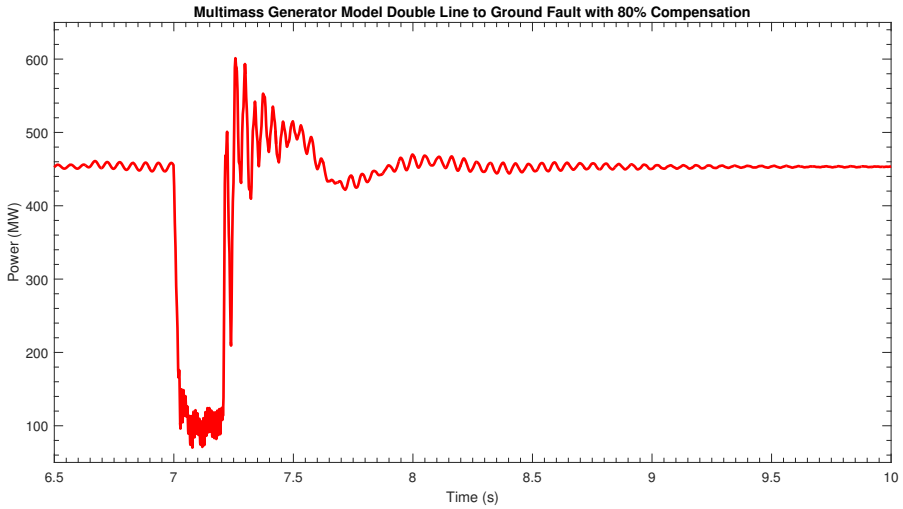

Figure 3.21: Double Line to Ground Fault Applied at 7 Seconds to the 80% Series Compensated Multi-mass System

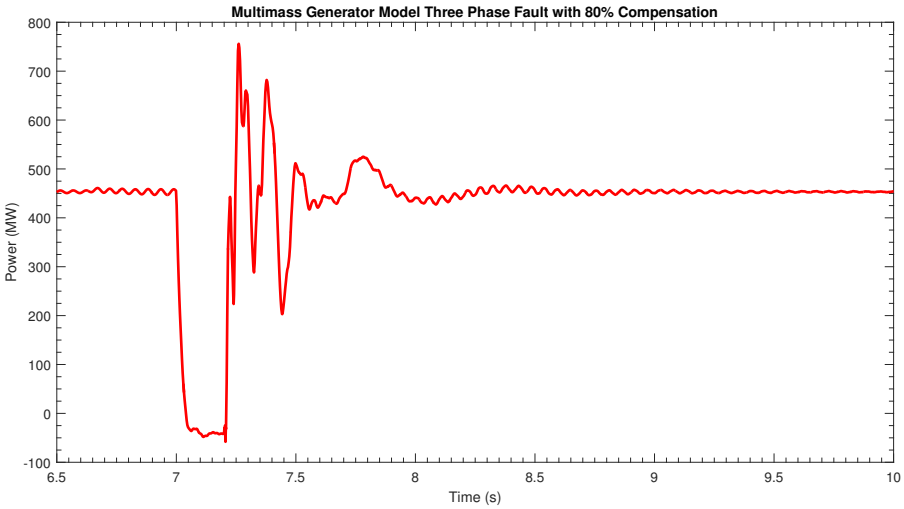

Figure 3.22: Three Phase Fault Applied at 7 Seconds to the 80% Series Compensated Multi-mass System

An overlay of all four faults occurring while the system is compensated to 80% appears in Figure 3.9.

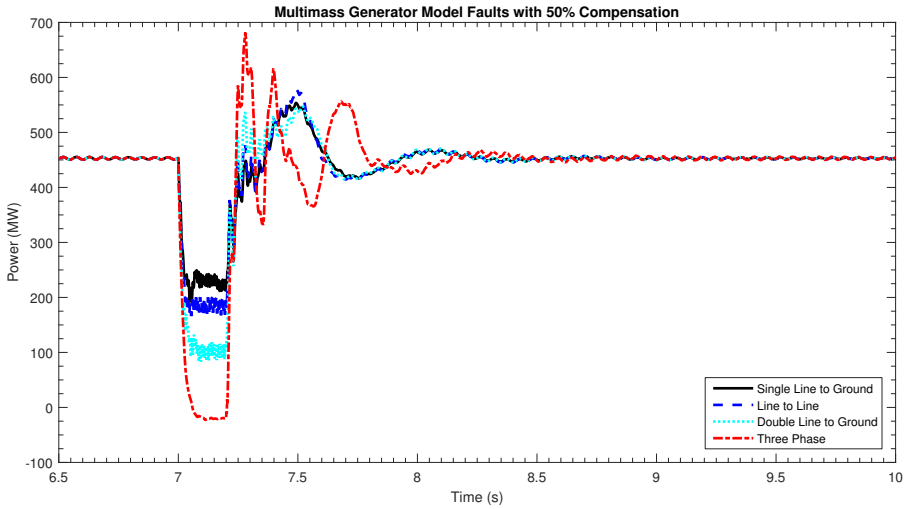

Figure 3.23: Comparison of 4 Fault Types Applied at 7 Seconds to the 80% Series Compensated Multi-mass System

Subsequent testing has revealed the system is able to maintain stability up to a level of 85% compensation with the MBSSDC (30 Hz and the 50 Hz damping bands) added to the base model. Higher levels of compensation resulted in an increasing oscillation in the output power.

The system response to the addition of 85% series compensation to the line is shown in Figure 3.24. The system response to four faults (SLG, L-L, DLG, and three phase) is shown in Figure 3.25.

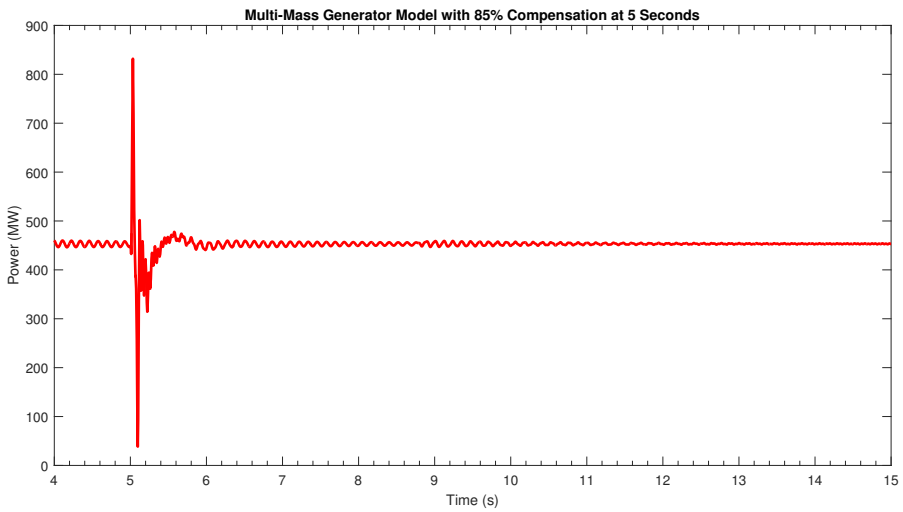

Figure 3.24: Response of the Multi-Mass MBSSDC to 85% Series Compensation

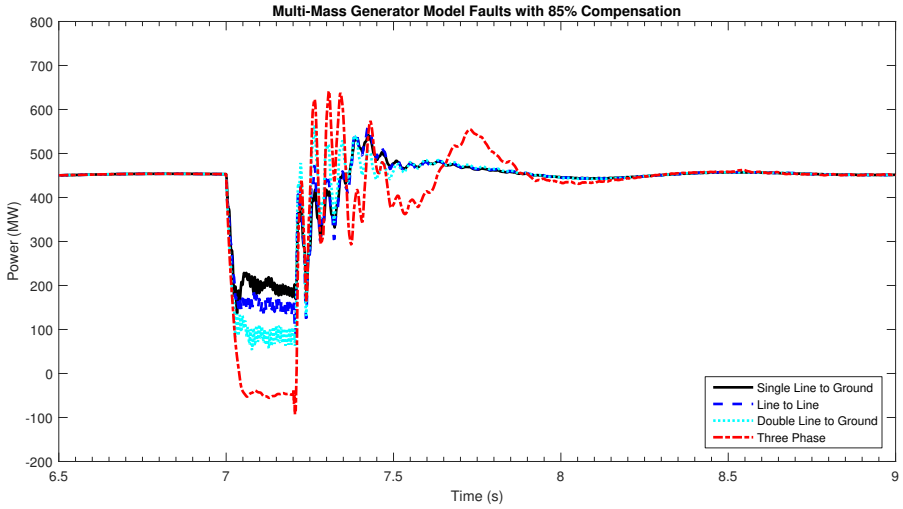

Figure 3.25: Response of the Multi-Mass MBSSDC to Various Faults with 85% Series Compensation

3.5 Summary of the Implementation of the MBSSDC on a Model System with a Multi-Mass Rotor Model

The use of the MBSSDC in the multi-mass rotor model system has greatly improved the stability of the system. Extremely high values of compensation, much higher than would

normally occur in practice, can be inserted in the line and system stability is maintained through normal operation and while faults are present in the system.

The stability improvement from the base system was remarkable, the original system was unstable at levels of compensation of 5% and greater, while the multi-mass rotor MBSSDC model is stable up to levels of 85% series compensation. A comparison of the original system and the multi-mass rotor model MBSSDC for series compensation levels of 8%, 50%, and 80% is shown in Figure 3.26.

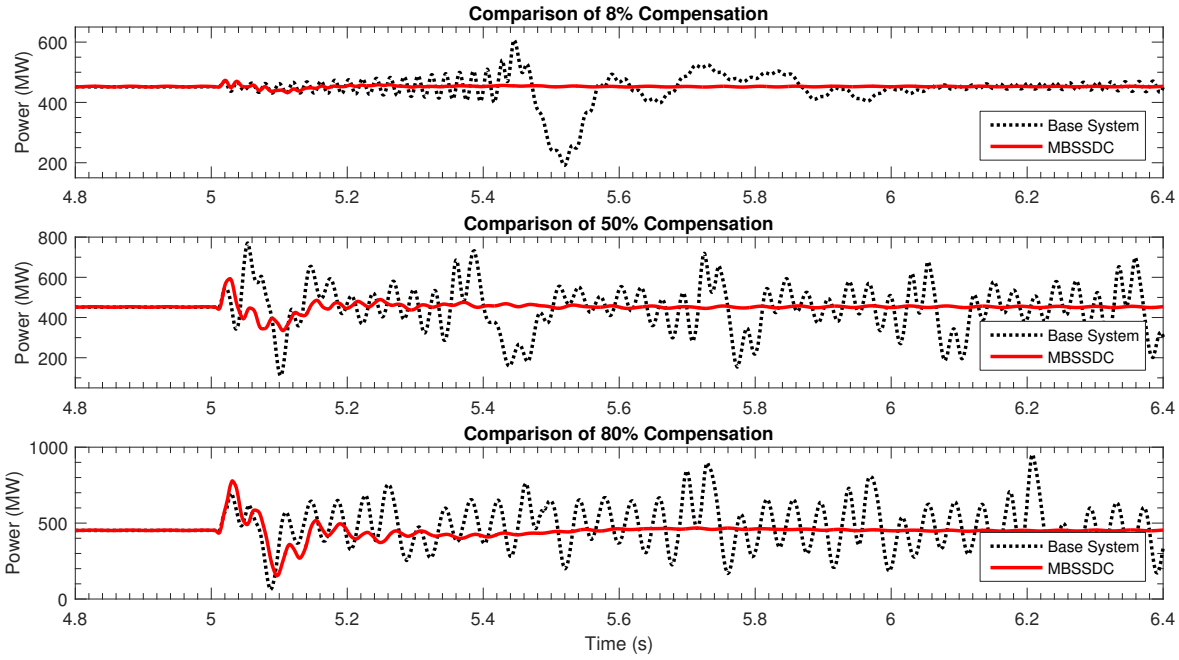

Figure 3.26: Comparison of the Base System to the Multi-Mass MBSSDC at Various Compensation Levels

The testing has shown that the performance of the system with the multi-mass rotor model is not as smooth as it is with the single mass rotor model system. This is to be expected, however as the multi-mass rotor model introduces additional inertial masses and thus additional torsional modes to the system [63]. This has the effect of introducing some additional oscillation in the system response as was seen in the above figures.

Torsional modes may be excited by the generator excitation system due to the low level of damping present in the generator itself [63]. The damping controller presented here has

shown sufficient damping to maintain system stability with the multi-mass rotor added to the system model.

Chapter 4

Simplex Optimization of the MBSSDC

4.1 Introduction

This chapter will detail the process of and results from the application of a simplex optimization on the MBSSDC. The optimization was run on both the single mass and multi-mass system models. The results from the testing of both systems responses to various levels of compensation and line faults is shown. The simplex optimization improved the response of both rotor model systems, decreasing the power swing when compensation was connected, while still maintaining stability through all fault situations tested. The maximum level of series compensation before stability loss occurred increased for the single mass rotor model as well.

4.2 Simplex Optimization

Once the initial results of the MBSSDC were satisfactory - the system response was stable for SSCI events and the controller was not detrimental to the system during normal operation - the design was optimized using a simplex algorithm. The eight time constants in the two supplementary control bands were optimized in this process.

The tuning of the parameters in the proposed MBSSDC controller is quite difficult as discussed earlier in Chapter 1. The multiple frequencies contained in the oscillations means typical control system techniques for tuning will not be effective, necessitating a nonlinear time domain optimization. The proposed MBSSDC utilizes a simplex optimization procedure

to tune the parameters of the controller.

The simplex method in combination with the EMT simulations provides a nonlinear time domain multi-run optimization of the objective function. A flow chart showing the steps involved in running the time simplex algorithm in conjunction with an EMT program (PSCAD in this case) is shown in Figure 4.1. The program is initialized with an initial feasible set of numbers for the time constants to be optimized. The values used will be the time constants designed in Chapters 2 and 3 for the single mass and multi-mass rotor systems.

The EMT program runs through the simulation and the data from the objective function is collected and analyzed by the simplex algorithm. If convergence has been reached, the optimization is complete, but if the program has not converged, a new set of time constant values is calculated based upon the results of the previous run and these new time constants are loaded into the EMT program and the simulation begins again with the updated values. Each iterartion of the algorithm will bring the system closer to the optimum point. This process is repeated until convergence is reached, the point where no adjacent solution is an improvement on the current points. The starting point of the optimzation must be a feasible solution or the algorithm will diverge.

The setup for the optimization routine within the PSCAD model appears below in Figure 4.2.

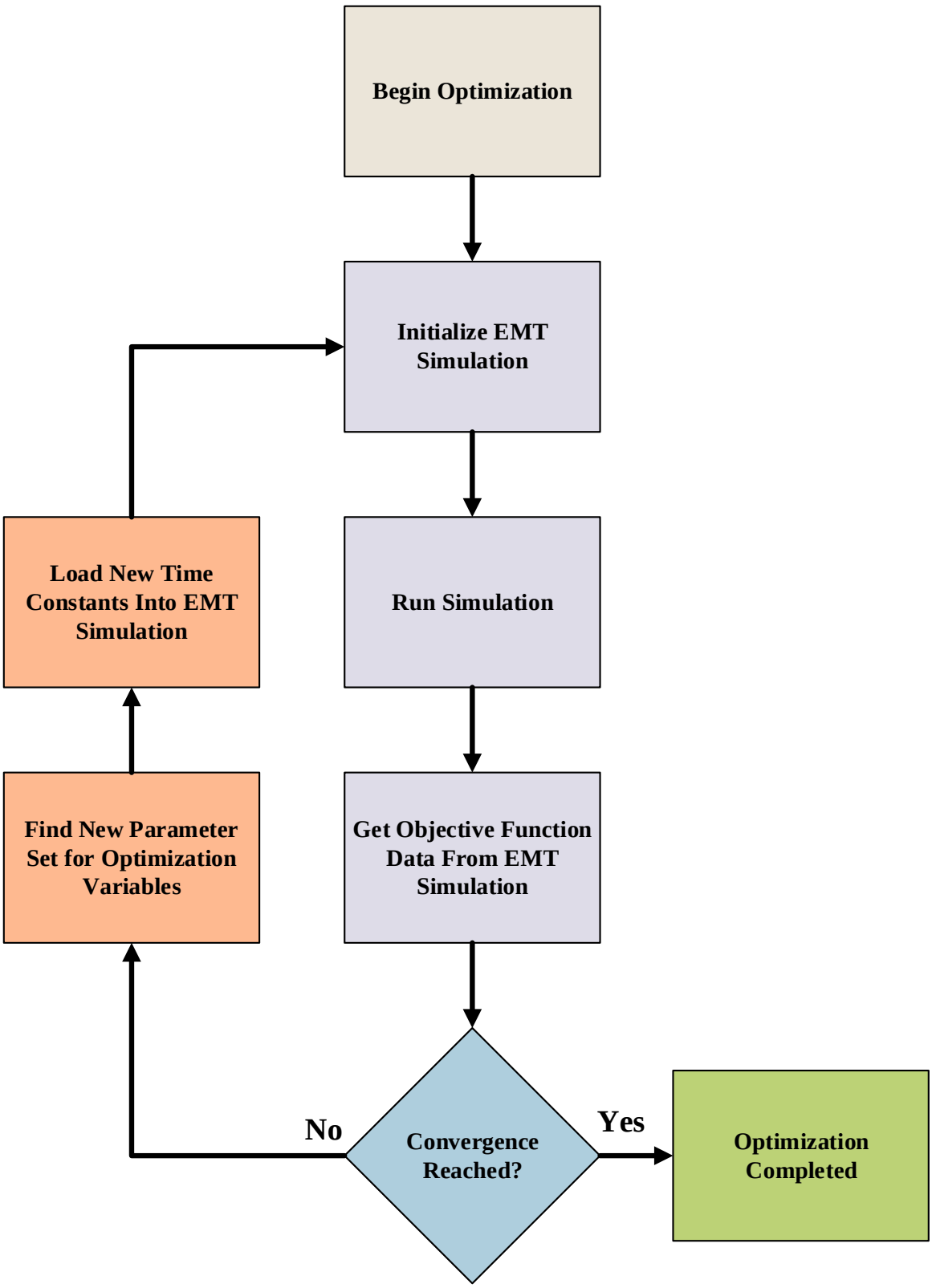

Figure 4.1: Simplex Optimization Flow Chart for EMT Simulation

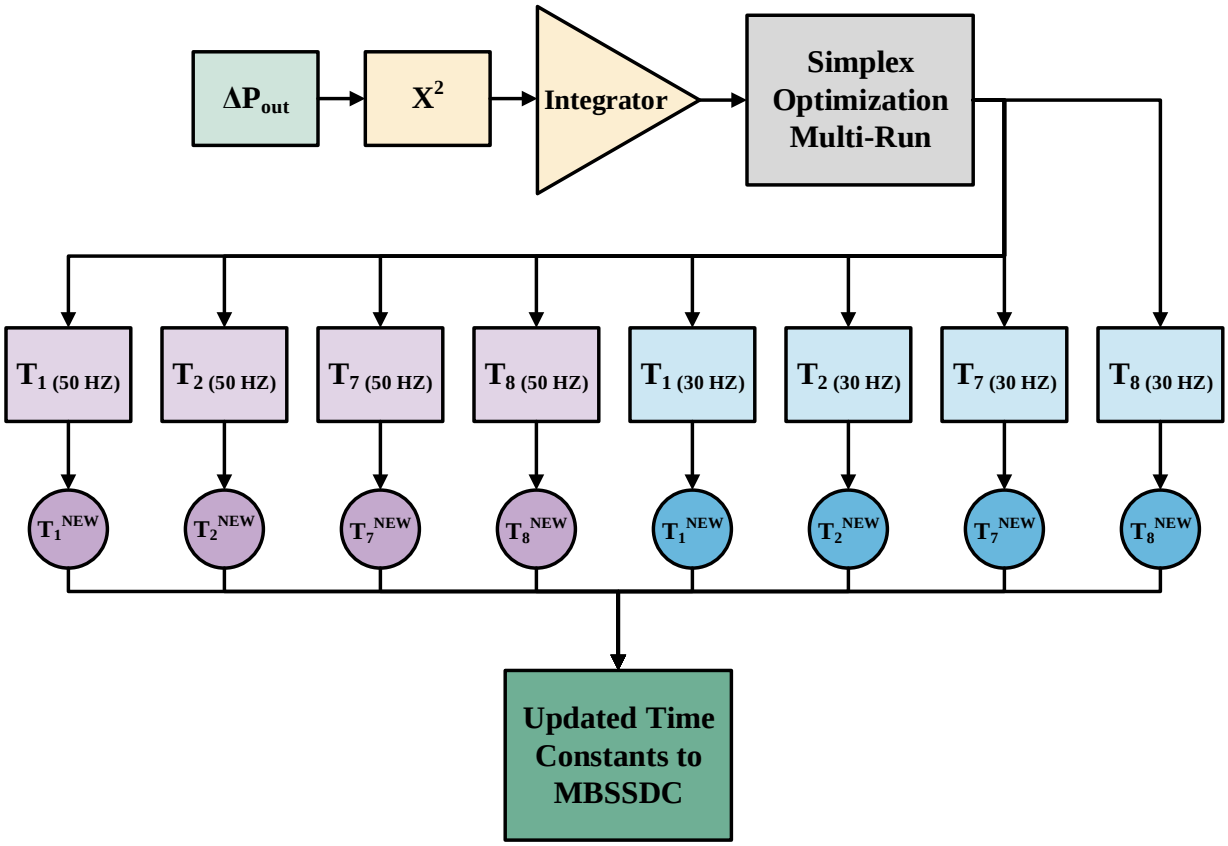

Figure 4.2: Simplex Optimization Setup for the MBSSDC Model

Figure 4.2 illustrates the setup of the optimization controller developed within the model. Eight different inputs have been setup to be used/tested during the optimization routine. simplex optimization works to minimize the objective function, which in this case is a signal representative of the change in output power of the wind farm. The Δ_P is squared to force all deviations from the set point to be positive. The squared Δ_P is then integrated to allow the error to be accumulated over the optimization period. The eight variables used within the optimization routine were applied to the eight time constants of the lead lag controllers in the MBSSDC.

Each run of the simulation consisted of the connection of 50% series compensation to the model system with the MBSSDC connected. Figure 4.3 shows the MBSSDC system with the addition of the simplex optimization setup.

The goal of the optimization was to minimize the brief disturbance experienced when the series compensation was first connected to the transmission line, while ensuring that the system remained stable when other levels of compensation were connected and while the system experienced a fault.

Simplex optimization is an algebraic iterative technique for the solving of multi-variable problems, or in this case, the minimization of an objective function [64] [65]. The objective function to minimize is the change in rotor speed ($\Delta\omega$) of the wind-farm, which is proportional to the change in output power (Δ_P). Minimizing the change in rotor speed (and thus the output power) achieves more efficient damping of the disturbances in the system.

The multi-run time domain optimization simplex optimization works algebraically to minimize the objective function, starting with an initial feasible solution (in this case the initial time constants for the lead-lag controllers of the MBSSDC shown in table 2.14) and iterating a variable and retesting the objective function [66]. The simplex optimization analyzed the Δ_P signal from 5 seconds (when the series compensation was connected) to 7 seconds (after the series compensation disturbance has settled).

The simulations were run on a computer using a Intel Core i7-2720QM Quad-Core processor (2.20GHz, 6MB L3, 1333MHz FSB) with 16 gigabytes of RAM and an SSD for the hard drive, each optimization run took approximately 30 seconds to complete.

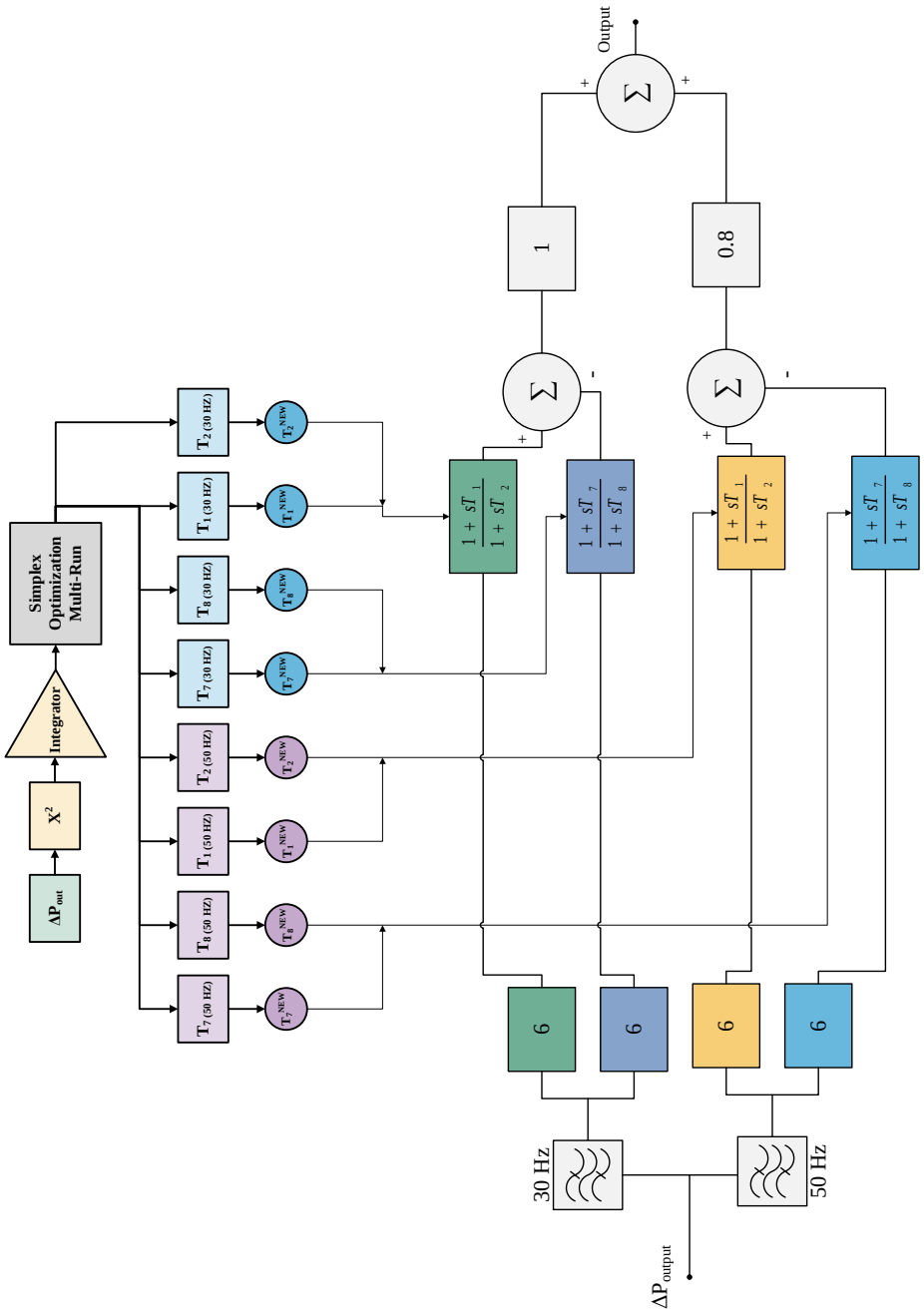

Figure 4.3: Simplex Optimization Setup for the MBSSDC Model

When there is no adjacent solution that is improved in comparison to the current solution, the problem is considered to be minimized [67]. This iterative optimization process is performed using all eight of the time constants used in the lead-lag controllers of the MBSSDC concurrently.

As the simplex algorithm moves through the various feasible states along an 'N' sided polygon during its multi-run optimization routine (with 'N' representing the number of variables being used by the algorithm in searching for an optimum solution, [this optimization used eight variables]), the complexity and time period of each iteration grows significantly with each variable added to the optimization.

4.3 Results from the Simplex Optimization of the Single-Mass Two Band MBSSDC

The simplex optimization was run on the single-mass MBSSDC using the eight time constants from the two bands of the differential lead-lag controllers as shown in Figure 4.3.

4.3.1 Initial and Final Time Constants Used in the Simplex Optimization of the Single-Mass Two Band MBSSDC

The initial values for the time constants used in the lead-lag controllers in each of the MBSSDC bands appear in Table 4.1.

Table 4.1: Initial Values for 50 Hz and 30 Hz Damping Bands during the Simplex Optimization

$Freq$	T_1	T_2	T_7	T_8
50 Hz	0.001125	0.00225	0.00225	0.0045
30 Hz	0.001876	0.003751	0.003751	0.007503

The final values for the time constants used in the lead-lag controllers in each of the MBSSDC bands are listed in Table 4.2. These are the values the simplex optimization converged to after 174 iterations taking about 90 minutes to complete.

Table 4.2: Optimized Values for 50 Hz and 30 Hz Damping Bands

$\boldsymbol{Freq}$	$\boldsymbol{T_1}$	$\boldsymbol{T_2}$	$\boldsymbol{T_7}$	$\boldsymbol{T_8}$
50 Hz	0.0011019498	0.0020701399	0.0021716501	0.004515348
30 Hz	0.0019792683	0.0035663708	0.0036798701	0.0077038205

The transfer function for simplex optimized dual band damping controller is shown in equation 4.1.

$$Y(s) = \frac{1.824 \times 10^{-10}s^4 + 4.28 \times 10^{-7}s^3 + 1.857 \times 10^{-4}s^2 + 21.22 \times 10^{-3}s}{2.568 \times 10^{-10}S^s + 2.863 \times 10^{-7}s^3 + 1.11 \times 10^{-4}s^2 + 17.86 \times 10^{-3}s + 1} \tag{4.1}$$

The system was tested under a variety of compensation levels and fault types to ensure the system remained stable. Figures 4.4, 4.5, and 4.6 show the responses of the simplex optimized single mass MBSSDC to the 4 different faults occurring while the system was compensated at 8%, 50%, and 80% respectively.

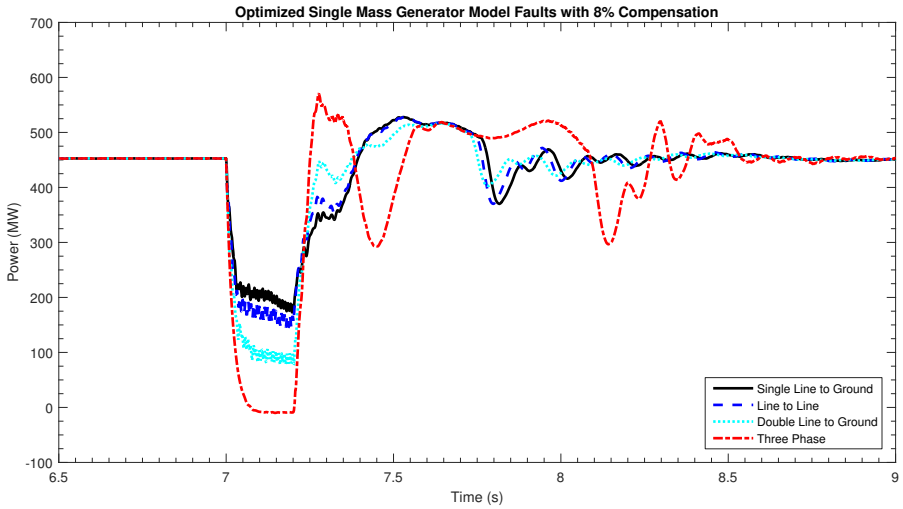

Figure 4.4: Comparison of the output waveforms for four faults on the simplex optimized single mass MBSSDC with 8% compensation

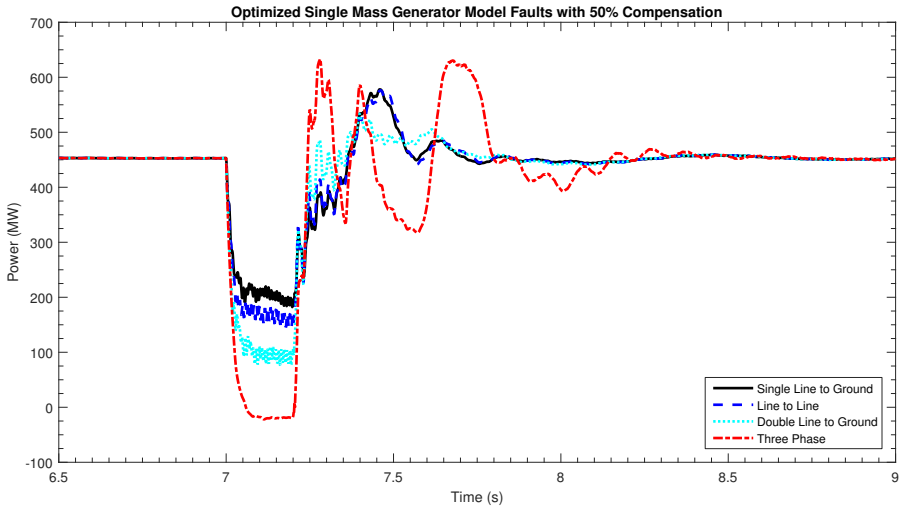

Figure 4.5: Comparison of the output waveforms for four faults on the simplex optimized single mass MBSSDC with 50% compensation

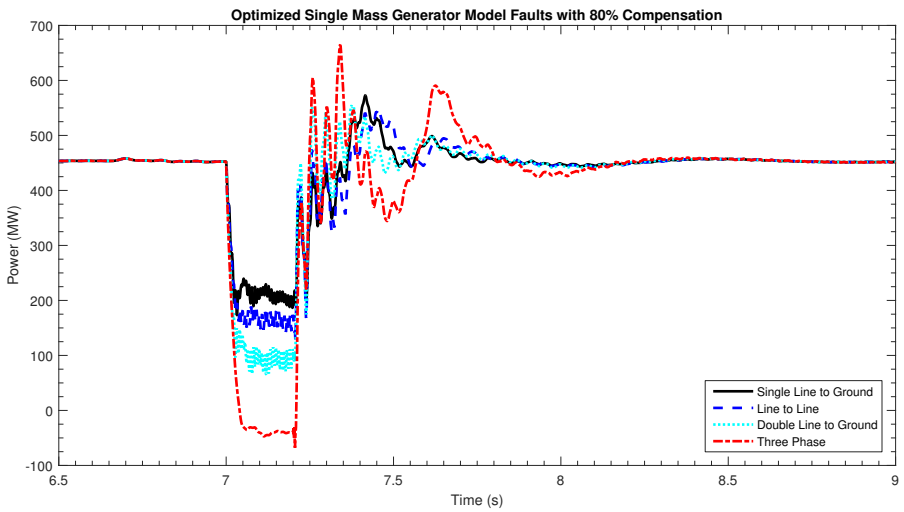

Figure 4.6: Comparison of the output waveforms for four faults on the simplex optimized single mass MBSSDC with 80% compensation

The results of the simplex optimization gave the design some modest but definite performance improvement. Graphs showing the system response to the addition of series compensation values of 8%, 50%, and 80% for both the non-optimized and optimized single mass model system are shown in Figures 4.7, 4.9, and 4.11.

While the two signals appear to overlap on each other for much of the transient period, it is visible that the optimized response has a lower change in power output indicating that the optimization was successful.

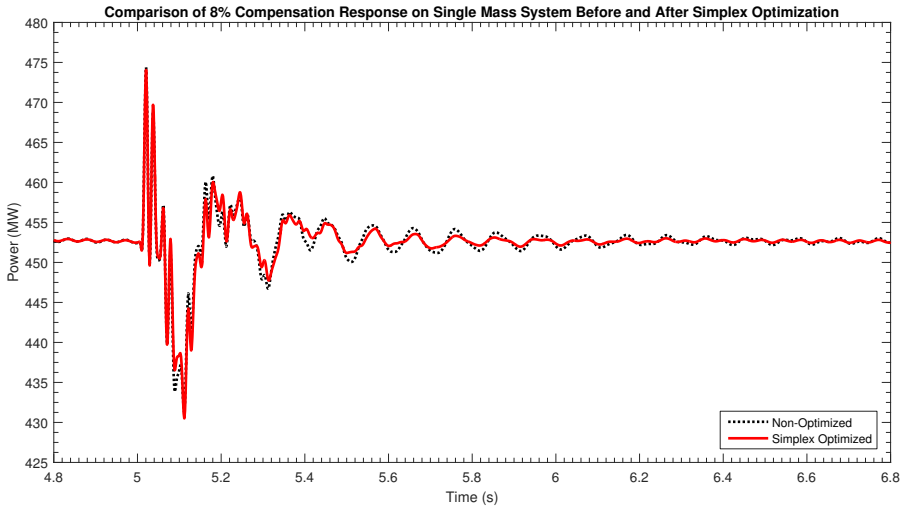

Figure 4.7: Comparison of the output waveforms for the non-optimized and the simplex optimized single mass MBSSDC for 8% compensation

Appearing in Figure 4.8 is a graph showing the response of the optimized and non-optimized MBSSDC system to various faults at the generation bus. These waveforms show there is some improvement with the optimized system.

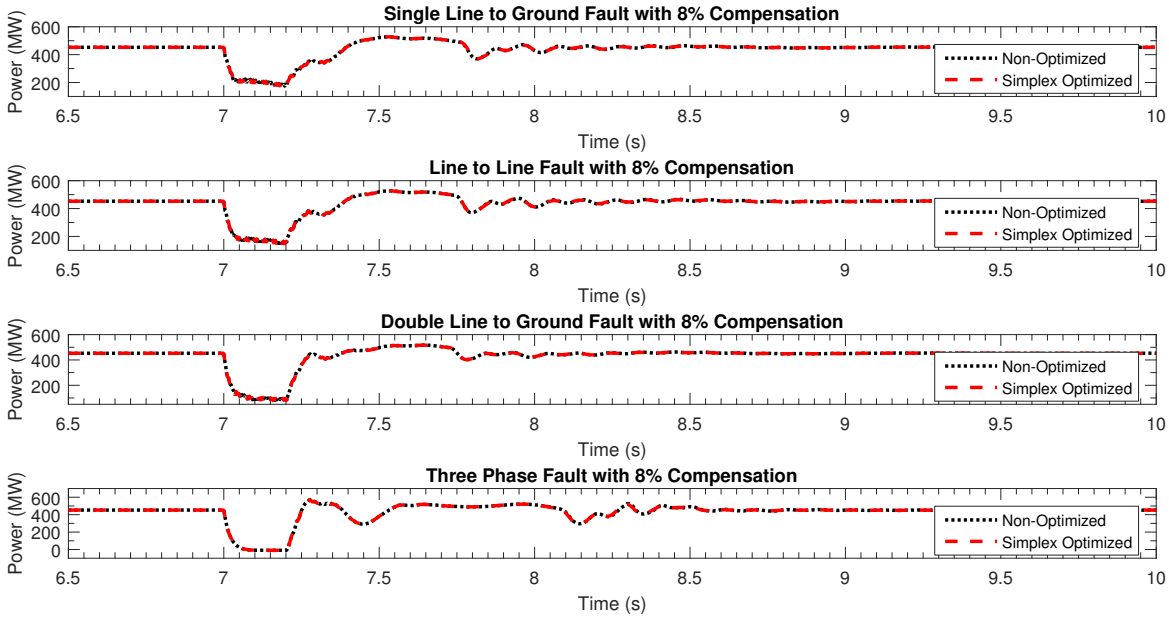

Figure 4.8: Comparison of the fault waveforms for the non-optimized and the simplex optimized single-mass MBSSDC for 8% compensation

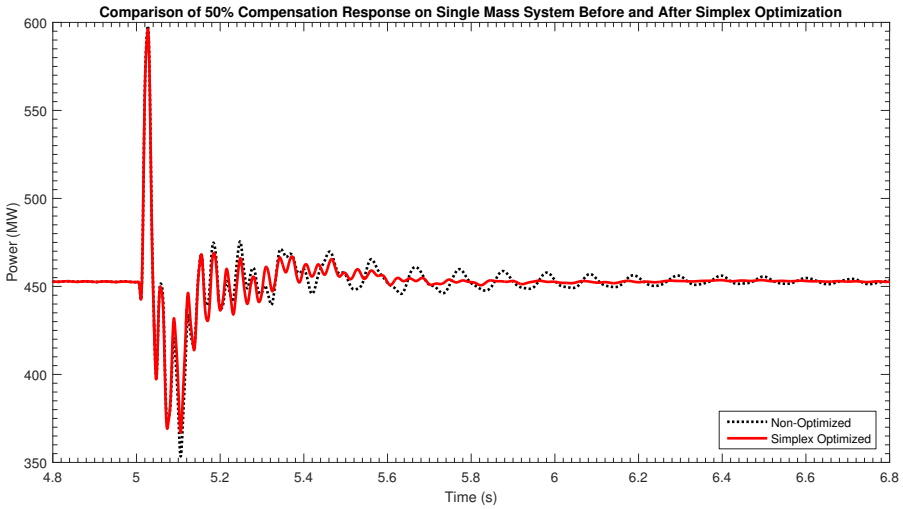

Figure 4.9: Comparison of the output waveforms for the non-optimized and the simplex optimized single mass MBSSDC for 50% compensation

Appearing in Figure 4.10 is a graph showing the response of the optimized and non-optimized MBSSDC system to various faults at the generation bus. These waveforms show there is some improvement with the optimized system.

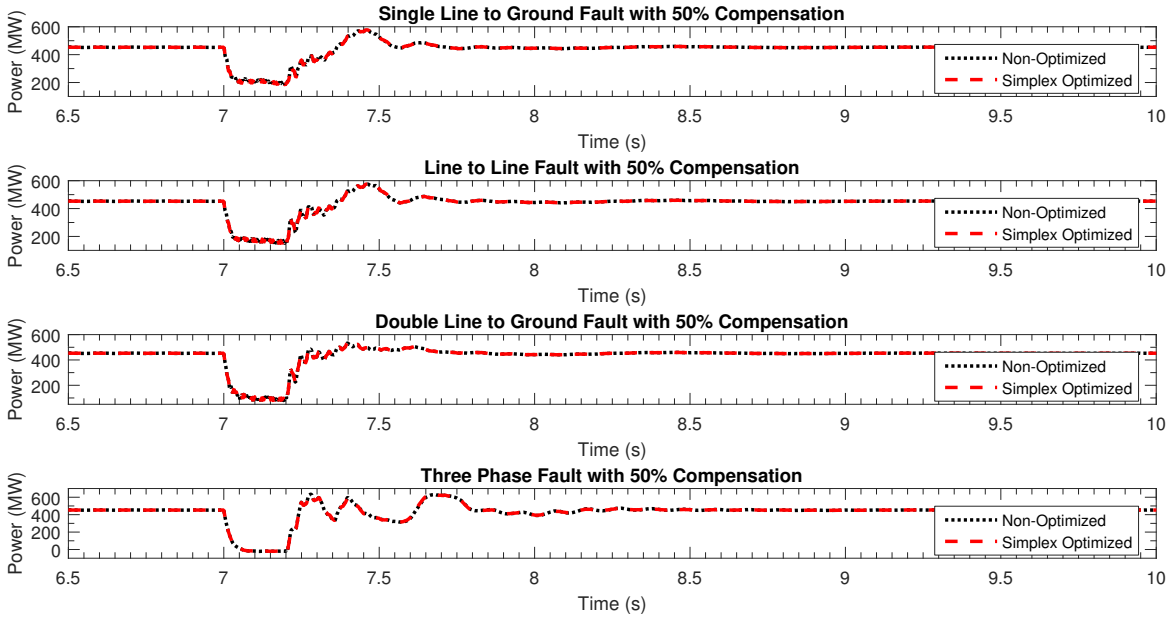

Figure 4.10: Comparison of the fault waveforms for the non-optimized and the simplex optimized single-mass MBSSDC for 50% compensation

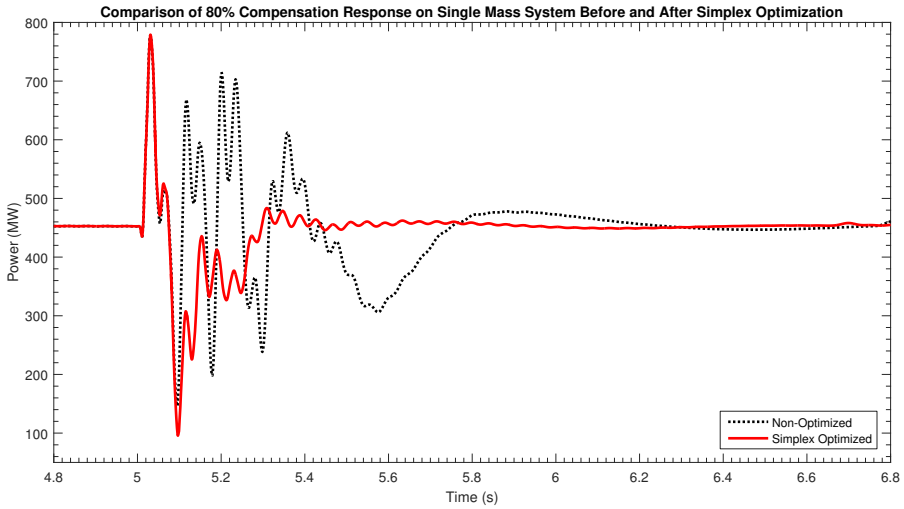

Figure 4.11: Comparison of the output waveforms for the non-optimized and the simplex optimized single mass MBSSDC for 80% compensation

Appearing in Figure 4.12 is a graph showing the response of the optimized and non-optimized MBSSDC system to various faults at the generation bus. These waveforms show there is some improvement with the optimized system.

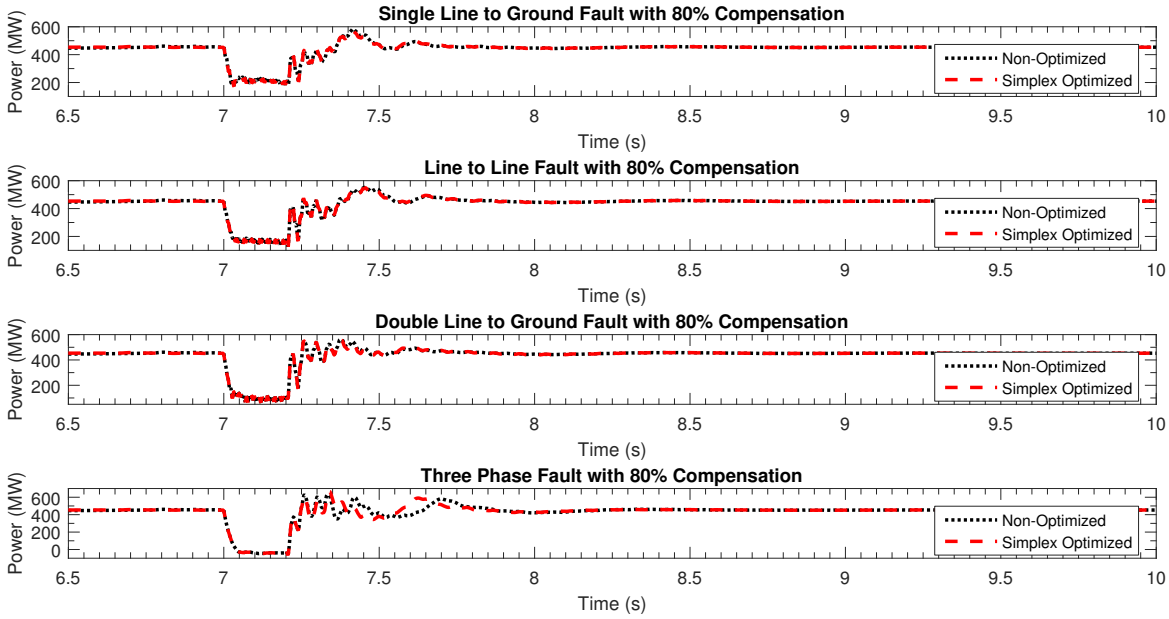

Figure 4.12: Comparison of the fault waveforms for the non-optimized and the simplex optimized single-mass MBSSDC for 80% compensation

One major result of the optimization procedure that is not visible in the above figures is that the level of compensation through which the system is able to deliver power through in a stable manner has increased. Before optimization the system would remain stable to approximately 94% compensation, while after the optimization process, this level increased to approximately 97%.

The system response to the addition of 97% series compensation to the line is shown in Figure 4.13. The system response to four faults (SLG, L-L, DLG, and three phase) is shown in Figure 4.14.

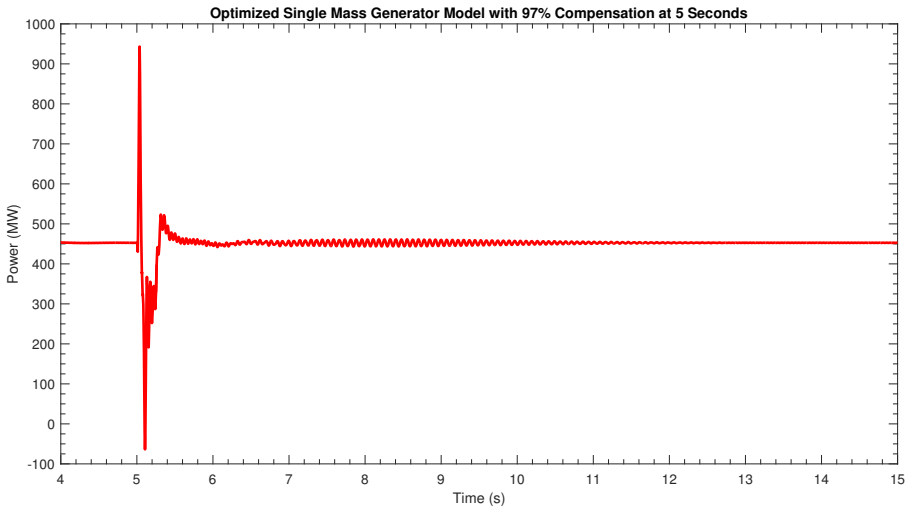

Figure 4.13: Response of the Simplex Optimized MBSSDC to 97% Series Compensation

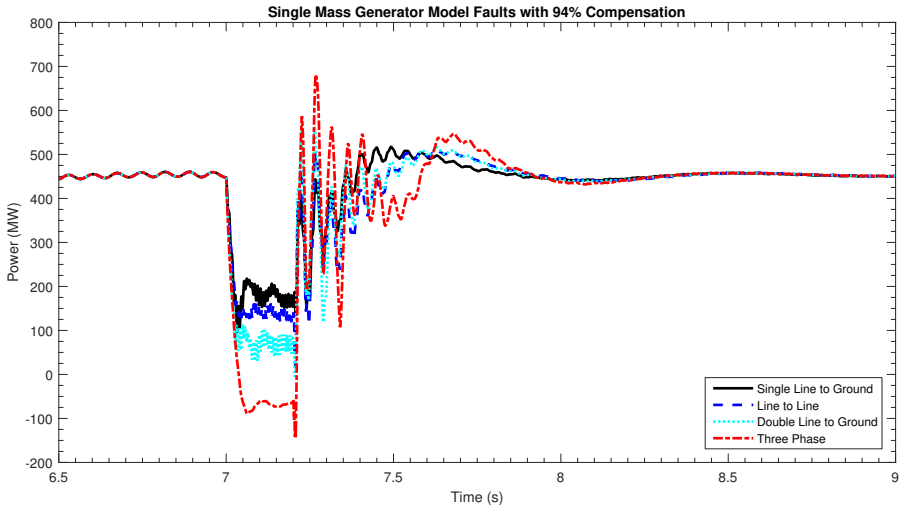

Figure 4.14: Response of the Simplex Optimized MBSSDC to Various Faults with 97% Series Compensation

A 3% increase in the maximum stable level of series compensation is a significant improvement that optimizing the system has achieved. Further gains could potentially be realized by using more variables in the simplex optimization, including the gain values in the MBSSDC, and possibly the proportional gain and integral time constant mentioned above in the PID controller section of the dq0 loop.

4.4 Results from the Simplex Optimization of the Multi-Mass Two Band MBSSDC

The simplex optimization was run on the multi-mass MBSSDC to optimize the values for the four time constants in each band of the MBSSDC (eight time constants in total) in the same manner as with the single mass MBSSDC. The multi-mass MBSSDC took much longer to converge than the single-mass MBSSDC. As mentioned, the single-mass MBSSDC converged in 174 iterations while the multi-band MBSSDC required 498 iterations to converge requiring about 4 hours of processing time. Series compensation was applied to the system at 5 seconds, while the objective function was recorded from 4 seconds to 7 seconds.

4.4.1 Initial and Final Time Constants Used in the Simplex Optimization of the Multi-Mass Two Band MBSSDC

Simplex optimization has resulted in the alteration of the time constants used in the lead-lag block of the MBSSDC. The initial values for the time constants used in the lead-lag controllers in each of the MBSSDC bands are listed in Table 4.3.

Table 4.3: Initial Values for 50 Hz and 30 Hz Damping Bands during the Simplex Optimization

$Freq$	T_1	T_2	T_7	T_8
50 Hz	0.001125	0.00225	0.00225	0.0045
30 Hz	0.001876	0.003751	0.003751	0.007503

The final values for the time constants used in the lead-lag controllers in each of the MBSSDC bands are shown in Table 4.4. These are the values the Simplex optimization converged to after 498 iterations.

Table 4.4: Optimized Values for 50 Hz and 30 Hz Damping Bands

$Freq$	T_1	T_2	T_7	T_8
50 Hz	0.0011261759	0.0022591941	0.0022636103	0.0045002771
30 Hz	0.0018882093	0.0037561412	0.0037449591	0.0075226409

The transfer function for simplex optimized dual band damping controller with the multi-mass rotor model is shown in equation 4.2.

$$Y(s) = \frac{2.185 \times 10^{-12}s^4 + 2.693 \times 10^{-7}s^3 + 1.378 \times 10^{-4}s^2 + 16.76 \times 10^{-3}s}{2.873 \times 10^{-10}s^4 + 3.057 \times 10^{-7}s^3 + 1.147 \times 10^{-4}s^2 + 18.04 \times 10^{-3}s + 1} \tag{4.2}$$

No time constant is significantly altered from its original value, but all 8 time constants did end being altered by the simplex optimization process.

The system was tested under a variety of compensation levels and fault types to ensure the system remained stable. Figures 4.15, 4.16, and 4.17 show the response of the simplex optimized multi-mass MBSSDC to the 4 different faults occurring while the system was compensated at 8%, 50% and 80%.

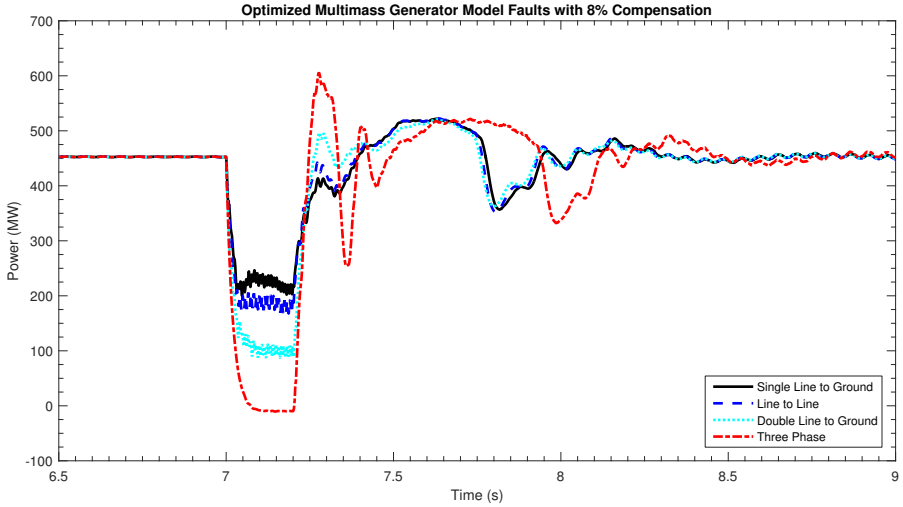

Figure 4.15: Comparison of the output waveforms for four faults on the simplex optimized single mass MBSSDC with 8% compensation

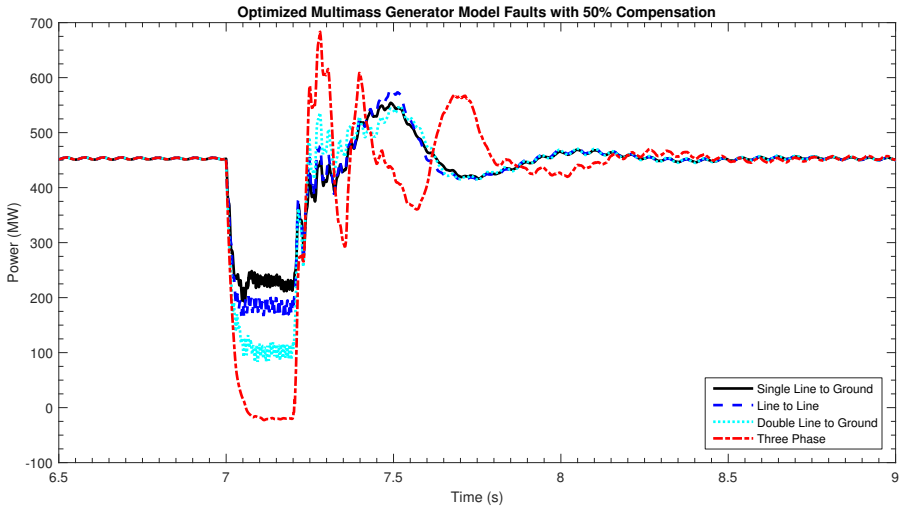

Figure 4.16: Comparison of the output waveforms for four faults on the simplex optimized multi mass MBSSDC with 50% compensation

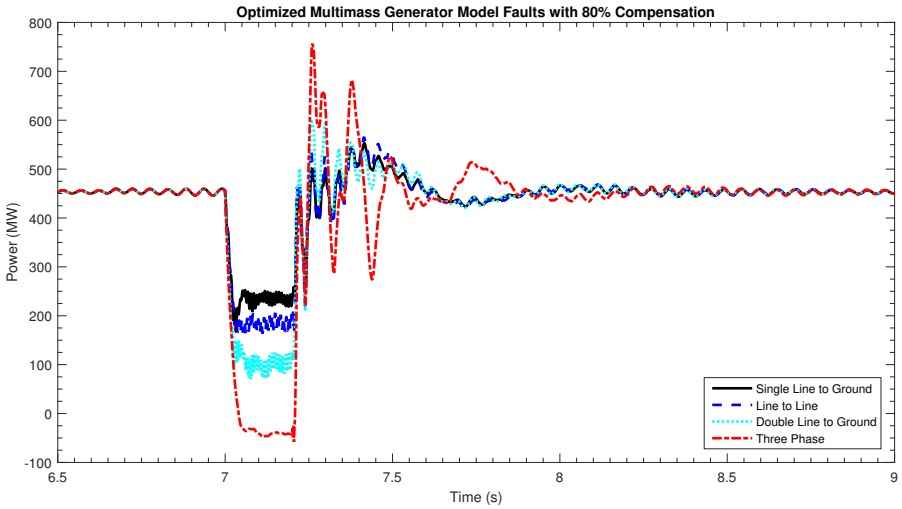

Figure 4.17: Comparison of the output waveforms for four faults on the simplex optimized multi mass MBSSDC with 80% compensation

The results of the simplex optimization gave the design some modest but definite performance improvement. Graphs showing the system response to the addition of series compensation values of 8%, 50%, and 80% for both the non-optimized and optimized multi-mass model system are shown in Figures 4.18, 4.20, and 4.22. It is clear that the improvement is modest in comparison to the improvement made on the single-mass model (Figure 4.9).

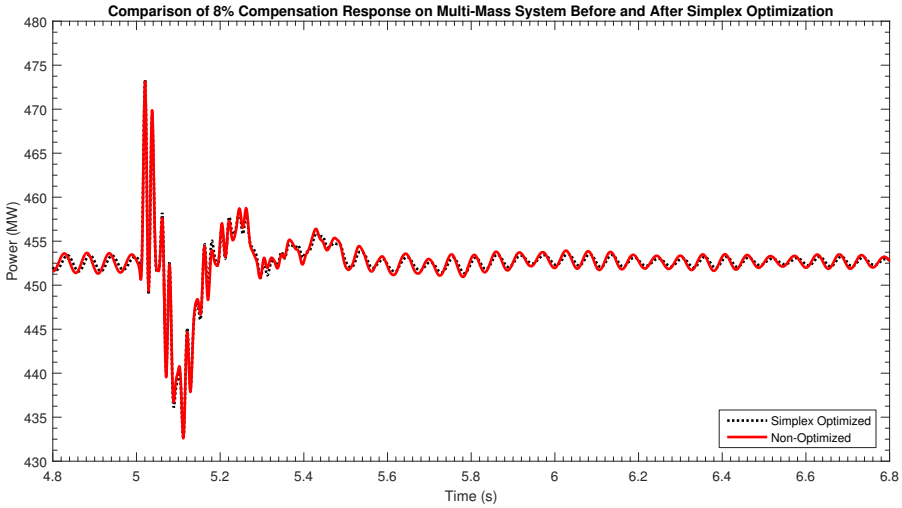

Figure 4.18: Comparison of the output waveforms for the non-optimized and the simplex optimized multi-mass MBSSDC for 8% compensation

Appearing in Figure 4.19 is a graph showing the response of the optimized and non-optimized MBSSDC system to various faults at the generation bus. These waveforms show there is some improvement with the optimized system.

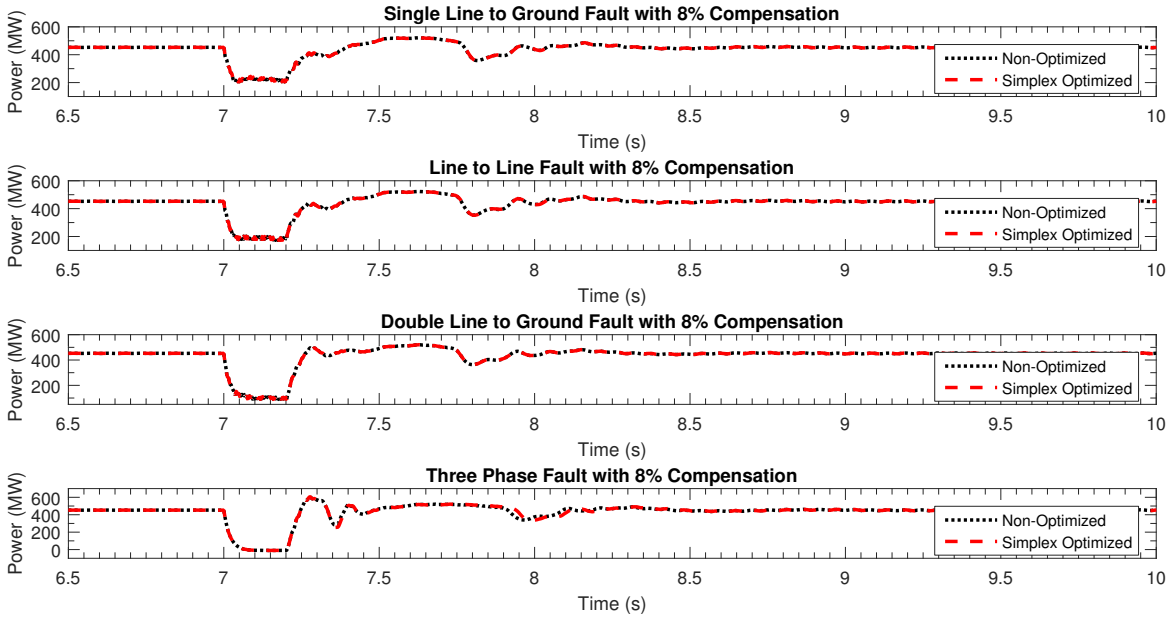

Figure 4.19: Comparison of the fault waveforms for the non-optimized and the simplex optimized multi-mass MBSSDC for 8% compensation

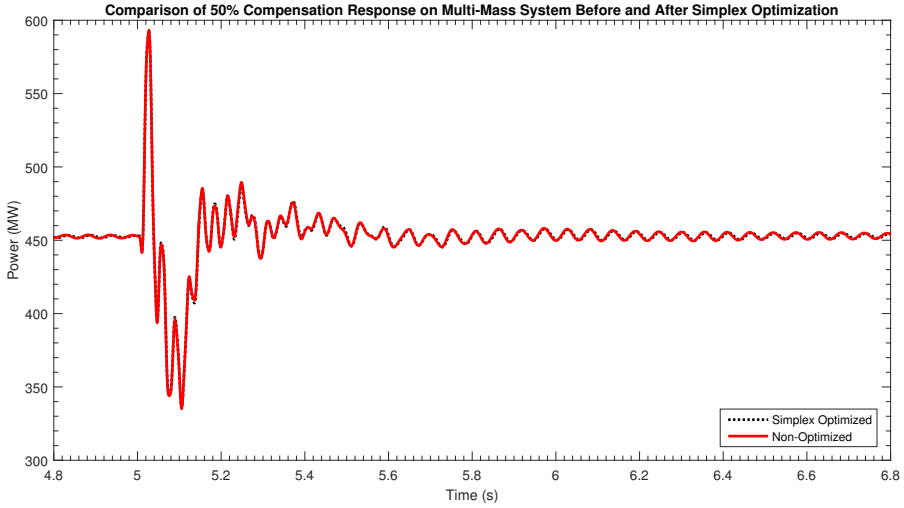

Figure 4.20: Comparison of the output waveforms for the non-optimized and the simplex optimized multi-mass MBSSDC for 50% compensation

Figure 4.21 is a graph showing the response of the optimized and non-optimized MBSSDC system to various faults at the generation bus. As with the previous compensation levels, these waveforms show there is some improvement with the optimized system.

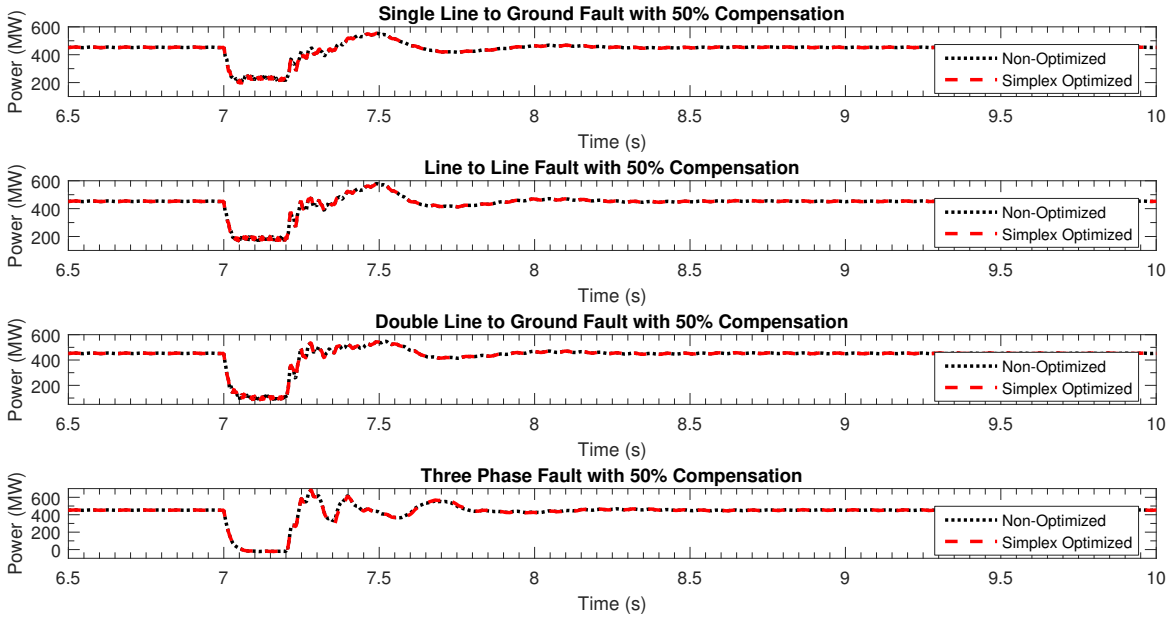

Figure 4.21: Comparison of the fault waveforms for the non-optimized and the simplex optimized multi-mass MBSSDC for 50% compensation

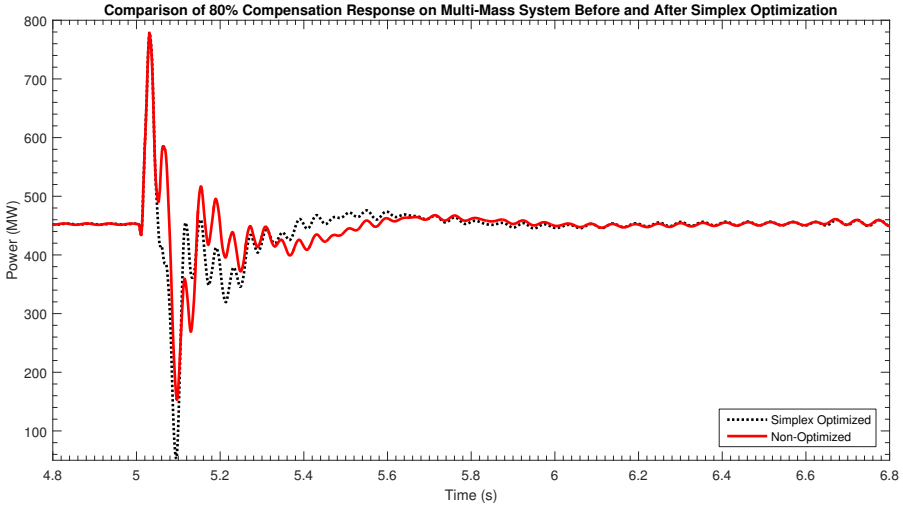

Figure 4.22: Comparison of the output waveforms for the non-optimized and the simplex optimized multi-mass MBSSDC for 80% compensation

Figure 4.23 is a graph showing the response of the optimized and non-optimized MBSSDC system to various faults at the generation bus. Again these waveforms show there is some improvement with the optimized system.

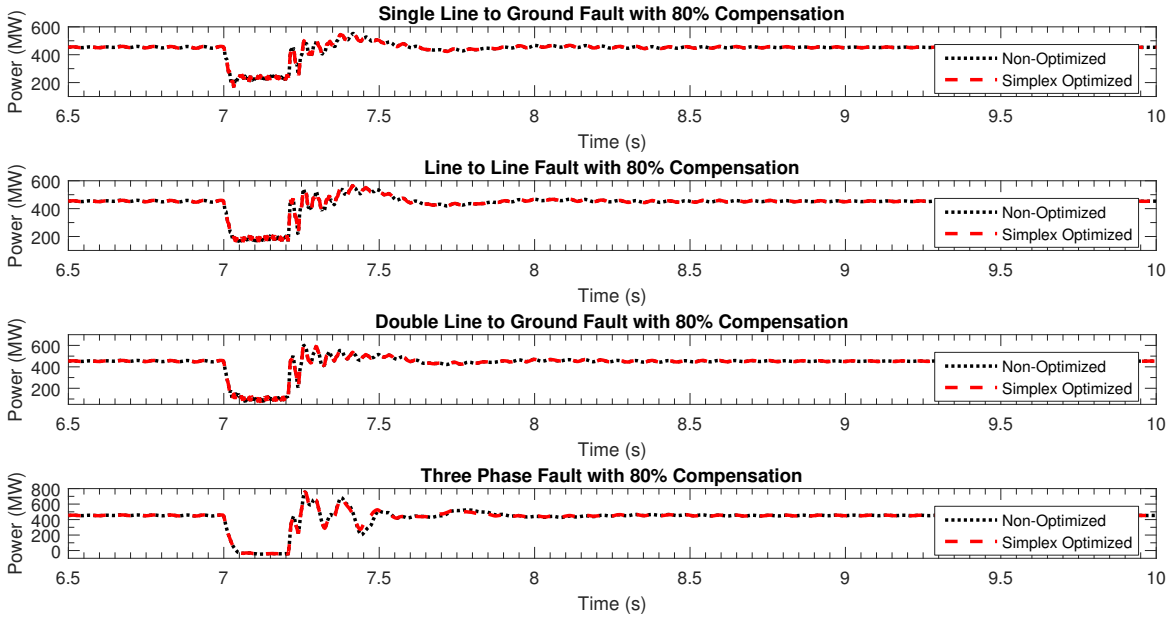

Figure 4.23: Comparison of the fault waveforms for the non-optimized and the simplex optimized multi-mass MBSSDC for 80% compensation

Unlike the improvement seen with the single-mass MBSSDC simplex optimization, the maximum level of compensation remained the same at 85% for the multi-mass MBSSDC after simplex optimization.

The system response to the addition of 85% series compensation to the line is shown in Figure 4.24. The system response to four faults (SLG, L-L, DLG, and three phase) is shown in Figure 4.25.

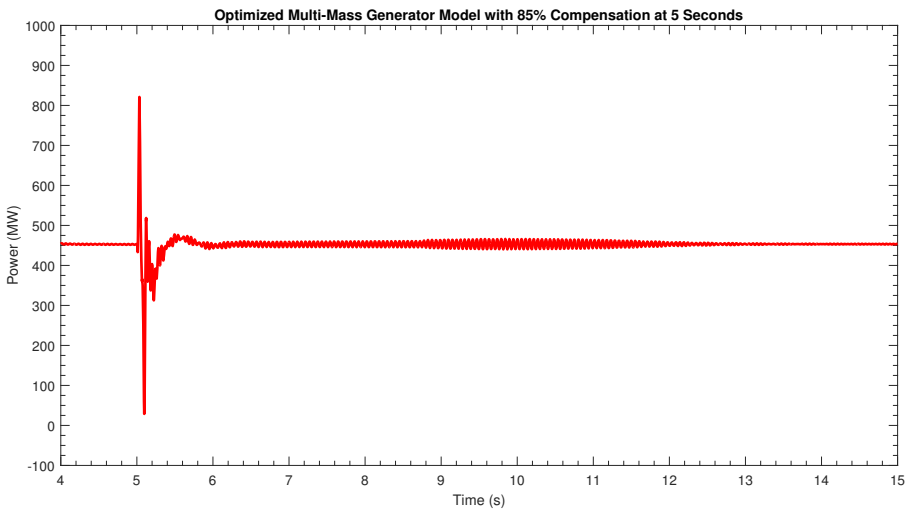

Figure 4.24: Response of the Simplex Optimized Multi-Mass MBSSDC to 85% Series Compensation

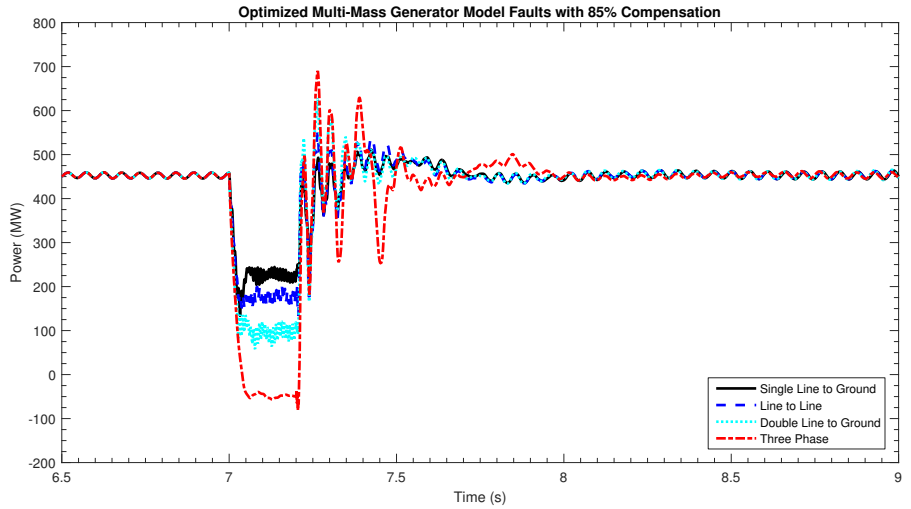

Figure 4.25: Response of the Simplex Optimized Multi-Mass MBSSDC to Various Faults with 85% Series Compensation

4.5 Summary of Simplex Optimization on the MB-SSDC

The use of the simplex optimization on both the single-mass and multi-mass MBSSDC yielded improvements in the system. The optimization took 174 iterations on the single-

mass model while the multi-mass model required 498 iterations to converge. Tables 4.5 and 4.6 shows some numerical results from the optimized and non-optimized systems.

Table 4.5: Numerical Comparison of Optimized and Non-Optimized Single Mass Rotor Model System

Parameter	***Optimized System***	***Non-Optimized System***
Maximum Series Compensation	97%	94%
8% Series Compensation Applied		
Overshoot	4.7%	4.8%
Undershoot	4.9%	4.8%
Settling Time (2% of Final Value)	0.1 s	0.1 s
50% Series Compensation Applied		
Overshoot	31%	32%
Undershoot	19%	22%
Settling Time (5% of Final Value)	0.143 s	0.247 s
80% Series Compensation Applied		
Overshoot	72%	72%
Undershoot	79%	68%
Settling Time (5% of Final Value)	0.351 s	0.962 s

Table 4.6: Numerical Comparison of Optimized and Non-Optimized Multi-Mass Rotor Model System

Parameter	***Optimized System***	***Non-Optimized System***
Maximum Series Compensation	85%	85%
8% Series Compensation Applied		
Overshoot	4.5%	4.6%
Undershoot	4.5%	4.5%
Settling Time (2% of Final Value)	0.135 s	0.135 s
50% Series Compensation Applied		
Overshoot	31%	31%
Undershoot	26%	26%
Settling Time (5% of Final Value)	0.373 s	0.373 s
80% Series Compensation Applied		
Overshoot	71.9%	72.2%
Undershoot	66.2%	88.3%
Settling Time (5% of Final Value)	0.463 s	0.553 s

The optimization was more effective on the single-mass model, decreasing the power output swings when the compensation was connected to the system, and increasing from 94% to 97% the maximum amount of compensation that the system could receive and maintain stability.

The optimization on the multi-mass model was less effective, yielding improvements on the output power swings when compensation was connected. The maximum level of compensation was not increased after the optimization was completed, remaining at 85% for both the non-optimized and optimized multi-mass MBSSDC.

The improvement from the simplex optimization process is primarily seen during the

disturbance that occurs when series compensation is connected to the system. As shown in Figures 4.7, 4.9, and 4.11, or the single mass system, and Figures 4.18, 4.20, and 4.22 for the multi-mass system, the power swings when the series compensation is connected is much lower for the optimized systems than the non-optimized systems. This is primarily due to the fact that the frequencies in the disturbance are mainly concentrated in the range that the bands of the MBSSDC is tuned to.

The waveforms generated from faults on the generator bus, Figures 4.8, 4.10, and 4.12 for the single mass system and Figures 4.19, 4.21, and 4.23, for the multi-mass system, show little difference from the same waveforms on the non-optimized system. This is due to the fact that the fault waveforms primarily contain low frequency waveforms that are below the range the MBSSDC has been tuned to.

Further improvement may be possible through the optimization of the gain three gain values in each of the two supplementary control bands.

Chapter 5

Thesis Summary and Conclusions

5.1 Summary

Wind energy provides a needed source of renewable energy to the electrical market; however, connecting this renewable energy to the grid can cause some challenges, and with the rapid increase of the proportion of renewables, these complexities are becoming more and more important to the power generation industry. Integration of renewable energy to the electrical system has seen a rapid increase over the past decade.

Currently wind power represents about 10% of the installed electrical generation capacity in Canada. The growing supply of wind power being connected to the grid, frequently in areas far from population centers, means that issues involved with the stable and reliable transmission of this energy to the main grid are likely to become very important in the near future.

5.2 Sub-Synchronous Interactions

As wind-farms are frequently connected to the main grid through a radial transmission line, efficient use of the transmission line often means the use of a series capacitor in the system. A specific type of SSI oscillation (SSCI's) can occur due to the interaction between an induction generator's power-electronic based excitation control and series compensated 'long' transmission lines. The purely electrical nature of this interaction means that stability can be lost nearly instantly.

Series compensated lines are often found in a typical wind-farm application, in a rural or remote area, where wind power is captured using an induction generator, then transmitted along the electrical grid to a population center. Even if the farm is not normally connected radially, it is possible for a wind-farm suddenly to find itself connected radially due to other faults on the system, causing lines to be removed from service [12].

5.3 Single Mass Rotor Model MBSSDC

The study of the model wind generation system in Chapter 2 showed the oscillations and instability that can result from even a small value of series compensation being added to an otherwise stable system under the correct conditions. Chapter 2 showed the development of the MBSSDC, a multi-band sub-synchronous damping controller, and its addition to the system model.

Testing showed that the MBSSDC allowed the system to remain stable in situations where it had been previously unstable. The addition of the MBSSDC allowed the system to remain stable with compensation levels of up to 94%. Fault testing was performed with the series compensation set to this 94% value to confirm that the system remained stable during the fault situations that can occur.

5.4 Multi-Mass Rotor Model MBSSDC

Chapter 3 showed the addition of a multi-mass rotor model to the system. The multi-mass rotor model is a more realistic rotor model than the simpler single mass rotor model used in Chapter 2. Testing of the MBSSDC was performed with the multi-mass rotor model in place with the results being quite acceptable. Stability of the system was maintained up to 85% series compensation. Fault testing was performed with the series compensation set to this 85% value in the same manner as the single-mass model from Chapter 2 showing that the system remained stable in fault situations.

5.5 Simplex Optimization

Chapter 4 documented the optimization of both the single mass and multi-mass systems using a nonlinear time domain optimization with a simplex algorithm. The optimization used the 8 time constants in the lead-lag blocks of the MBSSDC as the input variables and the change in output power as the objective function to minimize.

The optimization took 174 iterations on the single-mass model while the multi-mass model required 498 iterations to converge. The optimization was more effective on the single-mass model, decreasing the power output swings when the compensation was connected to the system. The maximum amount of series compensation that the system could receive and maintain stability increased from 94% to 97%. The optimization on the multi-mass model was less effective than with the single mass rotor model system, yielding modest improvements on the output power swings when compensation was connected.

The optimization had a larger impact on the disturbances created by the connection of series compensation, than on the disturbances created when a fault occurred due to the frequencies of oscillation in the fault waveforms being primarily low frequency, below the range of frequencies the MBSSDC bands are tuned for.

5.6 Thesis Contributions

This thesis has advanced the model of a Type III DFIG wind farm used in the Real-Time Simulation Laboratory at the University of Saskatchewan. Research from this thesis is contributing to the implementation of the modeling of Type III DFIG's on the RTDS system.

The main contributions of this thesis are summarized in the list below:

1. The MBSSDC is an innovative method of damping SSCI that develop in series compensated Type III DFIG wind farms. The MBSSDC provides a simple and elegant solution with the multi-band damper placed in parallel with the existing control system. Unlike several proposed control level solutions, the original control system is left

in place to operate as designed in normal operation, with the MBSSDC operating in parallel. The MBSSDC provides an economical control method.

In comparison, many of the proposed solutions call for placement of new SVCs, TCSCs, PSSs and FACTS devices. These solutions require high power devices that will increase the cost and footprint of the solution greatly in comparison to the control level MBSSDC.

2. Provides a method for the nonlinear time domain optimization of a multivariable system. The tuning of a control system for multiple frequencies is a very difficult task, and conventional methods using the transfer functions are not appropriate for the wide frequency range of oscillations seen in SSCI's.

   This thesis demonstrates a method to tune multiple variables in a control system using a nonlinear time domain simplex method. The optimization is performed using a multirun process in an EMT simulation (PSCAD).

5.7 Future Work

The following list explains some avenues where the research could be continued:

1. Optimization of the gain values in each band of the MBSSDC:
   - There are 3 gain values in each of the bands of the MBSSDC (6 total). Optimizing these in tandem with the time constants will be difficult as the simplex method is best suited to less than 10 variables.
2. Study of the implications of fault location on the response of the system:
   - All faults were placed directly after the wind farm collector bus.
3. Implementation of the MBSSDC on DSP hardware to test and verify the operation using the Real Time Digital Simulation (RTDS) platform:

4. Study the need for additional damping bands to be implemented on the multi-mass model due to the additional modes of oscillation added by the rotor.

    - Further improvements may be obtained in the performance of the multi-mass rotor system.

References

[1] J. Rose, "Series Compensation and SSR - Concepts," in *Workshop on NPRR 562, Subsysnchronous Oscillations*, September 2013.

[2] N. R. CANADA. (2016) About Renewable Energy. [Online]. Available: http://www.nrcan.gc.ca/energy/renewable-electricity/7295

[3] "Wind in Power, 2015 European Statistics," European Wind Energy Association, Tech. Rep., 2016.

[4] "Global Wind Report - Annual Market Update 2012," Global Wind Energy Council, Brussels, Tech. Rep., 2012.

[5] "Renewables 2016 Global Status Report," Renewable Energy Policy Network for the 21st Century (REN21), Tech. Rep., 2016.

[6] Canadian Wind Energy Association, "Powering Canada's Future," Canadian Wind Energy Association, Tech. Rep., 2015.

[7] E. V. Larsen, "Wind Generators and Series-Compensated AC Transmission Lines," in *IEEE PES Transmission and Distribution Conference and Exposition*, Orlando, Florida, USA, 2012, pp. 1–4.

[8] "Renewable Energy Essentials: Wind," International Energy Agency, Tech. Rep., 2008.

[9] "Electric Power Annual 2009," United States Energy Information Administration, Department of Energy, Tech. Rep., 2011.

[10] "Wind Power: Capacity Factor, Intermittency, And What Happens When The Wind Doesnt Blow?" Renewable Energy Research Laboratory, University of Massachusetts at Amherst, Tech. Rep., 2004.

[11] "Renewables 2015 Global Status Report," Renewable Energy Policy Network for the 21st Century (REN21), Tech. Rep., 2015.

[12] L. C. Gross, "Sub-Synchronous Grid Conditions: New Event, New Problem, and New Solutions," Relay Application Innovation Inc., Tech. Rep., 2010.

[13] S. H. Huang, D. Maggio, K. McIntyre, V. Betanabhatla, J. Dumas, and J. Adams, "Impact of Wind Generation on System Operations in the Deregulated Environment: ERCOT Experience," in *Power & Energy Society General Meeting, IEEE*, Calgary, Alberta, Canada, July 2009, pp. 1–8.

[14] G. D. Irwin, A. K. Jindal, and A. L. Isaacs, "Sub-Synchronous Control Interactions Between Type 3 Wind Turbines and Series Compensated AC Transmission Systems," in *Power and Energy Society General Meeting, IEEE*, Detroit, Michigan, USA, 2011, pp. 1–6.

[15] "Lesson Learned - Sub-Synchronous Interaction between Series-Compensated Transmission Lines and Generation," North American Electric Reliability Corporation, Tech. Rep., July 2011.

[16] J. G. Slootweg and W. L. Kling, "Aggregated Modelling Of Wind Parks In Power System Dynamics Simulations," in *Power Tech Conference Proceedings, 2003 IEEE Bologna*, vol. 3, June 2003, pp. 6 pp. Vol.3–.

[17] C. Abbey, J. Morneau, J. Mahseredjian, and G. Joos, "Modeling Requirements For Transient Stability Studies For Wind Parks," in *2006 IEEE Power Engineering Society General Meeting*, 2006, pp. 6 pp.–.

[18] T. Ackermann, *Wind Power in Power Systems, Second Edition*. John Wiley & Sons, 2012.

[19] "Fault Current Contributions from Wind Plants," in *2015 68th Annual Conference for Protective Relay Engineers*, March 2015, pp. 137–227.

[20] M. Poller and S. Achilles, "Aggregated Wind Park Models for Analyzing Power System Dynamics," in *4th Int. Workshop Large-Scale Integration of Wind Power and Transmission Networks for Offshore Wind Farms*, Billund, Denmark, Oct 2003.

[21] H. Liu and Z. Chen, "Aggregatedm odelling for Wind Farms for Power System Transient Stability Studies," in *2012 Asia-Pacific Power and Energy Engineering Conference*, March 2012, pp. 1–6.

[22] D. E. Kim and M. A. El-Sharkawi, "Dynamic Equivalent Model of Wind Power Plant using an Aggregation Technique," *IEEE Transactions on Energy Conversion*, vol. 30, no. 4, pp. 1639–1649, Dec 2015.

[23] S. M. Muyeen, M. H. Ali, R. Takahashi, T. Murata, J. Tamura, Y. Tomaki, A. Sakahara, and E. Sasano, "Comparative Study on Transient Stability Analysis of Wind Turbine Generator System using Different Drive Train Models," *IET Renewable Power Generation*, vol. 1, no. 2, pp. 131–141, June 2007.

[24] L. Harnefors, "Analysis of Subsynchronous Torsional Interaction with Power Electronic Converters," *IEEE Transactions on Power Systems*, vol. 22, no. 1, pp. 305–313, Feb 2007.

[25] G. Rogers, "Demystifying Power System Oscillations," *IEEE Computer Applications in Power*, 1996.

[26] D. N. Walker, C. E. J. Bowler, R. L. Jackson, and D. A. Hodges, "Results of Subsynchronous Resonance Test at Mohave," *IEEE Transactions on Power Apparatus and Systems*, vol. 94, no. 5, pp. 1878–1889, Sept 1975.

[27] C. Liu, R. Yokoyam, K. Koyanagi, and Y. Lee, "PSS Design for Damping of Inter-Area Power Oscillations by Coherency-Based Equivalent Model," *Electrical PowEr and Energy Systems*, vol. 26, 2004.

[28] J. W. Butler and C. Concordia, "Analysis of Series Capacitor Application Problems," *Transactions of the American Institute of Electrical Engineers*, vol. 56, no. 8, pp. 975–988, Aug 1937.

[29] K. A. Donohoo, "Planners Perspective on Series Compensated Transmission Lines," Oncor Electric Delivery Company LLC, Tech. Rep., 2012.

[30] J. Glover, T. Overbye, and M. Sarma, *Power System Analysis And Design*. Cengage Learning, 2016. [Online]. Available: https://books.google.ca/books?id=4ihTCwAAQBAJ

[31] H. Saadat, *Power System Analysis*. PSA Publishing, 2010. [Online]. Available: https://books.google.ca/books?id=s_IbSQAACAAJ

[32] J. Grainger and W. Stevenson, *Power System Analysis*, ser. McGraw-Hill series in electrical and computer engineering: Power and energy. McGraw-Hill, 1994. [Online]. Available: https://books.google.ca/books?id=NBIoAQAAMAAJ

[33] "Series Compensation Systems," General Electric Grid Solution, Tech. Rep., 2015.

[34] J. Adams, C. Carter, and S. H. Huang, "ERCOT Experience with Sub-Synchronous Control Interaction and Proposed Remediation," in *Transmission and Distribution Conference and Exposition, 2012 IEEE PES*, May 2012, pp. 1–5.

[35] S. Chandrasekar and R. Gokaraju, "Dynamic Phasor Modeling Of Type 3 DFIG Wind Generators (Including SSCI Phenomenon) For Short-Circuit Calculations," *IEEE Transactions On Power Delivery*, vol. 30, no. 2, pp. 887–897, April 2015.

[36] Z. Miao, "Impedance-Model-Based SSR Analysis For Type 3 Wind Generator And Series-Compensated Network," *IEEE Transactions On Energy Conversion*, vol. 27, no. 4, pp. 984–991, Dec 2012.

[37] B. Badrzadeh, M. Sahni, D. Muthumuni, Y. Zhou, and A. Gole, "Sub-Synchronous Interaction in Wind Power Plants Part I: Study tools and techniques," *Power and Energy Society General Meeting (2012), IEEE*, pp. 1–9, 2012.

[38] M. Sahni, D. Muthumuni, B. Badrzadeh, A. Gole, and A. Kulkarni, "Advanced Screening Techniques for Sub-Synchronous Interaction in Wind Farms," in *Transmission and*

Distribution Conference and Exposition (TD), 2012 IEEE PES, Orlando, Florida, USA, 2012, pp. 1–9.

[39] M. S. El Moursi, B. Bak Jensen, and M. H. Abdel Rahman, "Novel STATCOM Controller for Mitigating SSR and Damping Power System Oscillations in a Series Compensated Wind Park," *Power Electronics, IEEE Transactions on*, vol. 25, no. 2, pp. 429–441, 2010.

[40] R. K. Varma, S. Auddy, and Y. Semsedini, "Mitigation of Subsynchronous Resonance in a Series-Compensated Wind Farm Using FACTS Controllers," *IEEE Transactions on Power Delivery*, vol. 23, no. 3, pp. 1645–1654, 2008.

[41] H. Liu, X. Xie, Y. Li, H. Liu, and Y. Li, "Damping DFIG-Associated SSR with Subsynchronous Suppression Filters: A Case Study on a Practical Wind Farm System," in *International Conference on Renewable Power Generation (RPG 2015)*, Oct 2015, pp. 1–6.

[42] H. Liu, X. Xie, J. He, H. Liu, and Y. Li, "Damping DFIG-Associated SSR by adding Subsynchronous Suppression Filters to DFIG Converter Controllers," in *2016 IEEE Power and Energy Society General Meeting (PESGM)*, July 2016, pp. 1–5.

[43] L. Wang, X. Xie, Q. Jiang, and X. Liu, "Centralised Solution for Subsynchronous Control Interaction of Doubly Fed Induction Generators using Voltage-Sourced Converter," *IET Generation, Transmission Distribution*, vol. 9, no. 16, pp. 2751–2759, 2015.

[44] M. A. Chowdhury, M. A. Mahmud, W. Shen, and H. R. Pota, "Nonlinear Controller Design for Series-Compensated DFIG-Based Wind Farms to Mitigate Subsynchronous Control Interaction," *IEEE Transactions on Energy Conversion*, vol. PP, no. 99, pp. 1–1, 2017.

[45] M. Edrah, K. L. Lo, and O. Anaya-Lara, "Reactive Power Control of DFIG Wind Turbines for Power Oscillation Damping under a wide range of Operating Conditions," *IET Generation, Transmission Distribution*, vol. 10, no. 15, pp. 3777–3785, 2016.

[46] X. Zhang, Y. Chen, X. Zhu, Y. Fu, Q. Yan, J. Chen, and X. Wang, "Improved Control of DFIG-Based Wind Turbines for Frequency Response and Power Oscillation Damping," in *International Conference on Renewable Power Generation (RPG 2015)*, Oct 2015, pp. 1–5.

[47] S. Filizadeh, A. M. Gole, D. A. Woodford, and G. D. Irwin, "An Optimization-Enabled Electromagnetic Transient Simulation-Based Methodology for HVDC Controller Design," *IEEE Transactions on Power Delivery*, vol. 22, no. 4, pp. 2559–2566, Oct 2007.

[48] J. A. Nelder and R. Mead, "A Simplex Method for Function Minimization," *Computer Journal*, vol. 7, pp. 308–313, 1965.

[49] A. M. Gole, S. Filizadeh, and P. L. Wilson, "Inclusion of Robustness into Design using Optimization-Enabled Transient Simulation," *IEEE Transactions on Power Delivery*, vol. 20, no. 3, pp. 1991–1997, July 2005.

[50] A. Gole, S. Filizadeh, R. Menzies, and P. Wilson, "Optimization-Enabled Electromagnetic Transient Simulation," in *IEEE Power Engineering Society General Meeting, 2004.*, June 2004, pp. 1133 Vol.1–.

[51] "Wind Power Turbine Calculations," Royal Academy of Engineering, Tech. Rep., 2014.

[52] L. Xu and P. Cartwright, "Direct Active and Reactive Power Control of DFIG for Wind Energy G'eneration," *IEEE Transactions on Energy Conversion*, vol. 21, no. 3, pp. 750–758, Sept 2006.

[53] S. Muller, M. Deicke, and R. W. D. Doncker, "Doubly Fed Induction Generator Systems for Wind Turbines," *IEEE Industry Applications Magazine*, vol. 8, no. 3, pp. 26–33, May 2002.

[54] N. S. Nise, *Control Systems Engineering - 6th Ed.* John Wiley & Inc., 2011.

[55] S. Filizadeh, "Optimization-Enabled Electromagnetic Transient Simulation," Ph.D. dissertation, University of Manitoba, 2004.

[56] *PSCAD Users Guide V4.6.*

[57] A. Fitzgerald, C. Kingsley, and S. Umans, *Electric Machinery*. McGraw-Hill, 1983.

[58] R. Grondin, I. Kamwa, G. Trudel, L. Gerin-Lajoie, and J. Taborda, "Modeling and Closed-Loop Validation of a new PSS Concept, the Multi-Band PSS," in *Power Engineering Society General Meeting, 2003, IEEE*, vol. 3, July 2003, p. 1809 Vol. 3.

[59] "Tsat - Transient Security Analysis Tool."

[60] J. F. Hauer, C. J. Demeure, and L. L. Scharf, "Initial Results in Prony Analysis of Power System Response Signals," *IEEE Transactions on Power Systems*, vol. 5, pp. 80–89, 1990.

[61] R. Ramanujam, *Power System Dynamics: Analysis And Simulation*. PHI Learning Private Limited, 2009. [Online]. Available: https://books.google.ca/books?id=LdwREiT-yI4C

[62] W. Qiao, "Dynamic Modeling and Control of Doubly Fed Induction Generators driven by Wind Turbines," in *2009 IEEE/PES Power Systems Conference and Exposition*, March 2009, pp. 1–8.

[63] P. Kundur, *Power System Stability and Control*. New York: McGraw-Hill, 1994.

[64] K. Miura, K. Hashimoto, J. Gangloff, and M. de Mathelin, "Visual Servoing Without Jacobian Using Modified Simplex Optimization," *Proceedings Of The 2005 IEEE International Conference On Robotics And Automation*, pp. 3504–3509, April 2005.

[65] A. Tsatsoulas, J. Barkate, C. Baylis, and R. J. Marks, "A Simplex Optimization Technique For Real-Time Reconfigurable Transmitter Power Amplifiers," *2016 IEEE MTT-S International Microwave Symposium (IMS)*, pp. 1–4, May 2016.

[66] V. Braziunas and P.-Y. Woo, "Optimal Controller Parameter Design Using Simplex Optimization," *Intelligent Control and Instrumentation, 1992. SICICI '92. Proceedings., Singapore International Conference on*, vol. 1, pp. 59–63, Feb 1992.

[67] F. Hillier and G. Lieberman, *Introduction To Operations Research*, ser. Business Quantitative Series. McGraw-Hill Higher Education, 2005. [Online]. Available: https://books.google.ca/books?id=C8xfQgAACAAJ

Appendix A

System data

A.1 Type III Wind Generator Test System Parameters

Table A.1: Type 3 wind generator test system data

Generator data	$3.4\,MVA$, $0.69\,kV$, $60\,Hz$, $J = 1.856\,s$, $R_{stator} = 0.0054\,p.u$, $R_{rotor} = 0.00607\,p.u$, $L_m = 4.362\,p.u$, $L_{stator} = 0.102\,p.u$, $L_{rotor} = 0.11\,p.u$
Crowbar circuit	$R_{crowbar} = 0.1\,\Omega$, $R_{IGBT-ON} = 0.01\,\Omega$, $R_{IGBT-OFF} = 1.0e6\,\Omega$, $V_{dc-UL} = 1.3\,p.u$, $V_{dc-LL} = 1.05\,p.u$
Back to back converter	$R_{IGBT-ON-GSC} = 0.0005\ \Omega$, $R_{IGBT-ON-RSC} = 0.01\ \Omega$, $R_{IGBT-OFF} = 1.0e6\,\Omega$.
Rotor side controller	$K_{P,Q_s} = 1.0$, $K_{I,Q_s} = 1.0\ s$, $K_{P,P_s} = 1.0$, $K_{I,P_s} = 1.0\ s$, $K_{P,i_{r,d}} = 1.0$, $K_{I,i_{r,d}} = 2.0\ s$, $K_{P,i_{r,q}} = 1.0$, $K_{I,i_{r,q}} = 2.0\ s$
Grid side controller	$K_{P,Q_g} = 1.0$, $K_{I,Q_g} = 0.02\ s$, $K_{P,V_{dc}} = 1.0$, $K_{I,V_{dc}} = 0.02\ s$, $K_{P,i_{g,q}} = 0.1$, $K_{I,i_{g,q}} = 0.1\ s$, $K_{P,i_{g,d}} = 1.0$, $K_{I,i_{g,d}} = 0.02\ s$
Transmission line data	$240kms$, $R_{Line} = 0.3107e{-}7p.u/m$, $X_{Line} = 0.3479e{-}6p.u/m$, $B_{Line} = 5.1885e-6\,p.u/m$
Generator Transformer data	$3.4\,MVA$, $60\,Hz$, $Y-Y-Y$, $0.482/33/0.688\,kV$, $X_{1-2} = 0.0888\,p.u$, $X_{1-3} = 0.1663\,p.u$, $X_{2-3} = 0.0875\,p.u$
Station Transformer data	$600MVA, 60Hz, Y{-}\Delta{-}Y, 345/13.8/33kV$, $X_{1-2} = 0.24p.u$, $X_{1-3} = 0.12\,p.u$, $X_{2-3} = 0.16\,p.u$

A.2 Single Mass Shaft Model

Table A.2: Mechanical Drive Train parameters

Parameter	Value
Angular Moment of Inertia	1.856 sec
Mechanical Damping	0.01 $P.U.$

A.3 Multi-Mass Shaft Model

Table A.3: Mechanical Drive Train parameters

Parameter	Value
Turbine 1 Inertia Constant	2.1 sec
Turbine 2 Inertia Constant	0.1556 sec
Torque Share for Turbine 1	0.9 PU
Torque Share for Turbine 2	0.1 PU

Appendix B

PSCAD Model Diagrams

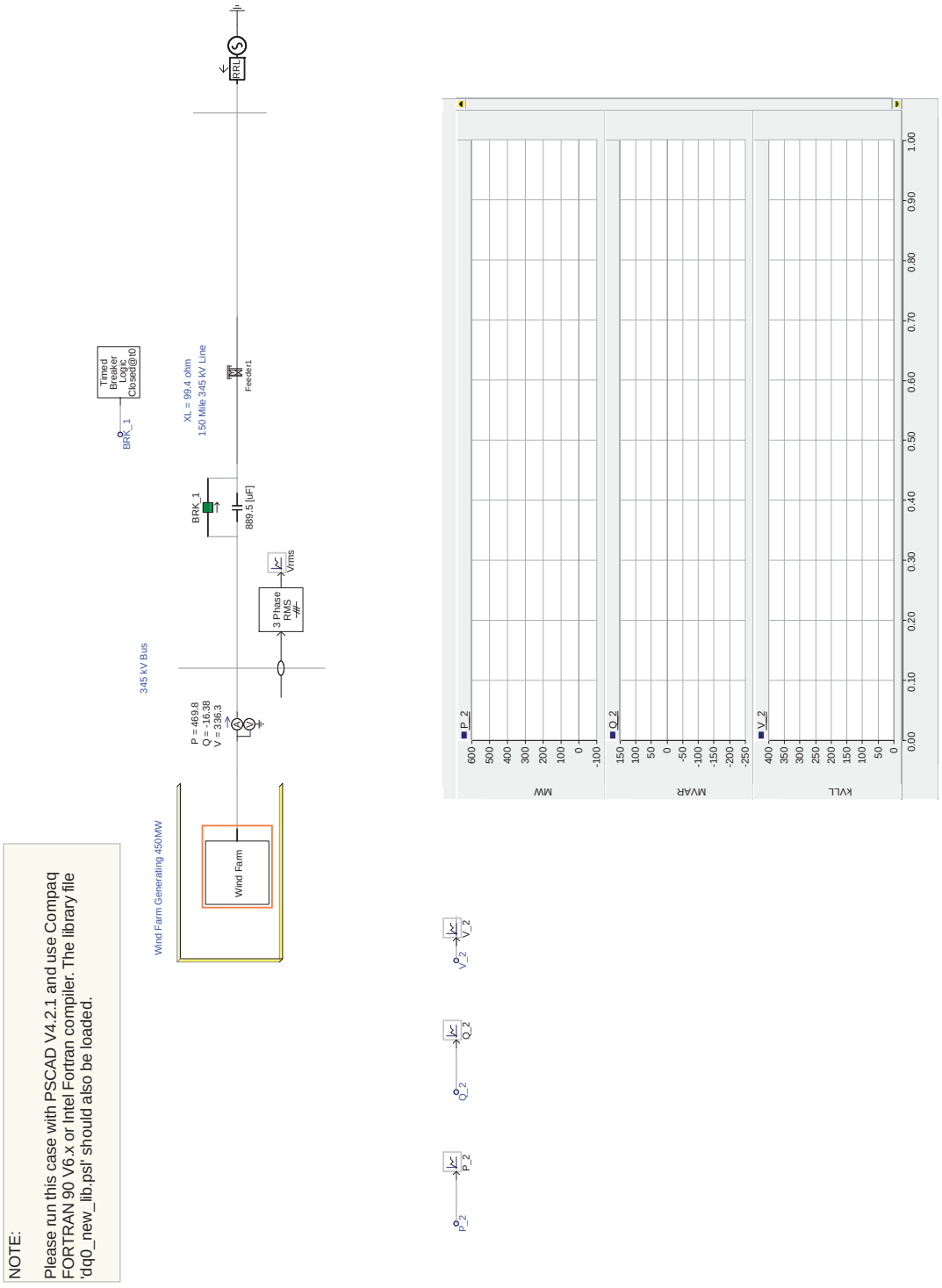

Figure B.1: Top Level View of Windfarm

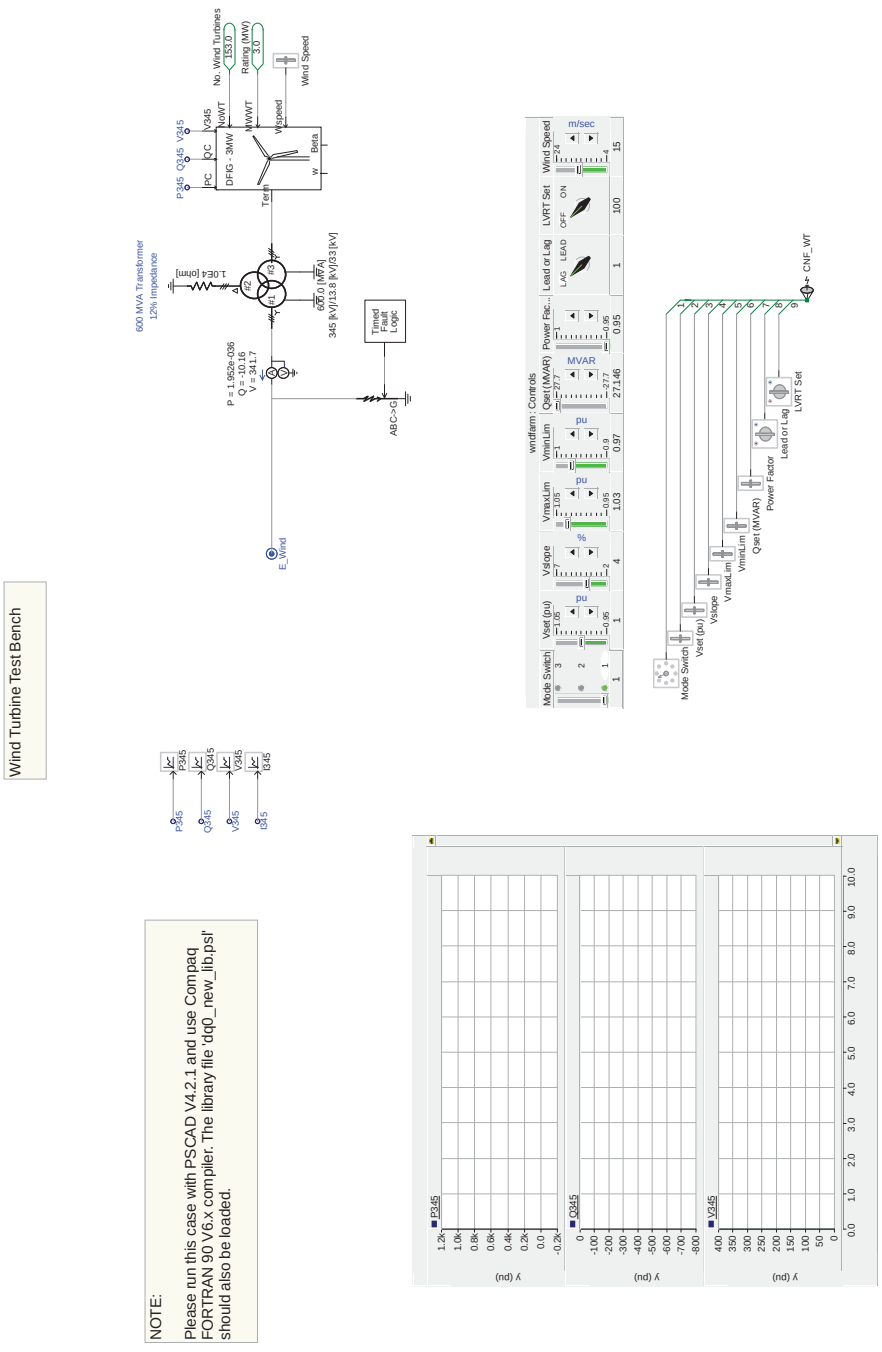

Figure B.2: Mid Level View of Windfarm

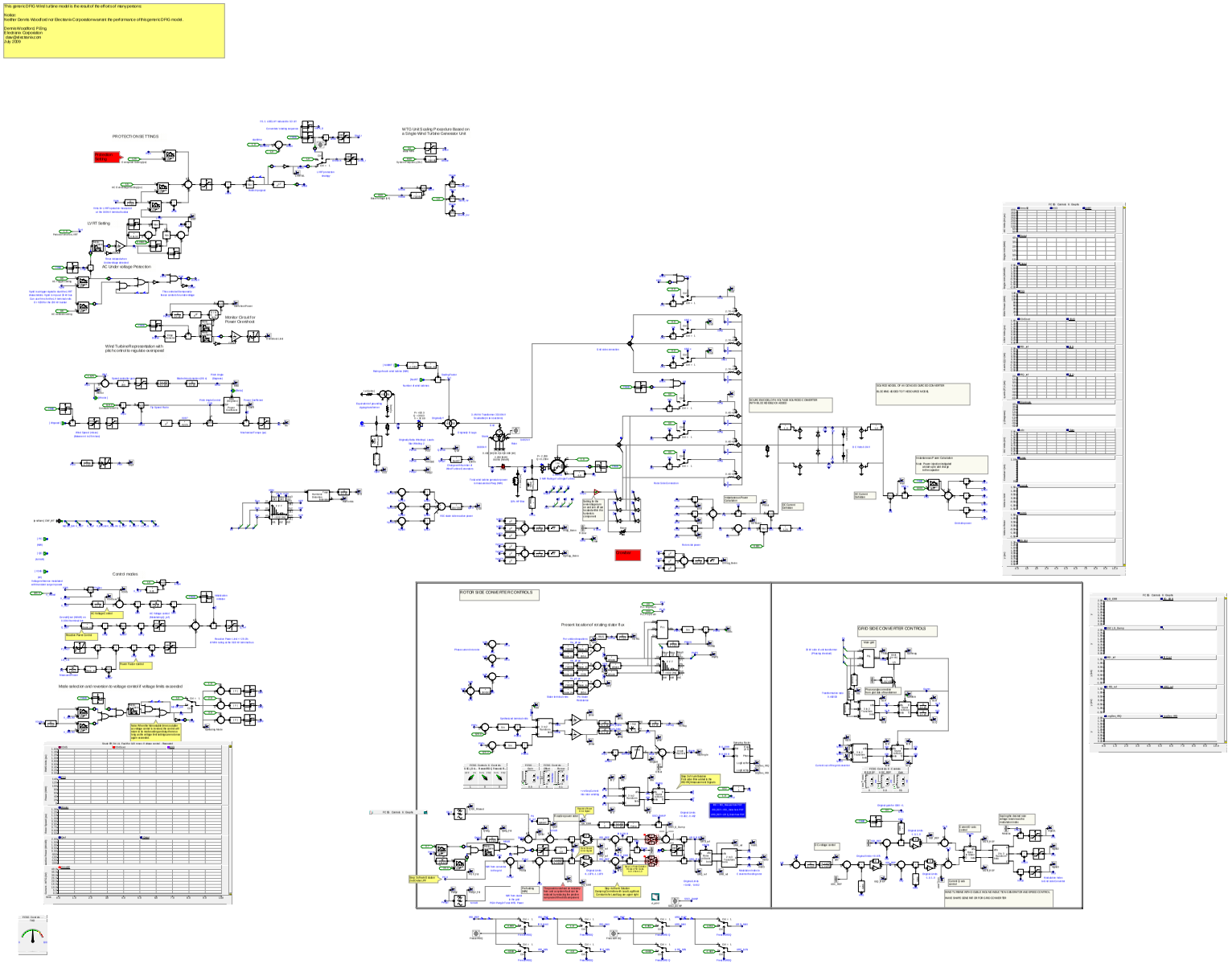

Figure B.3: PSCAD Single Mass Windfarm

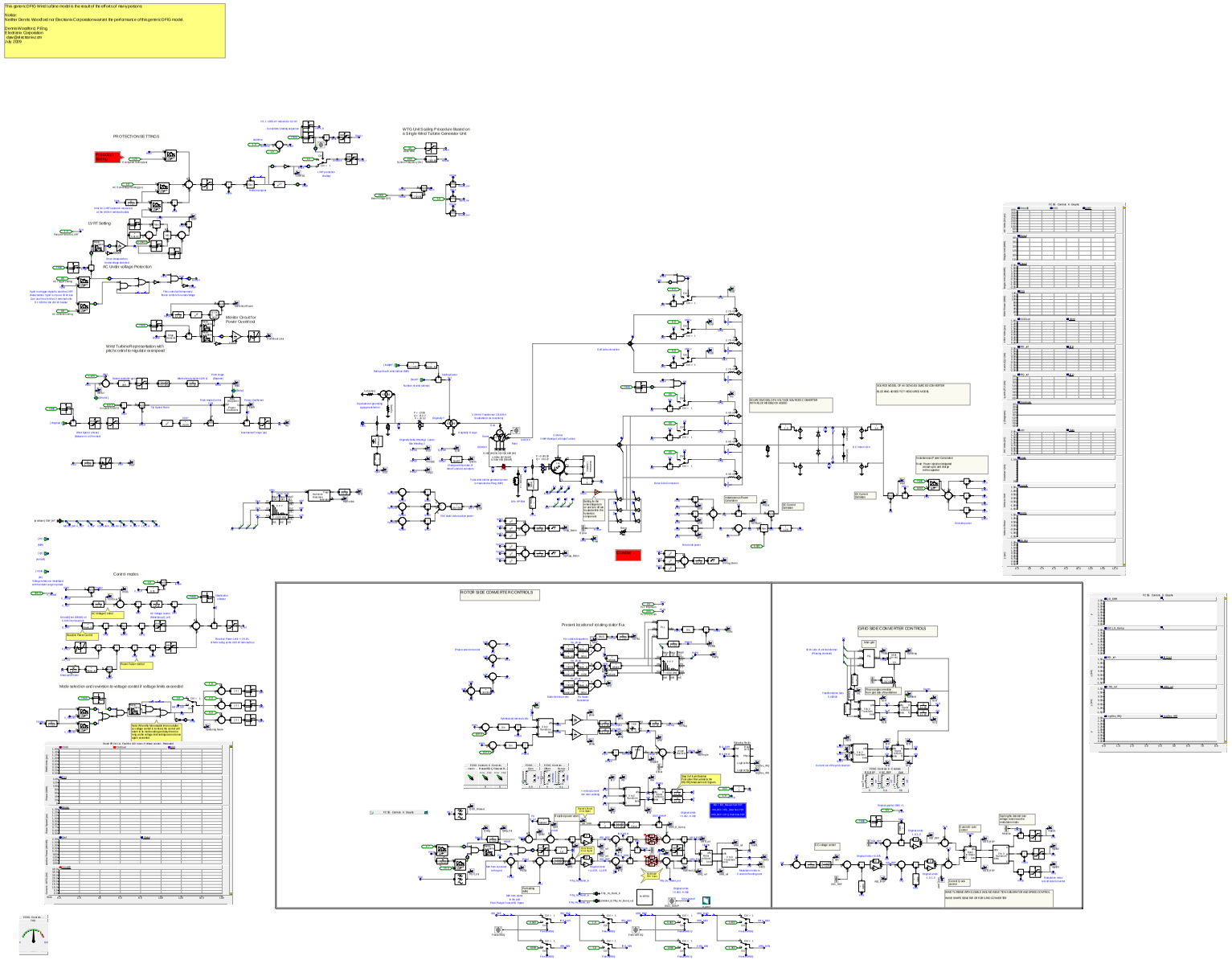

Figure B.4: PSCAD Multi-Mass Windfarm

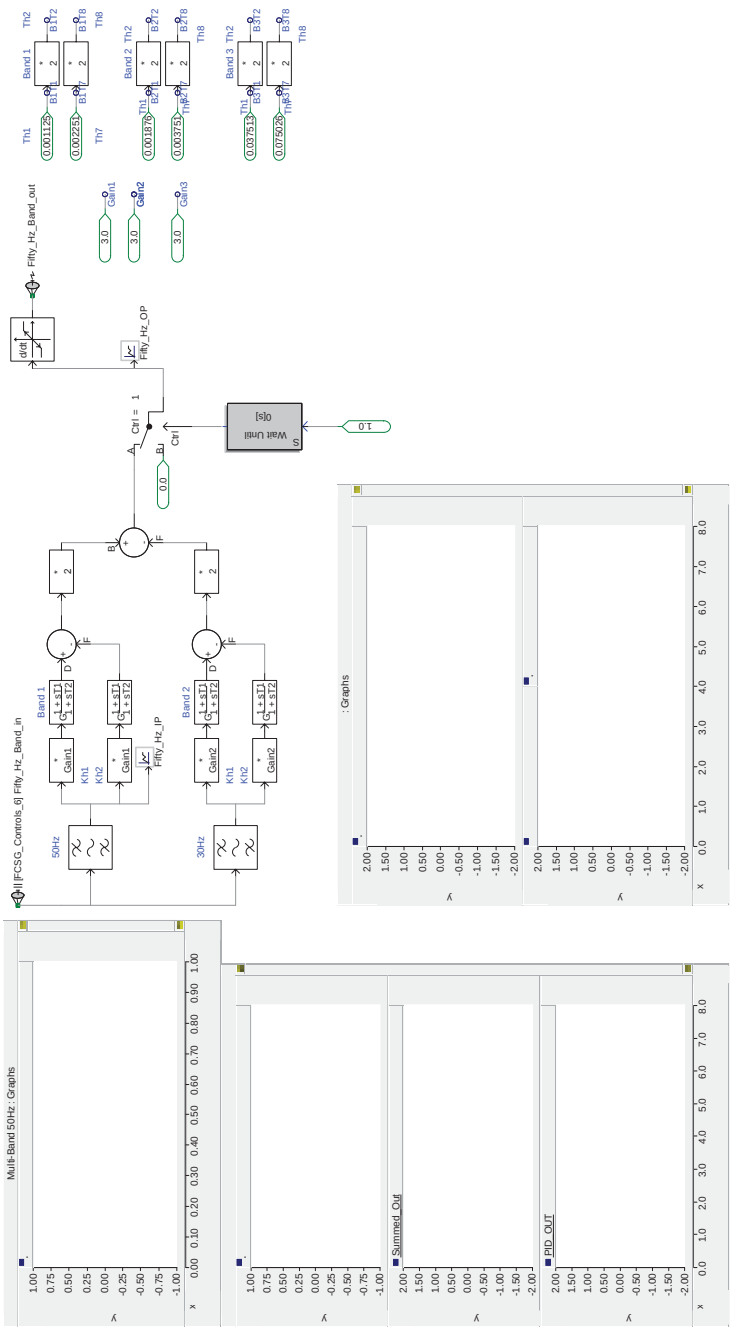

Figure B.5: PSCAD MBSSDC Setup

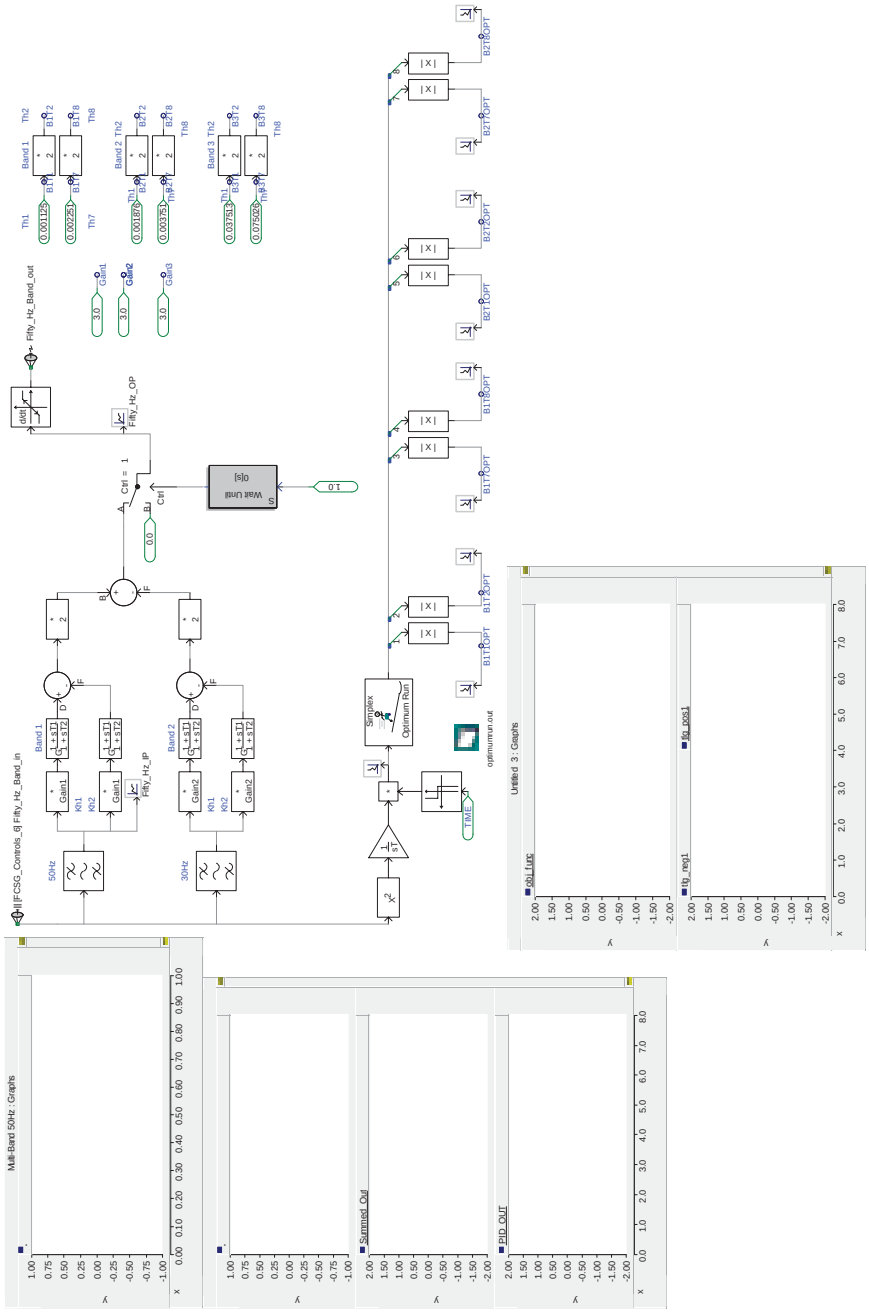

Figure B.6: PSCAD Simplex Optimization Setup